UNIVERSITY OF CALIFORNIA

Santa Barbara

Nitrogen Dynamics in Coastal California Watersheds, Beaches, and the Nearshore Ocean

A Dissertation submitted in partial satisfaction of the requirements for the degree of

Doctor of Philosophy in Environmental Science and Management

by

Blair MacPherson Goodridge

Committee in charge:

Professor John M. Melack, Chair

Professor Patricia A. Holden

Professor David L. Valentine

September 2014

The dissertation of Blair Goodridge is approved.

_____

Patricia A. Holden

_____

David L. Valentine

_____

John M. Melack, Committee Chair

July 2014

Nitrogen Dynamics in Coastal California Watersheds, Beaches, and the Nearshore Ocean

by

Blair MacPherson Goodridge

ACKNOWLEDGEMENTS

I would like to thank my advisor, John Melack, and committee members, Trish Holden and Dave Valentine, for their support and guidance throughout my studies. I would like to acknowledge the Santa Barbara Coastal Long-Term Ecological Research project at the UCSB Marine Science Institute for providing me the opportunity to discover my interest in biogeochemistry and funding many of the supplies and analytical work I used in my research. I would like to thank the sources of financial support throughout my time as a Ph.D. student, including the UCSB Associated Students Coastal Fund, Luce Environmental Science to Solutions Fellowship program, Susan and Bruce Worster (Worster Undergraduate Mentorship Program), and UCSB Graduate Division.

I am grateful for all the efforts and assistance provided by the many individuals who contributed to my research. Scott Coombs, Tim Robinson, Al Leydecker, Frank Setaro, and numerous undergraduate sampling assistants collected and provided much of the data used in my second chapter. Doug Hammond at USC provided invaluable advice and generously lent his time, knowledge, and equipment, allowing me to conduct my own radon work that I otherwise would not have been able to carry out. Peter Swarzenski at the USGS generously loaned me his RAD7 instrument for my pore water radon analyses. Jenifer Dugan provided useful advice and information on local beaches, allowing me to design and hone my beach sampling routines. Michael Benaron and Matt Meyerhof got to work on their suntans at the beach, providing invaluable assistance in collecting pore water samples. Matt Meyerhof also ran pore water ammonium and nitrate samples, and helped me work through CO_2 headspace equilibration calculations. The Carlson Lab at UCSB (Craig Carlson, Maverick Carey, Ellie Halewood, and Anna James) provided DOC and TDN analysis, and generously lent water filtration equipment and supplies. Steve Sadro was always there to help out with advice on certain analyses or methods when I needed it. Sage Davis was always willing to help with equipment construction, troubleshooting, and logistics, even though he was doing a million other tasks maintaining our research building.

I am so very grateful to my family; Mom, Dad, Colin, Puff, Maggie, Mira, and Boomer, for helping me persevere in times of doubt and celebrate in times of joy, I love you all. Finally, to my wife Ali, your love and support has meant everything to me. I couldn't have done this without you.

VITA OF BLAIR MACPHERSON GOODRIDGE
September 2014

Education

Ph.D. Bren School of Environmental Science and Management University of California Santa Barbara (UCSB) Santa Barbara, California	September 2014
B.A. Environmental Biology (with honors) Colgate University Hamilton, New York	May 2003

Professional and Research Experience

Research Associate UCSB Marine Science Institute Santa Barbara, California	2006 – 2013
Research Associate UCSB Earth Research Institute Santa Barbara, California	2006 – 2008
Environmental Careers Organization (ECO) Associate San Diego Coastkeeper San Diego, California	2006
Environmental Scientist Tetra Tech EM, Inc. San Diego, California	2003 – 2004
Undergraduate Research Assistant Department of Biology, Colgate University Hamilton, New York	2003

Peer-Reviewed Publications and Technical Reports

Goodridge B.M. and J.M. Melack. Radon residence times reveal temporal evolution and variability of dissolved inorganic nitrogen in beach pore water. Environmental Science & Technology (in review).

Brzezinski M.A., D.C. Reed, S. Harrer, A. Rassweiler, J.M. Melack, **B.M. Goodridge**, J.E. Dugan. 2013. Multiple sources and forms of nitrogen sustain year-round kelp growth on the inter-continental shelf of the Santa Barbara Channel. Oceanography 26(3),114-123.

Goodridge B.M. and J.M. Melack. 2012. Land use control of stream nitrate concentrations in mountainous coastal California watersheds. Journal of Geophysical Research – Biogeosciences 117(G2), G02005.

Melack J.M., S.D. Cooper, **B.M. Goodridge**. 2008. Development of a stream monitoring program for Santa Rosa Island, Channel Islands National Park, California. Final Report. U.S. National Park Service.

Hoham R.W., F.M. Frey, J.D. Berman, J.B. Ryba, J.E. Duncan, A.A. Forbes, **B.M. Goodridge**, P.R.Miller. 2009. The effects of irradiance level, photoperiod, and cell density on sexual reproduction in the green snow alga, Chloromonas chenangoensis (Chlorophyta, Volvocales), from Upstate New York. Nova Hedwigia 89: 1-16.

Conference Presentations

Goodridge, B.M. and J.M. Melack. 2014. Timescale of stream nutrient recovery following wildfire in a Southern California upland chaparral watershed. Invited talk. 2014 Joint Aquatic Sciences Meeting. Portland, Oregon.

Goodridge, B.M. and J.M. Melack. 2013. Carbon and nitrogen stoichiometry regulates temporal dynamics of nitrogen concentration in sandy beach pore water. Contributed talk. 2013 American Geophysical Union (AGU) Fall Meeting. San Francisco, California.

Goodridge, B.M. and J.M. Melack. 2011. Land use control of stream nitrate concentrations in mountainous coastal California watersheds. Contributed talk. 2011 American Geophysical Union (AGU) Fall Meeting. San Francisco, California.

Fellowships, Scholarships, and Research Grants

UCSB Graduate Division Dissertation Fellowship	2014
Brython Davis Endowment Graduate Fellowship	2013
UCSB Associated Students Coastal Fund Research Grant. $1,000	2013
Worster Award for Undergraduate Mentorship	2012
UCSB Luce Environmental Science to Solutions Fellowship	2010 – 2012
UCSB Fee Fellowship	2009 – 2010
UCSB Associated Students Coastal Fund Research Grant. $3,554	2009
Colgate University Class of 1990 Endowed Scholarship	1999 – 2003

Honors

Honorable Mention, Graduate Research Fellowship National Science Foundation	2009
Member, Tri-Beta Biological Honors Society Colgate University, Upsilon Phi Chapter	2003
Recipient, Dean's Award for Academic Excellence (5 of 8 semesters) Colgate University	1999 – 2003

ABSTRACT

Nitrogen Dynamics in Coastal California Watersheds, Beaches, and the Nearshore Ocean

by

Blair MacPherson Goodridge

Nitrogen plays a dual role in coastal oceans. It sustains primary production, the foundation of coastal marine food webs, but can also cause degradation in the forms of eutrophication, harmful algal blooms, and hypoxia when supplied in excessive quantity from urban and agricultural land uses. In this dissertation, I examined the biogeochemical, land use, and hydrologic factors that regulate the concentration of dissolved inorganic nitrogen (DIN) in two nitrogen suppliers to the nearshore coastal ocean in the Santa Barbara, California region: watershed streams and beach pore water. In addition, I examined the influence of nearshore seawater and beach pore water dissolved organic matter (DOM) composition on the uptake of DIN by bacterioplankton, the primary decomposers in coastal oceans. I found that that the relationships between stream nitrate concentration and stream runoff were consistent within three broad land uses: agricultural, urban, and undeveloped. As stream runoff increased, three agricultural watersheds showed nitrate dilution, two urban watersheds showed invariance, and one undeveloped watershed showed nitrate enrichment. The undeveloped upper mountainous watershed regions were dominant contributors of water and nitrate to stream runoff and nitrate across the whole watershed during periods of high runoff, such that the variability in stream nitrate concentrations during stormflow (rainstorms) was ~ 12% of the nitrate variability during baseflow (dry periods). In beach pore water, fresh groundwater with potentially elevated nitrate is largely precluded from discharge through beach sands by

the dominant coastal bluff geomorphology of the region. However, tides circulate seawater into and out of beach sands, introducing marine particulate organic matter (POM), such as phytoplankton, giant kelp (*Macrocystis pyrifera*), and detrital material that is then degraded by heterotrophic microbes in beach sands to DOM and DIN. I integrated pore water radon residence time distributions with DIN temporal evolution curves to calculate volume-weighted mean (VWM) DIN concentrations, which represented the DIN concentration of pore water discharging to the coastal ocean. I found that the combination of temporal variability in the residence time distribution due to spring-neap tidal cycles with the temporal evolution of DIN concentrations due to POM and DOM loading can result in substantial variability in pore water VWM DIN concentrations that should be accounted for in calculating DIN flux to coastal oceans. When pore water mixes with nearshore seawater upon discharge from the beach sands, DIN that was produced within beaches becomes available for uptake by bacterioplankton. I used excitation emission matrix (EEM) fluorescence spectroscopy, respiratory quotient determinations (i.e., ratio of CO_2 production to O_2 consumption), and DIN concentration analysis in a 7-day time-series dark incubation to determine how variability in DOM composition in seawater and pore water influenced DIN uptake by bacterioplankton in nearshore seawater. I found that mixing of seawater and pore water promoted greater DIN uptake than occurred in pore water alone, which is likely the result of the presence of more labile seawater DOM and/or production of more labile DOM under seawater and pore water mixing. Together, the studies described herein enhance our understanding of nitrogen dynamics in coastal marine regions, and thus can enhance coastal zone management and development practices that seek to preserve the functioning of coastal marine ecosystems.

TABLE OF CONTENTS

Chapter 1. Introduction

Coastal marine regions lie at the boundary of terrestrial ecosystems, receiving a wide array of chemical elements discharged by coastal streams, rivers, and aquifers. Nitrogen is one of the most vital of these elements, as it is essential to the biosynthesis of amino acids, nucleic acids, and proteins. The inorganic precursors of this biosynthesis—ammonium (NH_4^+), nitrite (NO_2^-), and nitrate (NO_3^-)—are collectively referred to as dissolved inorganic nitrogen (DIN). DIN is delivered to the coastal ocean via streams, rivers, and groundwater, where it can be an important nitrogen source to primary producers, phytoplankton and macroalgae, which act as the foundation of all coastal marine food webs (Howarth, 1988; Valiela et al., 1990). However, urbanization and agricultural activity elevate this nitrogen delivery (Boyer et al., 2006; Galloway et al., 2004), which in turn alters coastal marine nitrogen cycling, causing eutrophication, harmful algal blooms, and hypoxic water masses (Anderson et al., 2002; Diaz and Rosenberg, 2008). Thus, stream, river, and groundwater delivery of nitrogen has the potential to both sustain and degrade coastal marine ecosystems. An understanding of the factors that regulate the timing and magnitude of nitrogen delivery from land to ocean is of prime importance to coastal zone management and development practices that seek to preserve the functioning of coastal marine nitrogen cycles and healthy coastal marine ecosystems.

The magnitude of DIN delivery, or DIN flux, to coastal oceans is a product of discharge and DIN concentration in the hydrologic source. Therefore, it is first necessary to identify the causes of DIN concentration variability in hydrologic sources to accurately assess DIN delivery rates to the coastal ocean. Land use is often a dominant determinant of stream and river DIN concentrations, in particular nitrate, which is the main form of DIN in

surface runoff due to the elevated nitrate loads streams and rivers receive from agricultural and urban land uses (Caraco and Cole, 1999). Beaches sit at the interface of terrestrial and marine ecosystems, where groundwater can discharge through beach sands to coastal oceans. However, the primary source of groundwater in beaches is seawater, continuously circulating into and back out of beach sands, driven by waves and tides (Li et al., 1999; Martin et al., 2007; Robinson et al., 2007; Urish and McKenna, 2004). This recirculating seawater, or saline pore water, delivers marine particulate and dissolved organic matter (POM and DOM, respectively) that is mineralized in beach pore water, producing high concentrations of DIN (Santos et al., 2009). When this high DIN concentration pore water is flushed back to the coastal ocean, the DIN becomes available for uptake by primary producers and bacterioplankton (i.e., heterotrophic floating bacteria). In addition to the production of high DIN concentrations, pore water DOM is altered by heterotrophic microbial processing in beach sands (Kim et al., 2012; Seidel et al., 2014), in turn influencing uptake by coastal seawater bacterioplankton which receive the DIN and DOM discharged from beaches.

In the second and third chapters of my dissertation I examined land use, biogeochemical, and hydrologic factors that determine DIN concentrations in coastal watershed streams and beach pore water in the Santa Barbara, California region. The coastal watersheds in the Santa Barbara region are small in area and drain from their headwaters in the Santa Ynez Mountains to the Santa Barbara Channel through the lower watershed regions which have distinctly different land uses. This feature allowed me to parse clear land use signals in stream nitrate concentrations and nitrate concentration relationships with stream runoff over the range in hydrologic conditions, from low runoff (i.e., base flow) to high runoff (i.e., stormflow). The beaches in the Santa Barbara region are primarily marine-

influenced due to predominant coastal bluff geomorphology that precludes significant groundwater inputs from shallow coastal aquifers. This feature allowed me to identify the magnitude of and temporal variation in DIN concentrations in beach pore water from the mineralization of marine dissolved and particulate organic matter (DOM and POM). In my fourth chapter, I examined the influence of seawater and pore water DOM composition on bacterioplankton uptake of DIN. Seawater and pore water DOM composition often differ due to the variable importance of autotrophic versus heterotrophic processing of DOM in each setting. Bacterioplankton are heterotrophic, meaning that they are solely dependent on DOM for energy and growth. The chemical composition of DOM therefore influences the lability of each DOM source to bacterioplankton, and thus their ability to maintain the metabolic functions that allow uptake of DIN from pore water that mixes with coastal seawater.

Chapter 2. Land use control of stream nitrate concentrations in mountainous coastal California watersheds

Introduction

Agriculture and urbanization have increased the amount of biologically-available nitrogen in streams through the application of fertilizer, aging and leaky water supply and sewage infrastructure, and creation of impervious landscapes (Galloway et al., 2003; Vitousek et al., 1997). Biologically-available nitrogen exists in three dissolved forms in stream water: ammonium (NH_4^+), dissolved organic nitrogen (DON), and nitrate (NO_3^-). Stream nitrogen composition is a product of inputs from land uses in the watershed and biogeochemical processes (Lischeid, 2008). Cation adsorption of ammonium to clay minerals (Dillon and Molot, 1990), nitrification of ammonium to nitrate (Vitousek et al., 1982), and mineralization of DON to ammonium and uptake by plant and microbial communities or subsequent microbial nitrification (Hill and Warwick, 1987; Peterson et al., 2001), are biogeochemical processes that can lead to nitrate being the most abundant form of dissolved nitrogen in streams. In addition, while agricultural and urban land uses increase the concentration of all three forms of dissolved nitrogen, nitrate concentration often has the strongest positive correlations with land use and human population size (Caraco and Cole, 1999).

Comparative studies in streams of concentration versus runoff relationships (i.e., C-Q) among watersheds of varying land use can provide insight into how watershed hydrology and land use interactively regulate nitrogen inputs to stream water and downstream aquatic ecosystems (DeFries and Eshleman, 2004; Jordan et al., 1997; Meixner and Fenn, 2004;

Shields et al., 2008). The simplest models have identified two end-member sources that contribute solutes to streams during times of low runoff (i.e., baseflow) and high runoff (i.e., stormflow), and are typically identified as groundwater and precipitation sources, respectively (Burns et al., 2001). Inclusion of a third end-member, soil water, is often found to be important (Christophersen et al., 1990; Hooper et al., 1990). Most of the studies that employ mixing models have focused on streams draining predominantly undeveloped watersheds (Poor and McDonnell, 2007). Watersheds characterized by urban and agricultural land uses can complicate interpretation of mixing models, as these land uses have other potential solute sources, including potable water and sewage from leaking infrastructure (Caraco and Cole, 1999; Lerner, 1986; Silva et al., 2002; Yang et al., 1999), impervious surface runoff from buildings and roads (Driscoll et al., 2003; Jaworski et al., 1997), and agricultural irrigation water (Carpenter et al., 1998; Di and Cameron, 2002). In such cases, a hyperbolic equation may have the requisite flexibility in fitting C-Q relationships (Barco et al., 2008; Godsey et al., 2009). A hyperbolic equation generates three parameters: a hyperbolic slope parameter that identifies dilution, invariance, or enrichment behavior, and two solute concentrations, which are baseflow and stormflow solute concentration modes. Dilution, invariance, and enrichment occur when the rate of solute mobilization per volume of water input to a stream decreases ($dC\ dQ^{-1} < 0$), remains constant ($dC\ dQ^{-1} = 0$), or increases ($dC\ dQ^{-1} > 0$), respectively, as runoff (Q) increases (Salmon et al., 2001). The baseflow and stormflow modes are estimates of the most frequently observed solute concentration at low runoff and high runoff, respectively. Coupled with additional hydrochemical and land use information, comparative analyses of C-Q behavior and

baseflow and stormflow solute concentration modes can allow important insights into probable solute sources and biogeochemical mechanisms.

In semi-arid Mediterranean climatic regions, nitrogen mobility in undeveloped watersheds is partly regulated by the timing and magnitude of precipitation (Avila et al., 1992; Butturini and Sabater, 2002; Poor and McDonnell, 2007). The dry season, with little to no measurable precipitation, causes depletion of soil water and shallow groundwater stores through streamflow and evapotranspiration (Avila et al., 1992; Biron et al., 1999). The arrival of the wet season replenishes soil and groundwater stores, but to a variable extent depending on the number of precipitation events and their magnitude (Beighley et al., 2008; Butturini and Sabater, 2002; Latron et al., 2009). These pulsed and irregular precipitation dynamics make the timing and amount of water delivery to streams a function of watershed soil moisture deficits (Bernal et al., 2004; Chamran et al., 2002; Latron et al., 2009), which dictate the degree of hydrologic connectedness of streams with their soil water and groundwater solute sources. Soil microbial nitrogen processing, which is coupled to drying and wetting, exerts some control on the timing and amount of nitrogen delivery to streams (Belnap et al., 2005; Fierer and Schimel, 2002; Miller et al., 2005), as does nitrogen build-up during the dry season, which can contribute to nitrogen flushing at the onset of the wet season (Meixner and Fenn, 2004; Sobota et al., 2009).

Streams are not only laterally connected to the landscape, but also are longitudinally connected as they flow from headwater regions to lower reaches. In some situations, headwater streams can contribute an average 70% of the mean annual water flux and 65% of the nitrogen flux to lower reaches and coastal oceans (Alexander et al., 2007). Hence, alteration of headwater regions can induce downstream ecological and biogeochemical

changes such as eutrophication and hypoxia, and impairment of drinking water quality (Freeman et al., 2007; Mitsch et al., 2001). The presence of urban and agricultural land uses can alter the hydrologic pathways that deliver nitrogen compounds to streams and watershed stores of nitrogen (Basu et al., 2010; Jordan et al., 1997), introducing additional solute sources that can change hydrologic and biogeochemical watershed functioning. It is therefore important to understand the factors that control the degree of hydrological linkage of the headwater regions to their lower receiving water bodies, and the biogeochemical and land use processes that influence solutes that these headwater regions deliver, in order to understand potential ecological alterations and water quality impairments to downstream ecosystems.

Our goal is to identify variation in nitrate-runoff relationships in coastal California watersheds with varying amounts of agricultural, urban/suburban, and undeveloped area (Figure 1, Table 1). Nitrate is the focus of our investigation because it comprises the largest fraction of total dissolved nitrogen. We generate hyperbolic equation parameters for nitrate-runoff relationships for each watershed to derive their C-Q type (i.e., dilution, invariance, and enrichment) and baseflow and stormflow nitrate modes. To assess source water mixing dynamics, we also use the hyperbolic equation to generate C-Q types and baseflow and stormflow electrical conductance (EC) modes for EC-runoff relationships. In light of the high inter- and intra-annual variability in precipitation characteristic of the Mediterranean climate in coastal California, we assess the suitability of using only one stormflow nitrate mode to characterize stream nitrate concentrations during high runoff using nitrate-EC plots. We determine if a comparison of inter-watershed variation in nitrate-runoff and EC-runoff

relationships, and nitrate-EC plots, allows us to identify the most probable sources of water and nitrate to streams given our knowledge of the spatial variation of land uses.

Methods

Physical setting and climate characteristics

The watersheds we sampled are located on the south-facing slopes of the coastal Santa Ynez Mountains (California) and are characterized by mountainous headwaters that drain across mildly sloping, narrow coastal plains and outlet into the Santa Barbara Channel (Pacific Ocean) (Figure 1). Over 80% of annual precipitation typically falls between December and March (Figure 2). The relief (Table 1), southern orientation of the watersheds, and the predominant south-southwest winds with the passage of storm systems during the rainy season cause substantial orographic enhancement of rainfall (Beighley et al., 2003). Mean annual precipitation at a ridgeline gauge (1000 m asl) during our period of study from 2002 to 2008 was 210% greater than that of a low elevation (30 m asl) gauge (Figure 2). Inter-annual rainfall variability was high; from 2002 to 2008 mean annual rainfall ranged from a low of 2.2% in 2007 to a high of 96.4% in 2005 of the long-term (1868 – 2008) annual rainfall maximum, respectively (Table 2).

Field measurements

Stream water level was measured at a five-minute frequency near the watershed outlet of each stream using a pressure transducer (Solinst Canada Ltd., Georgetown, Ontario) corrected for atmospheric pressure. These water level records were converted to stream discharge using geomorphic profiles surveyed for each stream and a hydraulic computation

program, Hydrologic Engineering Center-River Analysis Program (HEC-RAS) (USACE, 2005). Runoff was calculated as discharge divided by watershed area. Baseflow and stormflow measurements were averaged over 12-hour and 1-hour periods, respectively. Rain was collected during storm events in a sampler composed of a polyethylene funnel and 2-L bottle mounted 2 m above the ground. A 10 cm diameter manually-read rain gauge was used to measure rainfall in association with sampling for rain chemistry.

Baseflow samples were collected weekly from November through May and biweekly from June through October. These samples were filtered in the field through Gelman A/E glass fiber filters (1 µm nominal pore size) into 60 mL high density polyethylene (HDPE) bottles triple-rinsed with filtered stream water before sample collection. Samples were stored at 4^{o}C upon return to the laboratory.

Stormflow samples were collected hourly on the rising limb of the hydrograph, and every two to four hours on the falling limb. Stormflow samples were collected either manually in triple-rinsed 500 mL HDPE bottles or automatically using ISCO 6712C portable water samplers (Teledyne Isco, Inc., Lincoln, Nebraska). The 500 mL ISCO sample collection bottles were triple rinsed with deionized water prior to deployment. Autosampler deployments typically lasted 20-24 hours, and samples were iced during this period and stored at 4^{o}C after retrieval.

Analytical measurements

Dissolved ammonium and nitrate concentrations were determined on a Lachat flow injection autoanalyzer (Hach Company, Loveland, Colorado). Ammonium was measured by adding base to the sample stream, which converted NH_4^+ to NH_3. Nitrate was measured using the Griess-Ilosvay reaction after cadmium reduction. The detection limit for

ammonium and nitrate was 0.5 µM, sensitivity was ± 0.2 µM and accuracy was ± 5%. Filtered samples were assayed for total dissolved nitrogen (TDN) by alkaline persulfate digestion in an autoclave for 25 minutes followed by determination of nitrate as above. The detection limit for TDN was 1 µM, sensitivity was ± 0.5 µM and accuracy was ± 10%. Dissolved organic nitrogen (DON) was calculated as the difference between TDN and the sum of nitrate and ammonium. Specific conductance of unfiltered water was measured with a conductivity bridge (cell constant = 1.0) and readings were corrected to 25° C. A 1,400 µS cm^{-1} standard was used for calibration.

Land use analysis

Land use classification was performed using data obtained by the Airborne Visible/Infrared Imaging Spectrometer (AVIRIS), which is an optical sensor that captures reflected spectral radiances from the Earth's surface in 224 contiguous spectral channels with wavelengths from 400 to 2,500 nm. Two AVIRIS flightlines were flown on August 6, 2004 for the Santa Barbara region. Imagery from these two flights was processed and merged to form one scene. Spectral libraries were generated, and an iterative selection of the spectra was performed to identify spectral signatures for individual land use classes of interest. Multiple end-member spectral analysis was then used to produce a land use and land cover map (Roberts et al., 1998).

Data analysis

Volume-weighted mean (VWM) concentrations were calculated for each watershed for their respective period of sampling (Table 3) using the following equation:

$$\mathrm{VWM} = \frac{\sum_{i=1}^{N}(C_i \times Q_i)}{\sum_{i=1}^{N} Q_i} \qquad (1)$$

Where C_i = stream water concentration (µM), Q_i = watershed discharge (L hr^{-1}), and N = total number of data points. Median absolute deviations (MAD) were calculated since frequency distributions of stream water solute concentrations often exhibited skewness and had outlier values that biased a measure such as the standard deviation (Dennis and Hirsch, 1993). MAD is a robust measure of the variability of a uni-variate dataset, and is defined as the median of the absolute deviations from the dataset's median.

Electrical conductance has been used by researchers as a conservative tracer to identify the contribution of pre-event water (also referred to as baseflow or groundwater) and event water (also referred to as precipitation) to stream water during storms in both undeveloped (Laudon and Slaymaker, 1997; Pilgrim et al., 1979) and urban watersheds (Pellerin et al., 2008). Studies using EC to distinguish these two water sources have reported relatively small differences (<50 µS cm^{-1}) between groundwater and precipitation values in temperate, forested watersheds, creating uncertainty and ambiguity in assigning relative contributions of the two sources (Laudon and Slaymaker, 1997; Matsubayashi et al., 1993; McDonnell et al., 1991). In watersheds impacted by urban and agricultural land uses, baseflow EC values are often elevated by 1-2 orders of magnitude relative to precipitation EC values, reducing the uncertainty in two-source separations, but complicating identification of potential water and solute sources, as there are often a greater number of these sources and delivery pathways in urban and agricultural than in undeveloped watersheds. However, the mathematical form of EC-runoff relationships within individual watersheds and the identification of potential baseflow and stormflow EC modes, together

with additional hydrochemical information, can help determine potential solute sources during periods of low and high runoff.

Nitrate-runoff and EC-runoff relationships were investigated using locally-weighted scatter plot smoothing (LOWESS). LOWESS is an exploratory data analysis technique that assumes no pre-determined functional form of these relationships (Cleveland, 1979; Cleveland and Devlin, 1988). The main difference between the LOWESS technique and other polynomial regression techniques is that local, rather than global, first degree polynomial fits are computed, allowing potential non-linearity of relationships to emerge. A bandwidth parameter (f) is set by the data analyst, from 0 to 1, which controls the "smoothness" of the LOWESS fit. For each runoff value in the dataset, x_i, a local first order polynomial is fit to $[f \cdot n]$ of the data points whose abscissas are closest to x_i, where n is the total number of x-y pairs. Each of these local fittings is performed by weighted least squares in which data points close to x_i receive large weight and those farther away receive lower weight. LOWESS fits allow for the selection of appropriate parametric models that can reproduce the form of the fits, aiding mechanistic interpretation of bi-variate patterns. Bandwidths of 0.5 were used to generate LOWESS fits for nitrate-runoff and EC-runoff scatterplots (Figure 3a and 4a). This bandwidth was chosen based on plotting three bandwidths (0.25, 0.50, and 0.75) followed by visual inspection of the LOWESS fit for each bandwidth. A bandwidth of 0.5 adequately represented the non-linearity of the solute-runoff patterns without over-smoothing of the data or distortion of the trend (Cleveland, 1979). LOWESS procedures were implemented in MATLAB (The MathWorks, Inc., Natick, MA).

A hyperbolic equation was used to fit nitrate-runoff and EC-runoff relationships (Equation 2). This equation was selected based on examination of the shape of the LOWESS

fits (Figure 3a and 4a), which were log-sigmoidal as opposed to log-linear, indicating the appropriateness of a hyperbolic function rather than a power function in fitting both nitrate-runoff and EC-runoff relationships (Godsey et al., 2009). In addition, the flexibility of a hyperbolic equation in fitting bi-variate relationships affords the ability to examine intra- and inter-watershed variation in generated parameters such as slope, baseflow mode (i.e., low runoff), and stormflow mode (i.e., high runoff).

$$C_{Stream\ water} = \frac{\delta}{1+\beta Q} + C_S \qquad (2)$$

In equation 2, C_S ($C_{S\text{-}EC}$) = stormflow nitrate or EC mode (µM or µS cm^{-1}), δ (δ_{EC}) = baseflow nitrate or EC mode (C_B or $C_{B\text{-}EC}$; µM or µS cm^{-1}) minus C_S ($C_{S\text{-}EC}$), β (β_{EC}) = hyperbolic fitting parameter, and Q is watershed runoff (mm hr^{-1}). Equation parameters were derived using non-linear least squares fitting procedures implemented in MATLAB's Curve Fitting Toolbox.

Non-linear least squares fits and 95% confidence intervals (CI) were computed for the three hyperbolic parameters, δ (δ_{EC}), C_S ($C_{S\text{-}EC}$), and β (β_{EC}) (Tables 4 and 5). The F-statistic was used to test the validity of using the hyperbolic equation (Johnson et al., 1969). To accomplish this, the equation was made linear by taking $1/1 + \beta Q$ as the independent variable, and nitrate concentration or EC value as the dependent variable. The slopes of the relationships are equal to δ (δ_{EC}), and significant slope effects were defined as δ (δ_{EC}) > or < 0 at the $p < 0.05$ level of significance (Tables 4 and 5).

Nitrate-EC plots were examined to identify potential seasonal shifts in baseflow and stormflow nitrate modes, which if present could invalidate using fixed C_B and C_S values derived using hyperbolic nitrate-runoff relationships alone (Figures 3b – 3d and 4b – 4d). For each watershed, hyperbolic equation-derived baseflow and stormflow EC modes (i.e.,

$C_{B\text{-}EC}$ and $C_{S\text{-}EC}$) and their lower and upper 95% CI values were used to calculate nitrate VWM concentrations and MADs for nitrate samples that had EC values contained within the respective bounds (i.e., lower and upper 95% CI values) (Table 6). These nitrate VWMs were used to validate the hyperbolic baseflow and stormflow nitrate values (i.e., C_B and C_S), and the MADs, in combination with qualitative assessment of nitrate-EC mixing behavior, were used to evaluate potential seasonal variability in baseflow and stormflow nitrate modes. The use of MADs instead of standard deviations of nitrate concentrations contained within the upper and lower 95% CI bounds reduces the potential bias of assuming normality of the baseflow (i.e., samples contained within the lower and upper $C_{B\text{-}EC}$ 95% CI) and stormflow (i.e., samples contained within the $C_{S\text{-}EC}$ lower and upper 95% CI) nitrate concentration distribution (Dennis and Hirsch, 1993).

A two end-member mixing model was used to estimate lowland stream nitrate concentrations.

$$C_S = C_U P_U + C_L P_L \qquad (3)$$

$$C_L = \frac{C_S - C_U P_U}{P_L} \qquad (4)$$

In equations 3 and 4, C_S = stormflow nitrate mode (µM), C_U = upland stormflow nitrate mode (µM), C_L = lowland stormflow nitrate mode (µM), P_U = proportion of water export from the upland (from 0 - 1), and P_L = proportion of water export from the lowland (from 0 - 1).

Results

Ammonium, nitrate, and DON VWM concentrations (µM) ranged from 0.6 to 4.1, 67.9 to 407.0, and 19.2 to 127.5, respectively (Table 3). Rattlesnake Creek had the lowest

VWM concentrations for all dissolved species except nitrate, which was only slightly lower in Mission Creek. Franklin Creek had the highest VWM concentrations. Nitrate was the predominant form of dissolved nitrogen in the streams, comprising 73.8 ± 7.3% (± 1 SD) of total dissolved nitrogen (TDN) concentrations. DON was second highest, comprising 24.9 ± 6.5%. Ammonium was a minor fraction, comprising 1.3 ± 0.9%. Rain VWM concentrations of ammonium, nitrate, and DON were 4.1 µM, 6.4 µM, and 8.1 µM, respectively (Table 3).

Based on MADs, nitrate was the most temporally variable dissolved nitrogen species, DON was the second most variable, and ammonium was the least variable (Table 3). Ratios of nitrate MAD to DON MAD ranged from about 1.2 to about 3.5. The two urban watersheds, Mission and Arroyo Burro, had the lowest nitrate MAD:DON MAD ratios of 1.2 and 1.8, respectively, while the agricultural and undeveloped watersheds had the highest nitrate MAD:DON MAD ratios (mean of 3.3 ± 0.2). This pattern can be seen in the LOWESS plot (Figure 3a), with nitrate concentrations for the two urban watersheds having lower variance over the runoff range than the agricultural and undeveloped watersheds.

LOWESS fits and hyperbolic equation slopes (δ) indicated that nitrate- runoff relationships for five of the six watersheds were hyperbolic (Figure 3a; Table 4). The three agricultural watersheds—Franklin, Bell Canyon, and Carpinteria—had significant dilution ($\delta > 0$). The undeveloped watershed, Rattlesnake, and one of the two urban watersheds, Arroyo Burro, had significant enrichment ($\delta < 0$). The other urban watershed, Mission, was invariant ($\delta = 0$). Arroyo Burro watershed had a lower p-value than four of the watersheds (Table 4), with a nitrate-runoff pattern more similar to Mission watershed's invariance rather than enrichment. In contrast to nitrate-runoff relationships, which had all three C-Q types (dilution, enrichment, and invariance), EC-runoff relationships for all six watersheds had

only dilution ($\delta_{EC} > 0$) and were highly significant (Table 5). The $C_{S\text{-}EC}$ values are a minimum of 16.8 to a maximum of 38.7 times higher than the precipitation EC VWM value of 15.7 µS cm^{-1} (MAD of 13.6 µS cm^{-1}), as the $C_{S\text{-}EC}$ values represent a mixture of water sources during rainstorms.

Nitrate VWMs calculated using $C_{B\text{-}EC}$ 95% CI bounds (i.e., baseflow) and $C_{S\text{-}EC}$ 95% CI bounds (i.e., stormflow) showed close agreement with the hyperbolic nitrate-runoff C_B and C_S parameters (Table 6). The baseflow nitrate VWMs had a higher mean % difference relative to C_B values (13.5%) than the stormflow nitrate VWMs relative to C_S values (35.2%), reflecting mainly the large % differences for Rattlesnake Creek. Most of the baseflow nitrate VWMs are lower than the C_B values, which is a function of the hyperbolic equation identifying C_B values at runoff = 0, whereas the nitrate VWMs are calculated for a range of EC values that occur at lowest runoff.

Nitrate-EC plots had strong linear relationships for Franklin and Bell Canyon creeks (Figure 5a and 5b), and strong seasonal linear relationships for Rattlesnake Creek (Figure 6a). Therefore, in addition to stormflow C_S (Table 4) and stormflow nitrate VWMs (Table 6), an additional estimate of the stormflow nitrate mode can be calculated using the linear relationships (Figures 5a, 5b, and 6a). Nitrate-EC plots for Mission, Arroyo Burro, and Carpinteria creeks did not have clear linear relationships, but did have seasonal effects evident in the triangular shape of the data points, indicating a third nitrate mode in the beginning storms of the season, shown as the dark blue (i.e., "Fall") points on the nitrate-EC plots (Figures 6b, 7a, and 7b). Overall, nitrate-EC plots for all watersheds had patterns consistent with their nitrate-runoff relationships; dilution in agricultural watersheds (although

a relatively less clear pattern for Carpinteria, discussed further below), invariance in urban watersheds, and enrichment in an undeveloped watershed (Figure 8).

Discussion

Nitrate-runoff relationships were consistent within land use types; dilution in agricultural watersheds, enrichment in an undeveloped watershed, and invariance in urban watersheds. The consistency of these nitrate-runoff relationships within land use types implicates nitrogen inputs related to land use as a primary driver of these patterns. The percentage ratios of the standard deviation of C_S to C_B parameters and stormflow nitrate VWMs to baseflow nitrate VWMs are ~12%. The percentage ratio of the standard deviations of $C_{S\text{-}EC}$ to $C_{B\text{-}EC}$ values are ~21%. These observed 4.8 to 8.8 fold reductions in variability, which are similar for both nitrate and EC, in spite of different land uses, implies different nitrate sources to streams during baseflow (i.e., low runoff), but similar nitrate sources during stormflow (i.e., high runoff). Further, unlike humid temperate regions with small differences between baseflow and stormflow EC values (Laudon and Slaymaker, 1997; Matsubayashi et al., 1993; McDonnell et al., 1991), these coastal California watersheds have baseflow/stormflow EC differences of a minimum of 599 µS cm^{-1} to a maximum of 2005 µS cm^{-1}, and all EC-runoff relationships demonstrate significant dilution during stormflow (Table 5). The strength of these hyperbolic EC-runoff relationships implies bimodal EC behavior, allowing us to examine nitrate-EC plots to identify probable land use and biogeochemical mechanisms underlying seasonal shifts in nitrate modes during periods of high runoff (i.e., stormflow). The following discussion addresses two fundamental questions that arise from the observed nitrate-runoff patterns with land use: how is the variability of

stormflow nitrate modes reduced during high runoff despite divergent land uses, and how does seasonality (i.e., pronounced dry/wet dynamics characteristic of a Mediterranean climate) potentially alter nitrate-runoff patterns and stormflow nitrate modes?

Baseflow nitrate variability

Baseflow nitrate concentrations (i.e., C_B) in the three agricultural watersheds were roughly 5 to 20 times greater than the two urban watersheds, and 67 to 241 times greater than the undeveloped watershed (conservative estimate using C_B lower 95% CI values for agricultural watersheds and C_B upper 95% CI values for urban and undeveloped watersheds). The elevation of agricultural C_B values relative to urban and undeveloped watersheds indicates nitrogen fertilizers as the likely source of elevated baseflow nitrate concentrations in agricultural streams. Nitrate is a common groundwater pollutant in agricultural regions, largely resulting from application of nitrogen fertilizer (Almasri and Kaluarachchi, 2004; Nolan et al., 1997; Spalding and Exner, 1993). A proportion of these fertilizers either leaches through soils into groundwater (Di and Cameron, 2002), the primary source of stream water during baseflow periods, or is directly discharged to streams through storm and/or tile drains. Estimates of mean nitrogen fertilizer application rates for agricultural land use in the eastern portion of our study region, which encompasses Franklin and Carpinteria watersheds, are 2,200 kg N km^{-2} $year^{-1}$ for young (<4 years old) avocado orchards, 5,100 kg N km^{-2} $year^{-1}$ for mature (>8 years old) avocado orchards, 36,400 kg N km^{-2} $year^{-1}$ for greenhouses, and 39,000 kg N km^{-2} $year^{-1}$ for nurseries (Robinson et al., 2005). These fertilizer application rates are a minimum of 5 to a maximum of 574 times higher than estimates of other nitrogen inputs to watersheds, such as wet deposition (68 kg N km^{-2} $year^{-}$

^{1}), dry deposition and plant foliar leaching (430 kg N km^{-2} year^{-1}) (Schlesinger et al., 1982), and nitrogen fixation by *Ceanothus* communities (110 kg N km^{-2} year^{-1}) (Kummerow et al., 1978), which are abundant members of plant communities in the upper watersheds.

In the undeveloped watershed, Rattlesnake, baseflow nitrate concentrations are the lowest of all watersheds (Table 4). There are two non-mutually exclusive explanations for these low nitrate values, the importance of each depending on the hydrologic pathways that feed streams during baseflow periods. The first explanation is that nitrogen removal mechanisms (e.g., denitrification, plant and microbial uptake) reduce soil water and groundwater nitrate concentrations before percolation into the stream. The stormflow nitrate modes for Rattlesnake Creek (112.5 and 49.6 µM) are a significant enrichment relative to the precipitation nitrate VWM of 6.4 µM and the baseflow nitrate mode of 0.2 µM, indicating nitrate removal along the soil/groundwater flowpaths to the stream. The second potential explanation for the low baseflow nitrate concentration in Rattlesnake watershed is that there are hydrologic pathways that bypass nitrate-enrichment in the soil. The Santa Ynez Mountains are composed of highly fractured arkosic sandstones and shales, with bedding planes that are nearly vertical due to intense faulting and folding (Rademacher et al., 2003). These bedding planes act as groundwater conduits within the mountains, directing groundwater flow vertically and laterally. If recharge to these bedrock aquifers mainly bypasses upper organic soil layers, then we might expect nitrate concentrations of bedrock groundwater to be similar to precipitation nitrate values in the absence of appreciable microbial transformation, uptake, and/or organic matter mineralization within the aquifer. For our 2002-2008 study period, the nitrate VWM concentration of precipitation for 75 recorded storms was 6.4 µM, with a MAD of 8.7 µM. This value lies within Rattlesnake

watershed's C_B upper 95% CI value of 6.7 µM, suggesting that if a hydrologic connection exists between bedrock groundwater and the stream, then stream water nitrate during baseflow periods may be sourced from bedrock groundwater inputs that have bypassed nitrate-enrichment in organic soil layers.

The C_B values for the two urban watersheds are intermediate between the agricultural and undeveloped values. It is difficult to estimate nitrate sources in these watersheds because urban land use is characterized by a diversity of activities and landscape properties that mobilize multiple nitrate sources (Spalding and Exner, 1993; Wakida and Lerner, 2005). Dry weather flows that entrain atmospherically-deposited nitrogen compounds from impervious surfaces (Driscoll et al., 2003; Jaworski et al., 1997), leaking sewage infrastructure (Caraco and Cole, 1999; Silva et al., 2002) , and lawn and golf course fertilizers (Shuman, 2001; Wong et al., 1998) likely all contribute to elevated nitrate concentrations in streams during baseflow periods. Storm drains are thought to discharge human waste to our urban watershed streams based on elevated fecal indicator bacteria and human-specific *Bacteroides* marker counts, implicating leaky sanitary sewer lines (Sercu et al., 2008).

Reduction in inter-watershed stormflow nitrate variability

The reduced variability of stormflow nitrate and EC modes relative to baseflow nitrate and EC modes implies a common nitrate and water delivery mechanism for all watersheds despite their differing land uses, muting the high inter-watershed nitrate variability evident during baseflow (Tables 4 and 5). Hydrological studies have identified the spatial variation in runoff-generating regions of our watersheds under varying land use scenarios. Beighley et al. (2008) examined storm runoff responses of a Santa Barbara

watershed (Atascadero, urban classification under our scheme) over historical and projected ranges of land use conditions (1929, 1998, 2050) for a 14-year precipitation record (October 1, 1988 through September 30, 2002). They examined these storm runoff responses at three different scales: whole watershed, lowland regions (low elevation coastal plain), and upland regions (steep, mountainous headwaters). For the 1929 conditions, with relatively low urban land use (5% versus 39% and 50% for 1998 and 2050 conditions, respectively), 78% of mean annual watershed storm runoff originated from the uplands region, dropping to 51% under 2050 conditions. They concluded that the majority of runoff originating from the uplands is a product of 1) the orographic enhancement of precipitation along the Santa Ynez Mountains and 2) the geomorphology of the uplands region of Santa Barbara watersheds, characterized by steep slopes, thin soils, and rock outcroppings, which promotes saturated overland excess flow and shallow soil interflow that rapidly delivers water from hillslopes to upland streams (Latron et al., 2009).

Upland, undeveloped watershed nitrate-runoff dynamics

Rattlesnake Creek is an upland watershed (Figure 1). Unlike the other watersheds, Rattlesnake's nitrate-runoff behavior shows an enrichment (Table 4). Examination of the nitrate-EC plot for Rattlesnake Creek reveals two linear relationships, with nitrate-EC pairs along the upper regression line occurring earlier in the wet season than the pairs along the lower regression line, which occur later (Figure 6a). The slopes of the two regression lines are not significantly different from one another, but their intercepts are significantly different with the difference equal to 62.8 µM. This difference is likely the result of nitrate flushing, whereby soil nitrate that has accumulated in upper soil layers during the dry season is flushed

during the first storms as water enters the previously dry, organic-rich soil horizons (Meixner and Fenn, 2004; Sobota et al., 2009). A possible source of this nitrate is nitrogen-containing osmolyte compounds that soil microbial communities synthesize during the dry season to prevent desiccation (Fierer and Schimel, 2002; Miller et al., 2005). Upon rewetting, the microbial cells release the compounds to the infiltrating soil water to maintain osmotic potential, as the hypertonicity of their cellular fluids would otherwise cause rapid water influx and cell bursting. Once released to the soil water, these substrates are available for mineralization and nitrification, increasing the nitrate concentration of soil water which is transported to the stream. Additionally, the wetting of the upper soil layers could mobilize non-microbial nitrogenous soil organic matter, making it increasingly accessible to microbial mineralization and nitrification and transport to the stream (Bernal et al., 2005; Butturini and Sabater, 2002).

The distinct linear nitrate-EC relationships observed for Rattlesnake Creek suggests that the timing and magnitude of precipitation events interacts with the mountainous geomorphology of the upland watersheds to control the hydrologic connectivity and soil microbial activity, which in turn regulates earlier versus later wet season nitrate flushing. Therefore, defining only one stormflow nitrate mode (85.2 µM using hyperbolic nitrate-runoff equation and 92.5 µM using the lower and upper $C_{S\text{-}EC}$ 95% CI bounds) appears to be a simplification of upland watershed nitrate-runoff behavior. Instead, two nitrate modes can be estimated using the two linear equations derived for the Rattlesnake nitrate-EC relationship and the stormflow $C_{S\text{-}EC}$ value (264.5 µS cm^{-1}) (Table 6), yielding 112.5 µM for the non-supply limited (i.e., higher intercept) regression line and 49.6 µM for the supply-limited (i.e., lower intercept) regression line (Figure 6a). The supply-limited regression line

occurs later in the wet season, when the more labile and/or abundant soil nitrogen pool that supported enhanced nitrate delivery to the stream is likely exhausted.

Lowland, urban watershed nitrate-runoff dynamics

For the urban watersheds, Mission and Arroyo Burro, it appears that the nitrate-EC plots show early wet season nitrate flushing, with progressive decreases (for a given EC value) of nitrate concentrations with later season storms. Urban watersheds are characterized by a diversity of activities and landscape properties that mobilize multiple temporally-variable nitrate sources over the course of storm events. The source of the early season nitrate flushing could be atmospherically-deposited nitrogen compounds from impervious surfaces that accumulated during the dry season (Driscoll et al., 2003; Jaworski et al., 1997), nitrate from leaking sewage pipes and septic tanks (Caraco and Cole, 1999; Silva et al., 2002), or upland nitrate. The seasonal flushing evident in the urban watersheds appears to be well approximated by using the nitrate VWM ± MAD limits as stormflow nitrate modes, which correspond to 107.8 and 154.1 µM in Mission and Arroyo Burro watersheds, respectively, for earlier wet season storms, and 29.6 and 70.7 µM for later wet season storms. Mission watershed has higher impervious surface coverage than Arroyo Burro watershed, 12.7% versus 8.6% (Peters et al., 2005), which increases the contribution of surface runoff from the urban lowland region to the stream (Beighley et al., 2008; Beighley et al., 2003). Arroyo Burro watershed has a higher percentage of agricultural land use than Mission watershed, introducing a potential nitrogen fertilizer source (Table 6), although this agricultural area is located to the north (upstream) of urban land use (Figure 1), and is likely diluted by impervious surface runoff before discharge to the ocean. Roughly 7 and 2 percent

of Mission and Arroyo Burro watersheds, respectively, have septic systems instead of sewage connections (Hantszche et al., 2003). While roughly a third the size in area, the density of septic systems in Arroyo Burro are twice that of Mission, and are situated closer to the watershed outlet to the ocean (i.e., on the coastal plain versus the foothills lowland-upland transition). The lower impervious surface area, higher percentage of agricultural land use, higher density of septic systems, and closer proximity of the septic region to the watershed outlet is the likely cause of a stormflow nitrate mode that is higher by 46.3 µM (154.1 – 107.8 µM) for earlier wet season storms, and 41.1 µM (70.7 – 29.6 µM) for later wet season storms for Arroyo Burro watershed relative to Mission watershed. For both watersheds, the lowest EC values converge toward a nitrate mode of ~25 µM, likely indicating an impervious surface contribution after the initial nitrate flushing, where nitrate and other solute sources are exhausted and stream nitrate and EC are influenced by mixing with a dilute water source (e.g., precipitation from impervious surfaces).

Lowland, agricultural watershed nitrate-runoff dynamics

In the agricultural watersheds, Franklin, Bell Canyon, and Carpinteria, linear nitrate-EC relationships are evident for Franklin and Bell Canyon watersheds (Figures 5a and 5b), but not for Carpinteria watershed (Figure 6b). This difference is likely a result of lower agricultural land use in Carpinteria (9%) versus Franklin (21%) and Bell Canyon (19%) watersheds. In the nitrate-EC plot for Carpinteria watershed, early season flushing is apparent with nitrate concentrations in the 750 - 1,500 µM range, which is approximately 1.5- to 3.5-times above the C_B value (489.2 µM) and baseflow nitrate VWM (410.5 µM). This early season flushing is similar to that in urban watersheds, although the nitrate

concentrations are higher. The seasonal difference may be the result of riparian and/or hyporheic denitrification removing groundwater nitrate before it enters the stream during low runoff (Ostrom et al., 2002; Seitzinger et al., 2006). During the initial storms of the wet season, hydraulic gradients between the lowland groundwater and stream steepen, as groundwater mixes with oxygenated infiltrating soil water and residence times in the riparian and hyporheic zones decrease, causing reduced denitrification capacity and thus high nitrate concentrations in the streams. The flushing of high nitrate groundwater represents a shift from a high EC-high nitrate mode (~1,500 µS cm^{-1}, 400 µM) in the beginning of the wet season to a low EC-low nitrate mode (~700 µS cm^{-1}, 40 µM) as the wet season progresses. The seasonal behavior of the stormflow nitrate mode appears to be well approximated by using the nitrate VWM ± MAD limits, which correspond to 236.1 µM for earlier wet season storms, and 34.4 µM for later wet season storms. The later wet season nitrate mode is the minimum of nitrate concentrations within the $C_{S\text{-}EC}$ 95% CI bounds, as the nitrate VWM minus the MAD would equal a negative value.

The linear nitrate-EC relationships for Franklin and Bell Canyon watersheds indicate little influence of seasonal drying/wetting dynamics on stream nitrate concentrations (Figures 5a and 5b). This is characteristic of intensively managed agricultural watersheds, whereby accumulated stores of nitrogen due to fertilizer use creates 1) transport- versus supply-limitation of nitrate delivery to streams and 2) delivery of water with relatively high and temporally similar nitrate concentrations that damps smaller magnitude nitrate variations due to other processes (Basu et al., 2010; Kemp and Dodds, 2002). In contrast to the early wet season flushing observed in Carpinteria watershed, which elevates nitrate concentrations well above the baseflow nitrate mode, Franklin and Bell Canyon watersheds do not show this

behavior, indicating the limited extent of nitrate removal pathways (e.g., denitrification) due to nitrate saturation in the lowland riparian and hyporheic zones during low runoff periods (Bernot and Dodds, 2005; Mulholland et al., 2008). Franklin watershed, which has 20% urban land use, has earlier wet season flushing of impervious surfaces, which is the reason that the EC-runoff relationship is not as strong as in Bell Canyon (Table 5). Using the nitrate-EC linear equations and $C_{S\text{-}EC}$ values for each watershed to determine their stormflow nitrate modes produces values of 265.7 and 240.9 µM for Franklin and Bell Canyon watersheds, respectively. These values agree well with C_S values of 289.8 and 245.8 µM (Table 6).

Overall, our examination of nitrate-EC plots for all watersheds indicates caution in using a single nitrate concentration (i.e., C_S) to characterize stormflow nitrate modes, as high intra-annual variation in precipitation can seasonally alter these nitrate modes for undeveloped (Rattlesnake Creek), urban (Mission Creek and Arroyo Burro Creek), and lower intensity agricultural (Carpinteria Creek) watersheds. The hyperbolic nitrate (i.e., C_S) and nitrate VWMs (Table 6) can be considered mean wet season nitrate modes, which in the case of Franklin and Bell Canyon, appear to sufficiently capture the dominant stormflow nitrate concentrations. For the other watersheds, accounting for seasonal nitrate flushing provides a more accurate depiction of dominant nitrate concentrations. Electrical conductance, despite potentially reflecting a variety of differing solute sources under varying land use, demonstrates significant dilution behavior in all watersheds (Figure 4; Table 5) and a pattern of reduced variability in stormflow values versus baseflow values similar to nitrate-runoff relationships (Tables 4 and 5). The 22% to 28% reduction in stormflow relative to baseflow EC modes for the five lowland watersheds indicates that during storms, the predominant

water and nitrate source to lowland streams is not lowland baseflow. If baseflow water sources were dominant, then dilution in all watersheds under variable land uses would not be evident (Figure 4; Table 5), consistent with studies conducted in many humid temperate watersheds that show little variation between stormflow and baseflow EC values (Laudon and Slaymaker, 1997; Matsubayashi et al., 1993; McDonnell et al., 1991). Further, we would expect comparable variability in both stormflow and baseflow EC modes between watersheds characterized by different land use mixtures, as baseflow water sources often comprise a large proportion of storm runoff volume (Buttle, 1994; Kirchner, 2003). In these coastal California watersheds, the magnitude of reduction in inter-watershed variability during storms is similar for both EC ($SD\text{-}C_{S\text{-}EC}$: $SD\text{-}C_{B\text{-}EC}$, 20.6%), a relatively conservative water source tracer, and nitrate ($SD_{Stormflow\ nitrate\ VWM}$: $SD_{Baseflow\ nitrate\ VWM}$, 11.3% and $SD\text{-}C_S$: $SD\text{-}C_B$, 12.0%), a biologically-reactive ion.

Upland-lowland watershed connectivity

In light of the above considerations, and hydrological modeling results of Beighley et al. (2008), we hypothesize that the upland, undeveloped watershed is important in regulating whole watershed (i.e., combined upland and lowland) stream nitrate dynamics (Figure 1). Using seasonally-refined stormflow modes, in concert with the hydrological modeling of Beighley et al. (2008), the potential role of the upland, undeveloped watershed regions in modifying stream nitrate concentrations during high runoff periods can be examined. We assume that the two stormflow nitrate modes for Rattlesnake Creek are representative of the undeveloped, upland watershed regions in the other five study watersheds during the earlier and later wet season (i.e., 112.5 and 49.6 μM). The stormflow nitrate modes for these five

watersheds represent a mixture of both upland and lowland watershed nitrate sources, allowing identification of the lowland nitrate modes. We can examine the seasonal variability in these estimates for Mission, Arroyo Burro, and Carpinteria watersheds using the identified range in nitrate VWMs for the urban watersheds and the lower intensity agricultural watershed, where the high concentration (nitrate VWM + nitrate MAD) equals the earlier wet season nitrate mode and the low concentration (nitrate VWM – nitrate MAD) equals the later wet season nitrate mode.

The results of the hydrologic modeling by Beighley et al. (2008) indicates that a minimum of 51% to a maximum of 78% of mean annual watershed runoff (i.e., over a 14-year period) is derived from the upland watershed regions for a range of historic, contemporary, and projected land use conditions in this coastal mountainous California region. The variance in mean annual upland water estimates is a function of urban land use, as increases in impervious surface cover in the lowland watershed regions progressively decreases the mean annual percentage contribution of the upland regions to whole watershed runoff. Using Beighley et al.'s 1929 and 2050 estimates of land use and mean annual upland runoff contributions, and assuming a linear relationship between urban land use percentage and mean annual upland contribution, we calculate mean annual upland contributions of 67% and 69% for Mission and Arroyo Burro watersheds, respectively, using AVIRIS-derived urban land use values (Table 1). For Mission watershed, the equation-derived value of 67% is similar to an empirical mean value of 62% for water years 2003, 2004, and 2005, during which annual precipitation was 83%, 15%, and 96%, respectively, of the long-term (1868-2008) annual maximum precipitation value in Santa Barbara. For agricultural watersheds, Franklin, Bell Canyon, and Carpinteria, we calculated upland contributions of 69% for

Franklin (20% urban land use, 21% agricultural land use) and 78% for Bell Canyon and Carpinteria (both 1% urban land use, which is below Beighley et al.'s 5% 1929 urban land use, and therefore likely a slightly lower estimate of upland contribution).

On an intra-annual timescale, per-storm upland water contributions are a function of the timing and amounts of antecedent precipitation, which in turn regulates watershed soil saturation and runoff-generation. This is demonstrated by increasing and plateauing upland water contributions for storm sequences in "wet" years 2003 and 2005, when annual precipitation was 83% and 96% of the long-term (1868-2008) annual maximum precipitation value in Santa Barbara (Figure 9a). However, during "dry" years such as 2004, where annual precipitation was 15% of the long-term annual precipitation maximum, upland water contributions remain low (Figure 9a). Using the range in upland water contributions for our three-year storm runoff series in Mission watershed, in concert with our seasonal stormflow nitrate modes (i.e., earlier and later wet season), we can identify the variation in lowland stormflow nitrate modes over the range in upland water contribution for our five developed watersheds. We represent these lowland nitrate modes as percentage changes relative to the whole watershed nitrate mode for each watershed (i.e., whole watershed nitrate modes which include the upland water and nitrate contribution) (Figure 9b). Doing so removes the upland water and nitrate contribution, revealing that lowland stream nitrate modes would be 3% lower to 6% higher for Mission, 2 to 219% higher for Arroyo Burro, 3% lower to 75% higher for Carpinteria, 5 to 582% higher for Bell Canyon, and 5 to 596% higher for Franklin than whole watershed nitrate modes. Using mean annual upland contributions from Beighley et al.'s model, calculated as a function of lowland urban land use, longer-term mean annual nitrate modes would be 3% lower for Mission, 64% higher for Arroyo Burro, 74% higher for

Carpinteria, 270% higher for Bell Canyon, and 278% higher for Franklin. Mean annual lowland stormflow nitrate modes would also be 470% more variable ($SD_{\text{Lowland nitrate modes}}$:$SD_{\text{Whole watershed nitrate modes}}$) with the removal of the upland contribution. The later wet season nitrate mode estimates for Mission and Carpinteria watersheds resulted in negative values for mean annual lowland nitrate mode calculations and much of the range in upland water contribution for intra-annual lowland nitrate mode calculations. Examination of nitrate results for Mission and Carpinteria watersheds revealed that later wet season nitrate VWM concentrations were on average 50 µM and 49.4 µM, respectively, which we chose to use as the later wet season nitrate modes instead of the nitrate VWM – MAD estimates.

As the percentage water contribution from the upland regions increases during the wet season, the lowland nitrate modes for all watersheds except Mission increase, off-setting the progressive decline in nitrate concentration of upland water during stormflow. However, the lowland nitrate mode for Carpinteria plateaus around 75% upland water contribution, sharply declining thereafter, indicating supply-limitation of nitrate to the lowland stream when the watershed is most saturated. Arroyo Burro and Carpinteria have roughly the same percentage of agricultural land use, and Arroyo Burro does not show a supply-limitation of nitrate, but rather an enhancement of lowland nitrate at the highest upland contribution levels. This difference may be due to enhanced nitrate input from leaking septic tanks, which are located near the watershed outlet to the ocean in Arroyo Burro (Hantszche et al., 2003), and thus would be relatively un-diluted by impervious runoff or upland water during storms. Regardless of this difference in lowland nitrate behavior at highest upland water contributions, all watersheds except Mission have appreciable lowland nitrate enhancement as the watersheds become progressively saturated with successive storms through the wet

season. We attribute this effect to enhanced soil saturation and rising shallow water tables in the lowland watersheds, which would enhance mineralization and nitrification of previously dry soil organic matter, and enhance transport of nitrate originating from fertilizers and leaking sanitary infrastructure. The minimal lowland nitrate enhancement in Mission watershed may be a function of high impervious surface cover and stream channelization in the lowland region, which reduces soil and groundwater nitrate inputs by restricting soil infiltration, lowering water tables, physically blocking soil and groundwater stream input, and delivering a higher fraction of dilute water from impervious runoff.

Our examination of nitrate-runoff relationships in six mountainous coastal California watersheds has revealed the following:

1. The stream nitrate-runoff relationships for six mountainous coastal California watersheds of varying land use were consistent within predominant land use class: enrichment in an undeveloped watershed (Rattlesnake), invariance in urban watersheds (Mission and Arroyo Burro), and dilution in agricultural watersheds (Bell Canyon and Franklin).

2. Nitrate-EC plots revealed seasonality in nitrate modes for the undeveloped (Rattlesnake), two urban (Mission and Arroyo Burro), and lower intensity agricultural watershed (Carpinteria), showing decreases in nitrate modes with the progression from the earlier to later wet season.

3. The variability of stormflow nitrate and electrical conductance (EC) modal concentrations and values, identified using a hyperbolic model, for these six watersheds were ~12% and ~21%, respectively, of baseflow nitrate and EC modes, implying a common water and nitrate source during storms, which previous hydrological modeling studies and a three-

year empirical runoff series for one of the watersheds (Mission) indicated was the undeveloped, upland watershed regions.

4. Removal of the water and nitrate contribution from the upland watershed regions using a two end-member mixing model revealed the lowlands stream nitrate modes for five developed watersheds on both multi-annual (i.e., 14-year mean annual upland water contribution) and intra-annual (i.e., empirical range in upland water contributions from three-year runoff series) timescales. In the absence of the moderating influence of the upland water and nitrate contribution, lowland mean annual nitrate modes would be 470% more variable than the whole watershed nitrate modes (i.e., combined lowland and upland), and would be 3% lower for Mission, 64% higher for Arroyo Burro, 74% higher for Carpinteria, 270% higher for Bell Canyon, and 278% higher for Franklin for the whole watershed nitrate modes. Lowland intra-annual nitrate modes, relative to the whole watershed nitrate modes, would be 3% lower to 6% higher for Mission, 2 to 219% higher for Arroyo Burro, 3% lower to 75% higher for Carpinteria, 5 to 582% higher for Bell Canyon, and 5 to 596% higher for Franklin. The lowest percentage changes correspond to the earlier wet season when the upland does not contribute much to the whole watershed runoff, and the highest percentage changes correspond to the later wet season, except in dry years, when the upland becomes a dominant contributor to whole watershed runoff and the lowland nitrate sources become increasingly activated and mobilized.

The upland regions of the watersheds thus appear to play an important role in regulating stream nitrate concentrations by reducing inter-watershed variability in nitrate concentrations during storms, thereby making whole watershed nitrate concentration an integrated product of upland watershed hydrology and nitrogen cycling and lowland

watershed nitrogen land use subsidies. This linkage may mitigate ecological and water quality impairments to downstream aquatic and marine ecosystems due to excessive lowland agricultural and urban nitrogen inputs during periods of highest water export (i.e., storms). The strength of this upland-lowland linkage is sensitive to climate in our semi-arid Mediterranean climate, weakening in drier years and strengthening in wetter years, regulating the relative importance of lowland land use versus upland nitrogen cycling on intra-annual timescales. In other mountainous watersheds, the controls on watershed stream nitrate concentrations may similarly shift from downstream human land use during dry periods to the undeveloped, upland headwaters during storms.

Tables and Figures

Table 1. Watershed topography and land use

	Rattlesnake	Mission	Arroyo Burro	Carpinteria	Bell Canyon	Franklin
Land use class	Undeveloped	Urban	Urban	Agricultural	Agricultural	Agricultural
Area (km^2)	8.29	30.04	25.44	39.21	15.82	11.62
Relief (m)	933	1201	1188	1405	928	504
Mean slope (degrees)	21	14	15	21	17	9
% Urban	0	23	20	1	1	20
% Agriculture	0	3	8	9	19	21
% Undeveloped	100	74	72	90	80	58

Table 2. 2002 - 2008 total annual precipitation for the City of Santa Barbara (elevation: 30 m asl)

Water year	Annual total (cm)	Percentile[a]
2002	22.9	8.8
2003	63.4	82.5
2004	27.2	14.6
2005	93.8	96.4
2006	57.0	74.5
2007	16.3	2.2
2008	44.8	59.1

[a] Percentile is calculated for water years 1868 through 2008

Table 3. Watershed and precipitation volume-weighted means (VWM) and median absolute deviations (MAD)

	Rattlesnake (2002-2008)		Mission (2002-2008)		Arroyo Burro (2002-2006; 2008)		Carpinteria (2002-2005)		Bell Canyon (2005-2008)		Franklin (2002-2005)		Precipitation (2002-2008)	
	VWM	n	VWM	n	VWM	n	VWM	n	VWM	n	VWM	n	VWM	n
Ammonium (µM)	0.6	986	2.9	1130	2.6	848	1.9	815	1.0	356	4.1	788	4.1	75
Ammonium MAD	0.5		7.3		4.6		8.8		0.7		5.8		7.1	
Nitrate (µM)	68.2	987	67.9	1131	92.0	852	110.6	815	228.6	356	407.0	788	6.4	75
Nitrate MAD	31.8		32.2		37.5		215.3		507.7		584.8		8.7	
DON (µM)	19.2	978	34.8	1117	40.2	842	40.4	812	38.9	355	127.5	783	8.1	75
DON MAD	10.0		25.9		20.8		61.6		159.9		177.0		24.0	
TDN (µM)	88.1	978	105.6	1117	134.7	842	153.0	812	268.6	355	538.6	783	18.6	75
TDN MAD	35.6		51.7		47.2		255.9		566.2		613.7		33.8	

Table 4. Hyperbolic model fits for nitrate-runoff relationships

	Rattlesnake	Mission	Arroyo Burro	Carpinteria	Bell Canyon	Franklin
C_S	85.2	65.4	90.2	93.1	245.8	289.8
C_S 95% CI lower	78.4	60.3	83.8	59.7	175.7	182.3
C_S 95% CI upper	92.0	70.5	96.7	126.4	316.0	397.2
β	8.4	72.0	100.7	69.8	140.4	36.9
β 95% CI lower	5.9	-961.2	-201.8	36.7	83.0	22.7
β 95% CI upper	10.9	1105.0	403.3	103.0	197.7	51.1
δ	-85.0	2.4	-18.9	396.1	1374.0	1454.0
δ 95% CI lower	-91.4	-5.1	-35.7	352.1	1240.0	1322.0
δ 95% CI upper	-78.5	9.9	-2.1	440.1	1509.0	1586.0
R^2	0.48	3.7E-04	0.01	0.28	0.60	0.39
F-statistic	925.1	0.4	8.9	313.4	520.0	497.7
p-value	<0.0001	0.52	<0.01	<0.0001	<0.0001	<0.0001
n	987	1131	852	815	356	788

Table 5. Hyperbolic model fits for electrical conductance-runoff relationships

	Rattlesnake	Mission	Arroyo Burro	Carpinteria	Bell Canyon	Franklin
$C_{S\text{-}EC}$	264.5	392.0	513.2	443.8	607.6	352.8
$C_{S\text{-}EC}$ 95% CI lower	242.1	361.8	442.2	412.1	497.2	249.4
$C_{S\text{-}EC}$ 95% CI upper	287.0	422.2	584.3	475.6	717.9	456.2
β_{EC}	24.5	254.3	58.9	292.7	82.9	22.3
β_{EC} 95% CI lower	19.8	172.9	38.5	216.4	51.5	14.1
β_{EC} 95% CI upper	29.1	335.7	79.3	369.1	114.2	30.6
δ_{EC}	598.7	1016.0	1496.0	1161.0	2005.0	1269.0
δ_{EC} 95% CI lower	572.9	928.3	1357.0	1081.0	1832.0	1160.0
δ_{EC} 95% CI upper	624.5	1105.0	1635.0	1240.0	2178.0	1377.0
R^2	0.69	0.49	0.44	0.62	0.62	0.43
F-statistic	2074.0	672.2	597.5	1222.6	570.5	468.1
p-value	<0.0001	<0.0001	<0.0001	<0.0001	<0.0001	<0.0001
n	915	1034	806	763	399	742

Table 6. Nitrate VWMs and MADs calculated using lower and upper $C_{S\text{-}CE}$ and $C_{B\text{-}CE}$ 95% confidence intervals

Stormflow	Rattlesnake	Mission	Arroyo Burro	Carpinteria	Bell Canyon	Franklin
Nitrate VWM	92.5	68.7	112.4	95.0	231.0	206.9
Nitrate MAD	32.8	39.1	41.7	141.1	49.8	94.9
Nitrate VWM - MAD	59.7	29.6	70.7	-46.1	181.2	112.0
Nitrate VWM + MAD	125.3	107.8	154.1	236.1	280.8	301.8
C_S (hyperbolic fit)	85.2	65.4	90.2	93.1	245.8	289.8
% difference (absolute)†	7.9	4.8	19.8	2.0	6.4	40.1

Baseflow	Rattlesnake	Mission	Arroyo Burro	Carpinteria	Bell Canyon	Franklin
Nitrate VWM	23.3	59.5	82.0	410.5	1315.8	1220.0
Nitrate MAD	10.0	25.1	21.9	134.2	309.2	310.7
Nitrate VWM - MAD	13.3	34.4	60.1	276.3	1006.6	909.3
Nitrate VWM + MAD	33.3	84.6	103.9	544.7	1625.0	1530.7
C_B (hyperbolic fit)	0.2	67.9	71.4	489.2	1619.8	1743.8
% difference (absolute)†	99.1	14.1	12.9	19.2	23.1	42.9

† $|(\text{Nitrate VWM}_{\text{Stormflow}} - C_S) * 100|$ and $|\text{Nitrate VWM}_{\text{Baseflow}} - C_B * 100|$

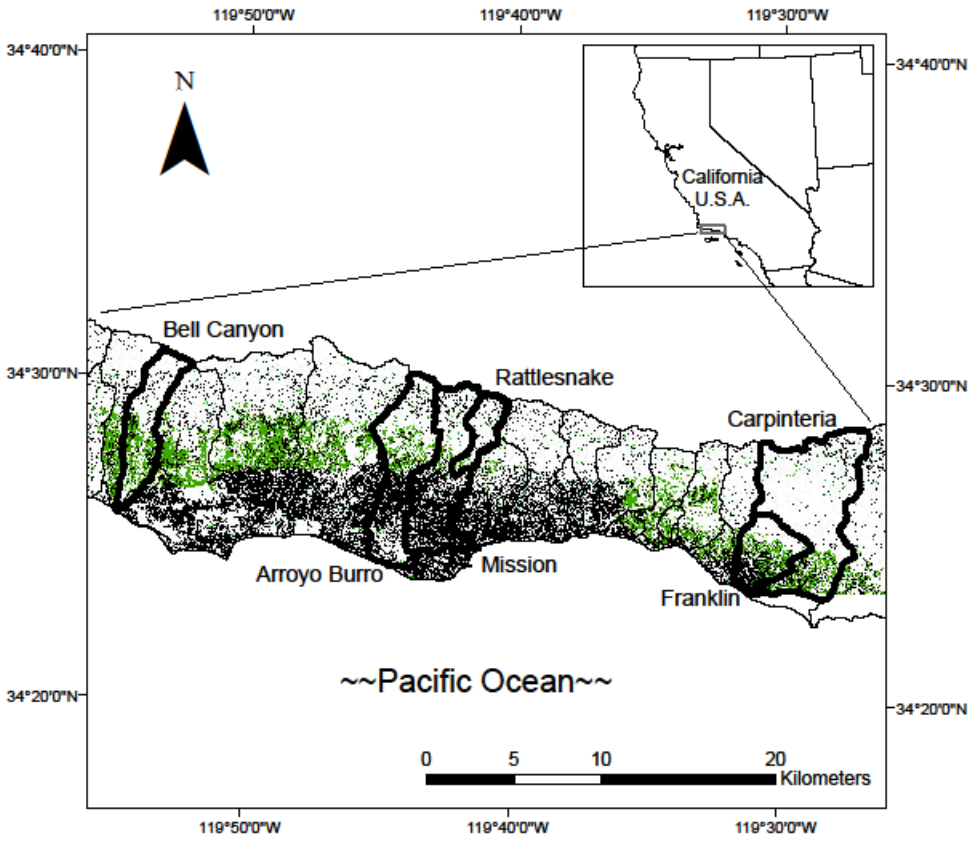

Figure 1. Locations of watersheds included in study. Land use is indicated by color: urban = black, agricultural = green, and undeveloped = white. Note: bare rock and urban/suburban land use have undifferentiated spectral signatures, hence the apparent urban/suburban land use in the upland (northern) region of the watersheds (black speckling pattern). This land use is in actuality bare rock (i.e., undeveloped).

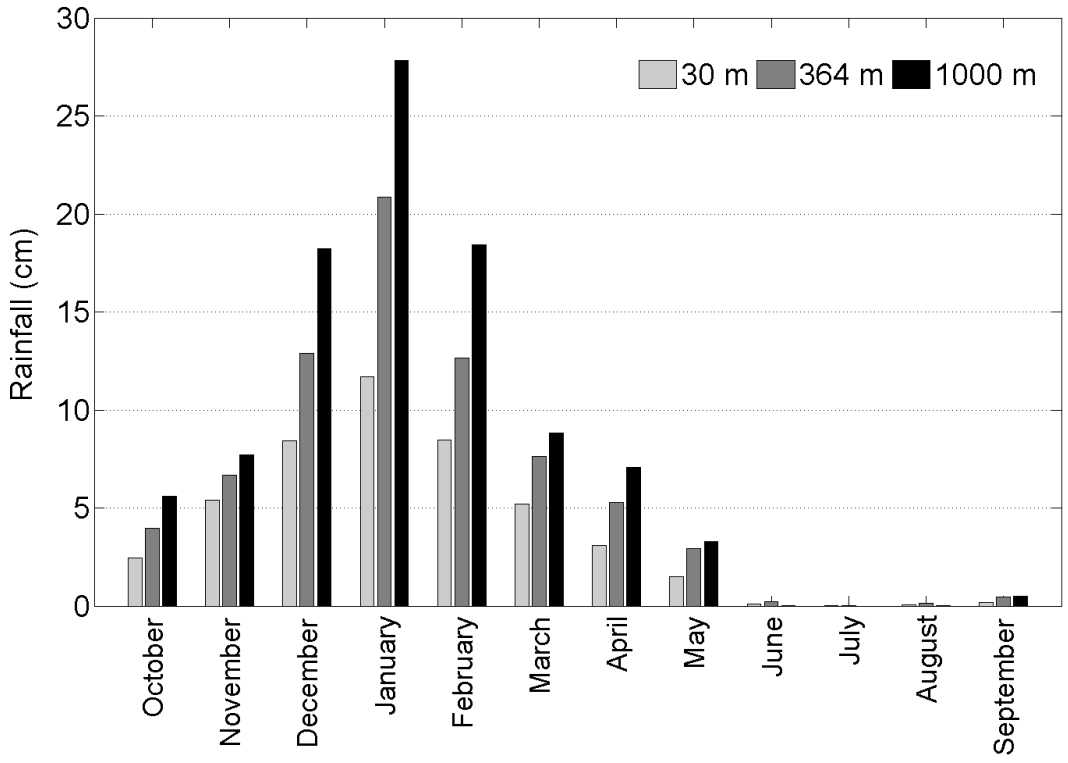

Figure 2. Mean monthly precipitation for three Santa Barbara precipitation gauges (water year ranges) located at elevations of 30 m (1868-2008), 364 m (1951-2008), and 1,000 m (1967-2008).

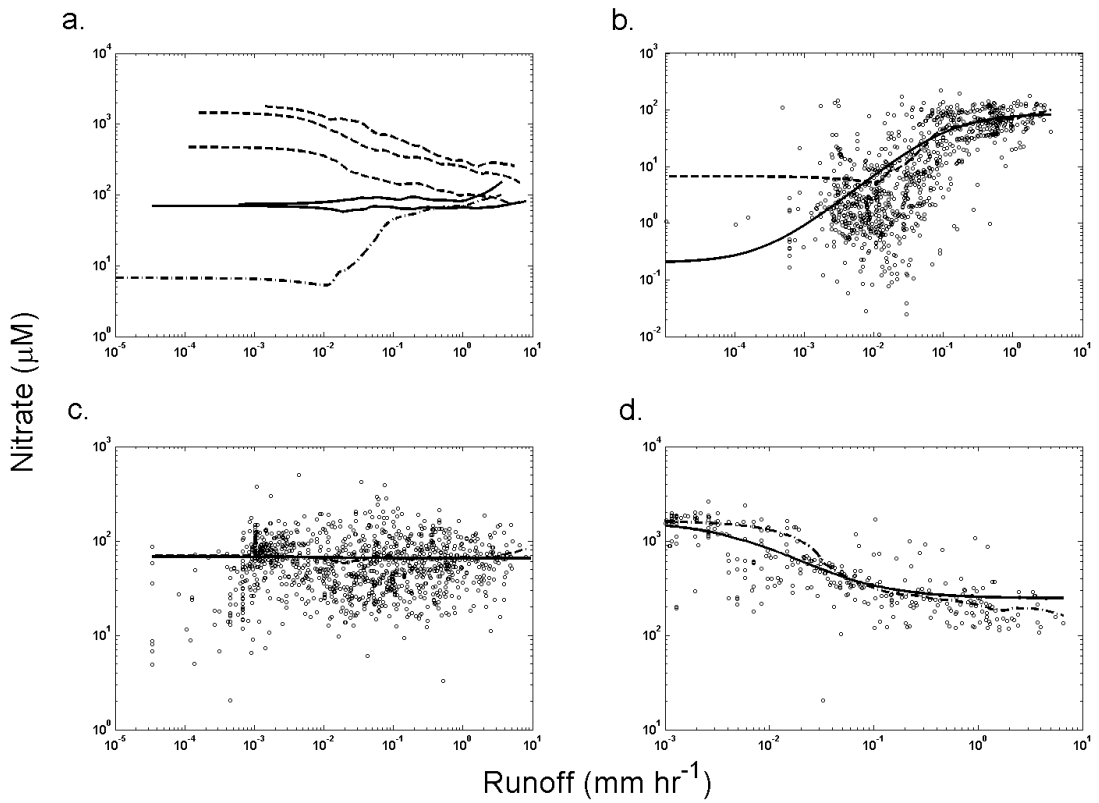

Figure 3. (a) Locally weighted scatter plot smooths (LOWESS) of nitrate concentration (µM) versus runoff (mm hr^{-1}) for watersheds delineated by land use class; undeveloped (- • -), urban (—), and agricultural (---) watersheds. From top to bottom, the smooths correspond to Franklin, Bell Canyon, and Carpinteria. (b-d) Scatter plots of nitrate versus runoff, LOWESS smooths (---), and hyperbolic equation fits (—) for (b) Rattlesnake, (c) Mission, and (d) Bell Canyon watersheds. Note: the apparent large deviation between the LOWESS smooth and hyperbolic equation fit for lower nitrate-runoff data points for Rattlesnake watershed is a function of the log-log scale, as the magnitude deviation in y-intercept nitrate concentrations is only ~7 µM.

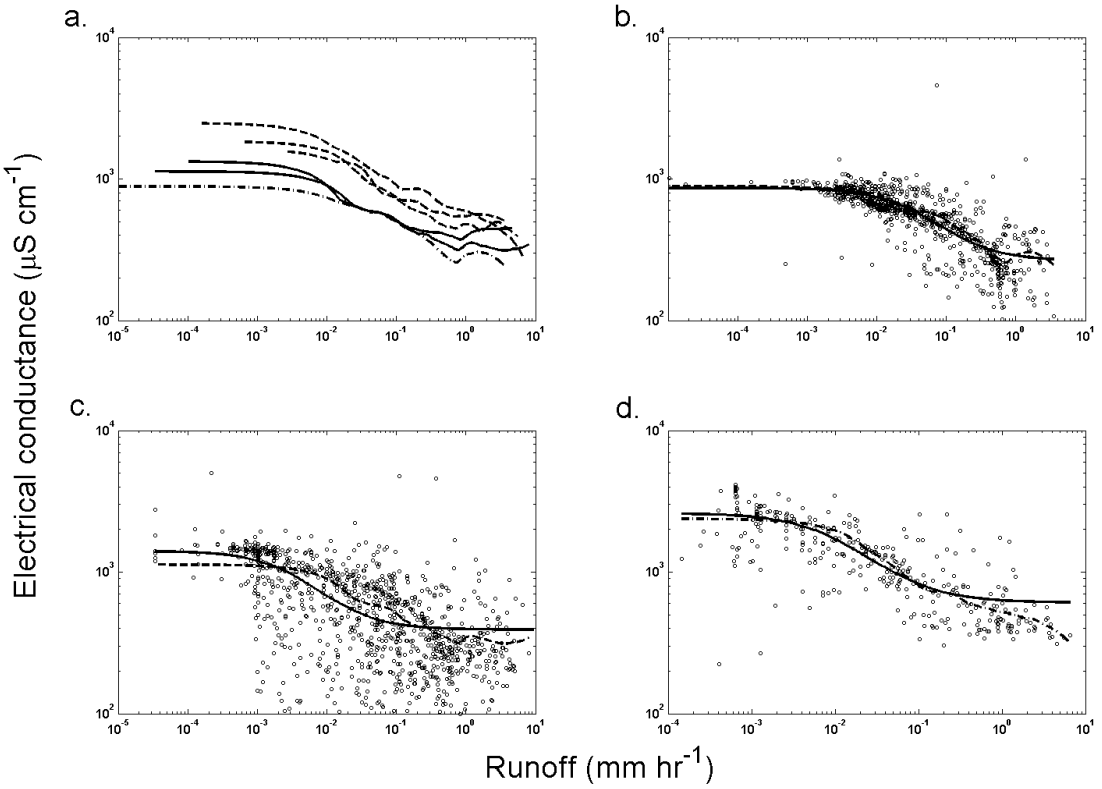

Figure 4. (a) Locally weighted scatter plot smooths (LOWESS) of electrical conductance (µS cm^{-1}) versus runoff (mm hr^{-1}) for watersheds delineated by land use class; undeveloped (- • -), urban (—), and agricultural (---) watersheds. (b-d) Scatter plots of electrical conductance versus runoff, LOWESS smooths (---), and hyperbolic equation fits (—) for (b) Rattlesnake, (c) Mission, and (d) Bell Canyon watersheds.

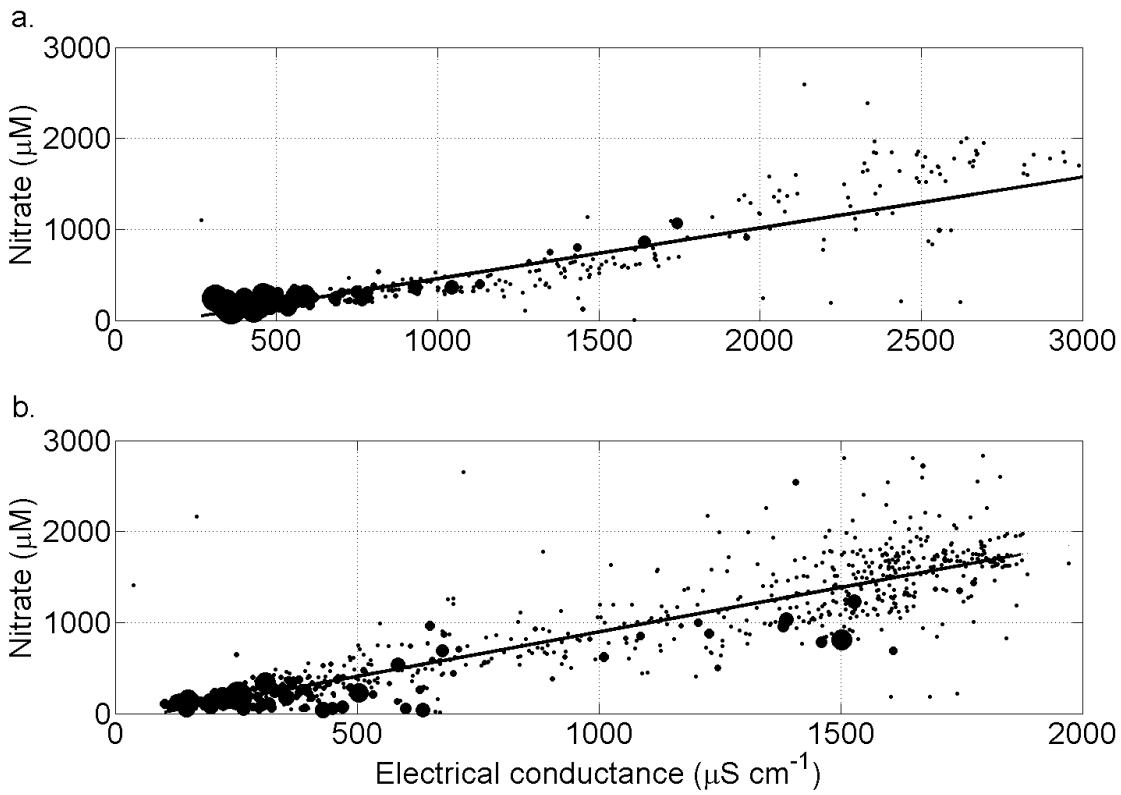

Figure 5. Nitrate versus electrical conductance plots for agricultural watersheds (a) Bell Canyon and (b) Franklin. Diameter of data points are proportional to runoff magnitude, except for the smallest diameter points, which have been enlarged for visibility. Linear regression equations are [Nitrate] = 0.56[EC] – 97.5 (R^2 = 0.87) for Bell Canyon and [Nitrate] = 0.98[EC] – 78.75 (R^2 = 0.88) for Franklin.

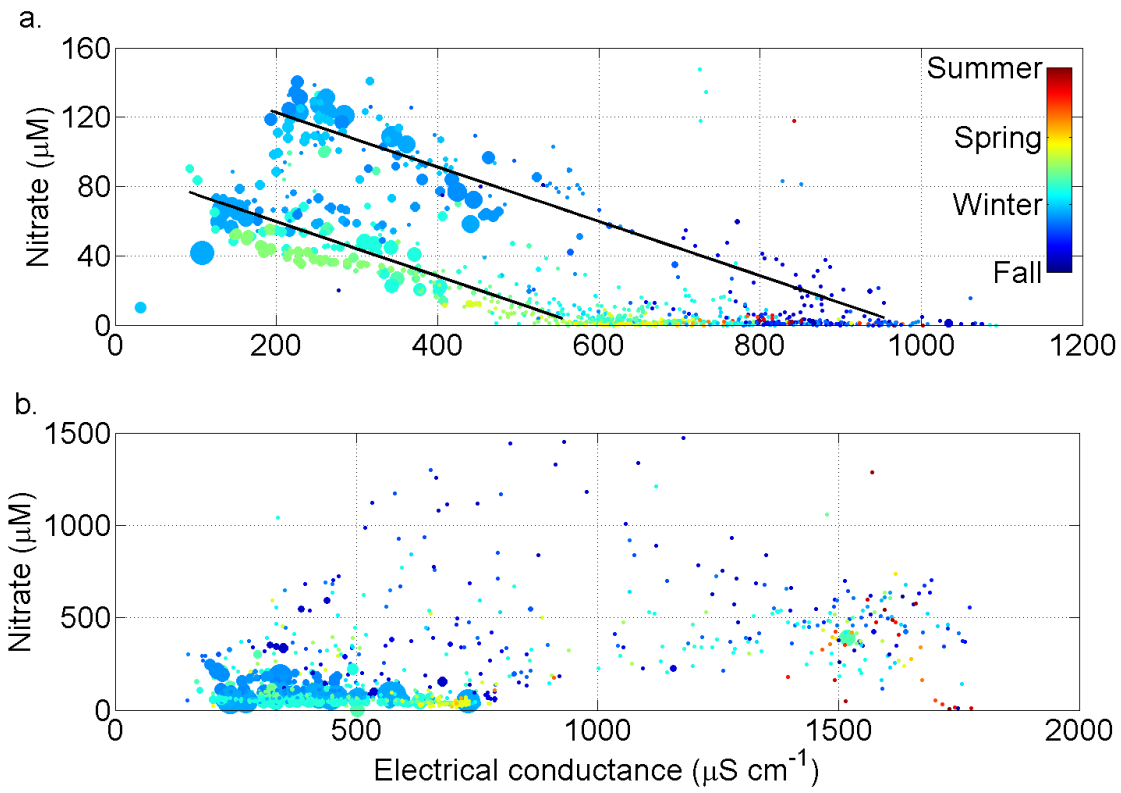

Figure 6. Nitrate versus electrical conductance plots for the undeveloped watershed (a) Rattlesnake and an agricultural watershed (b) Carpinteria. Diameter of data points are proportional to runoff magnitude, except for the smallest diameter points, which have been enlarged for visibility. Seasonal time of year of sample collection is denoted by data point color. Linear regression equations for Rattlesnake are [Nitrate] = -0.16[EC] + 154.0 (R^2 = 0.86) for the upper regression line and [Nitrate] = -0.16[EC] + 91.2 (R^2 = 0.76) for the lower regression line.

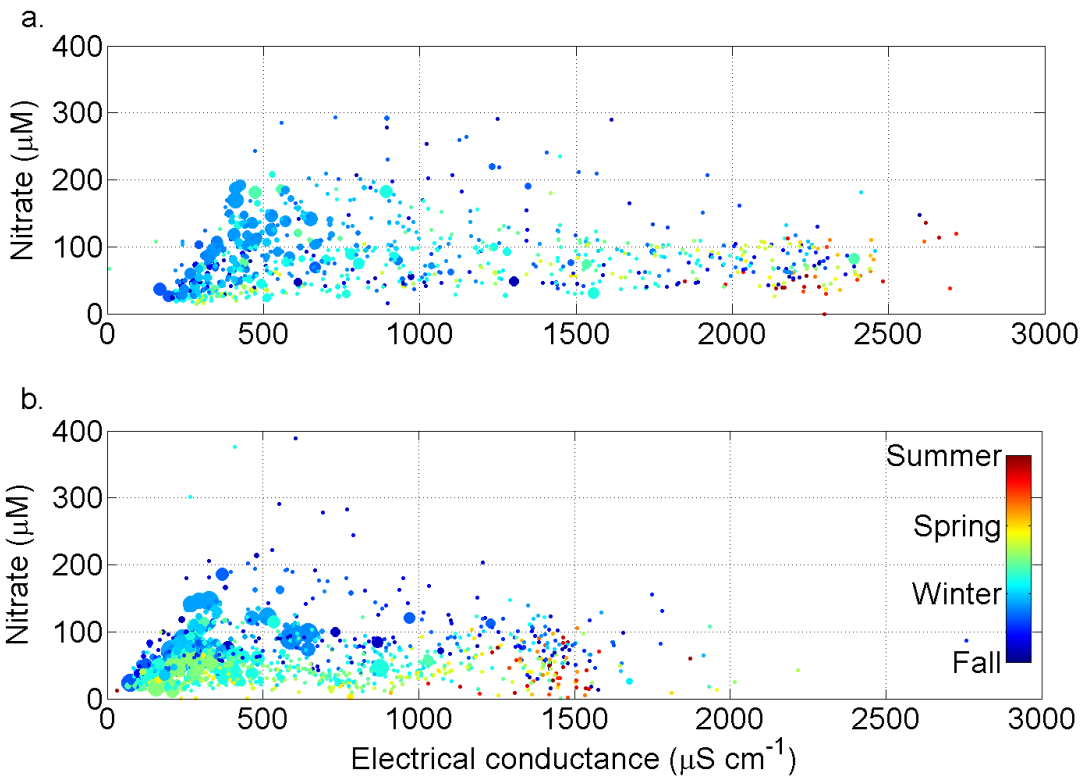

Figure 7. Nitrate versus electrical conductance plots for urban watersheds (a) Arroyo Burro and (b) Mission. Diameter of data points are proportional to runoff magnitude, except for the smallest diameter points, which have been enlarged for visibility. Seasonal time of year of sample collection is denoted by data point color.

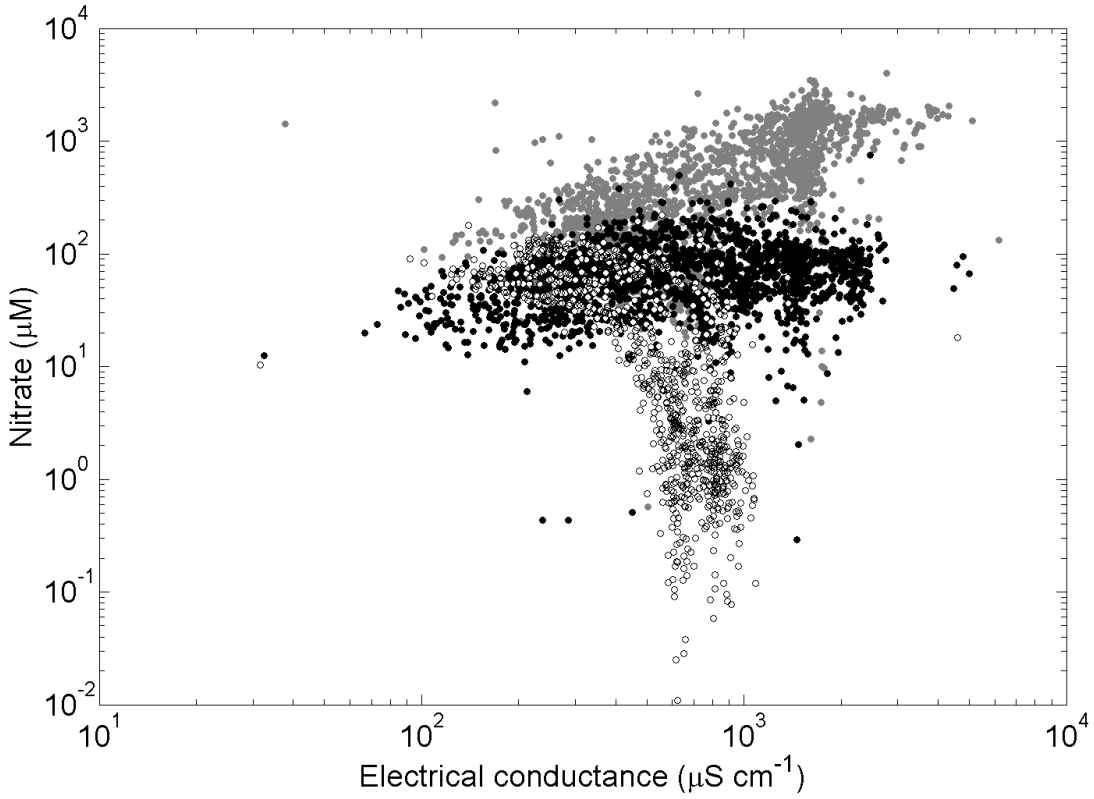

Figure 8. Nitrate versus electrical conductance plots for all watersheds grouped by land use: white data points with black outline = undeveloped watershed (Rattlesnake), black data points = urban watersheds (Arroyo Burro and Mission), and grey data points = agricultural watersheds (Carpinteria, Bell Canyon, and Franklin).

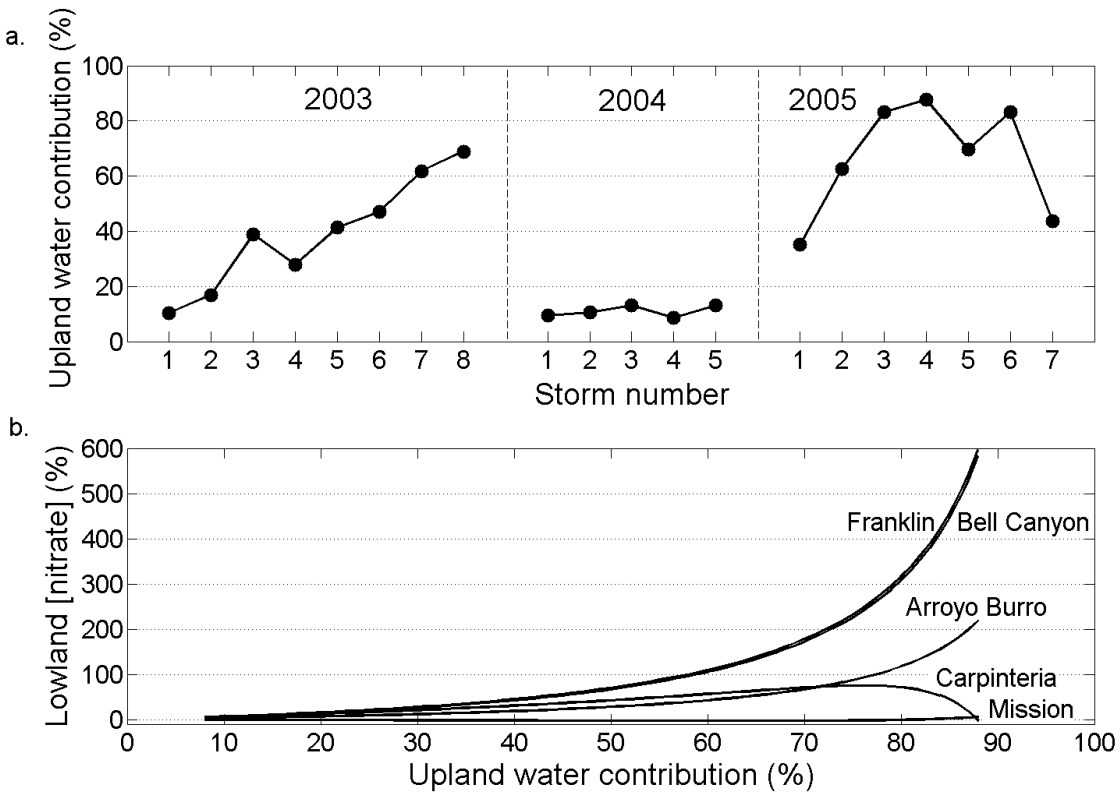

Figure 9. (a) Upland water contributions for storm series in 2003, 2004, and 2005 for Mission watershed. (b) Lowland nitrate modes for five developed watersheds as a function of upland water contribution over the observed 2003 through 2005 range (8% to 88%). Lowland nitrate modes are presented as percentage changes relative to the whole watershed (i.e., upland and lowland combined) nitrate mode for given upland water contributions.

Chapter 3. Radon residence times reveal temporal evolution and variability of dissolved inorganic nitrogen in beach pore water

Introduction

In coastal marine regions, dissolved inorganic nitrogen (DIN, the sum of ammonium, nitrite, and nitrate) can be a limiting nutrient for primary production (Howarth and Marino, 2006; Ryther and Dunstan, 1971) but pollutant when supplied in excess quantity, causing harmful algal blooms, eutrophication, and hypoxia (Cloern, 2001; Diaz and Rosenberg, 2008). Sandy intertidal beaches can function as both sink and source of DIN to coastal oceans, moderating excess fresh groundwater DIN delivery from coastal aquifers due to land use impacts, and regenerating DIN from marine particulate and dissolved organic matter (POM and DOM) in seawater that is continuously pumped through beach sands by waves and tides. This collective discharge of fresh groundwater and recirculating seawater to coastal oceans is termed submarine groundwater discharge (SGD) (Burnett et al., 2003). Recirculating seawater comprises a high percentage of SGD, even along coastlines with aquifer-ocean connectivity, ranging from 50% to over 99% of SGD (Li et al., 1999; Martin et al., 2007; Robinson et al., 2007; Urish and McKenna, 2004). As a result, the regeneration of DIN from marine POM and DOM in recirculating seawater can be a dominant source of DIN delivered to coastal oceans via SGD (Barreiro et al., 2013; Santos et al., 2009; Swarzenski and Izbicki, 2009), and is therefore an important process to understand when examining the role of beaches in coastal marine nitrogen cycles. However, characterizing this DIN delivery can be challenging due to high temporal variability in SGD and biogeochemical conditions in beach pore water.

The temporal variability and hydrologic controls of SGD have been studied using direct measurements, numerical modeling, and radioisotopic tracers such as radon (^{222}Rn) and the radium quartet (^{223}Ra, ^{224}Ra, ^{226}Ra, and ^{228}Ra) (reviewed in Burnett et al., 2003). However, the temporal variability and biogeochemical controls on pore water DIN concentrations have received less attention, despite recognition of the dynamic biogeochemical conditions in pore water that can significantly alter DIN concentrations through time (Santos et al., 2008; Santos et al., 2009). One way to identify this temporal variability is to couple DIN concentration measurements with residence time determinations using a residence time tracer. Residence time is defined as the amount of time that has elapsed since a volume of groundwater (or pore water) entered the subsurface hydrologic system (Bethke and Johnson, 2008). Radon, a conservative, radioisotopic gas with a 3.8 day half-life, is continuously produced from the radioactive decay of ^{226}Ra adsorbed to sediments (Swarzenski et al., 2003), and has been employed as a residence time tracer in terrestrial groundwater (Bertin and Bourg, 1994; Hoehn and Von Gunten, 1989) and beach pore water environments (Colbert et al., 2008). Radon is able to resolve residence times up to ~ 15 to 19 days, making it an effective residence time tracer in beach pore water (Colbert et al., 2008).

In this study, we demonstrate the first use of radon as a residence time tracer to identify the temporal evolution and variability of DIN concentrations in beach pore water. We coupled radon residence time determinations with measurements of DIN, total dissolved nitrogen (TDN), dissolved organic carbon (DOC), and particulate organic carbon and nitrogen (POC and PON, respectively) in beach pore water at four predominantly marine-influenced beaches along the Santa Barbara, California coastline. Tides have been shown to exert a dominant control on pore water discharge (Kim and Hwang, 2002; Li et al., 1999;

Taniguchi, 2002) and transit times (Robinson et al., 2007), so we hypothesized that pore water residence time distributions (RTDs) would shift as a function of tidal amplitude. As such, integrating modeled RTDs with modeled DIN vs. residence time relationships would allow a calculation of pore water volume-weighted mean (VWM) DIN concentrations, the variability of which could identify the interactive controls of temporal hydrologic and biogeochemical variability on DIN concentrations in beach pore water. SGD DIN delivery is routinely calculated assuming end-member concentrations that do not account for this variability. Our study 1) directly addresses the validity of this assumption, and 2) determines whether radon can be effectively employed as a residence time tracer to reveal patterns in the temporal evolution of DIN in beach pore water environments.

Methods

Sites description

The four study sites are located along the northern coast of the Santa Barbara Channel (Fig. 6). The coastal geomorphology of the region is characterized by unconsolidated sand beaches backed by 3 to 30 m high uplifted marine terraces (Patsch and Griggs, 2008) which preclude significant fresh groundwater inputs (Swarzenski and Izbicki, 2009). Beach sediments consist of well-sorted fine to medium sands with an overall median grain size of 281 µm and a range of median grain sizes of 207 to 483 µm (J. Dugan, personal communication). Beach widths during the study period (July 2012 through June 2013), measured from the base of the bluff on the back beach to the water line, averaged 35 m and ranged from 10 m to 55 m. Sand depths, measured from the sand surface to underlying bedrock, averaged 1.4 m and ranged from 0.4 m to 2.3 m. Sand density and porosity were

1.4 ± 0.1 g/mL and 0.34 ± 0.02 (mean ± 1σ; n = 25). The tidal regime in the Santa Barbara Channel is mixed semi-diurnal with tidal ranges less than 2 m (Dugan et al., 2011).

Pore water and nearshore seawater sample collection and analysis

Pore water samples were collected during ebb tides for ammonium, nitrite + nitrate (hereafter nitrate), total dissolved nitrogen (TDN), dissolved organic carbon (DOC), particulate organic carbon and nitrogen (POC and PON, respectively), and salinity using hollow-core stainless steel piezometers (2 cm screen) and a hand-held peristaltic pump (Woessner, 2007). Ammonium, nitrate, TDN, and DOC samples were filtered with 0.7 µm GF/F filters (Whatman), POC and PON samples were collected on 25 mm 0.7 µm GF/F filters (Whatman), and salinity samples were unfiltered. Nearshore seawater samples were collected for the same analytes as pore water samples on the ebb to flood tide transition by wading in ~ 1 m water depth. Pore water samples were collected at multiple locations (distance between sample locations was 6.3 ± 4.6 m; mean ± 1σ) and at multiple depths, where feasible, along shore-normal transects running from the base of the bluff on the back beach to the wave run-up line.

Ammonium and nitrate concentrations were determined on a Lachat Flow Injection Autoanalyzer (Hach Company). The detection limit for ammonium and nitrate was 0.5 µM, precision was ± 0.4 µM for ammonium and ± 0.1 µM for nitrate, and accuracy was ± 6% for ammonium and nitrate. DOC and TDN were measured by high temperature combustion (HTC) using a Shimadzu (Shimadzu) TOC-V_{CSH} system coupled with a Shimadzu Total Nitrogen analyzer (Letscher et al., 2013). The precision for DOC and TDN was ± 1 to 2 µM. Dissolved organic nitrogen (DON) was calculated as the difference between TDN and the

sum of ammonium and nitrate. POC and PON were pre-acidified with HCl and measured by high-temperature combustion using a CE440 CHN Elemental Analyzer (Exeter Analytical).

Pore water and nearshore seawater radon activity sample collection and analysis

Pore water and nearshore seawater radon activity samples (Rn_{pw} and Rn_{sw}, respectively) were collected at two study beaches, East Campus and Manzanita, in 615 mL glass bottles (radon bottles) with custom gas-tight sampling caps. Rn_{pw} were collected by driving piezometers to target sampling depths and filling with approximately 250 mL pore water (260 ± 22 mL). Rn_{sw} were collected during the ebb to flood tide transition in ~ 1 m water depth by filling with approximately 500 mL of surf zone seawater (452 ± 65 mL). Rn_{pw} and Rn_{sw} were determined on a RAD7 Radon-in-Air instrument (Durridge Company) using a closed-loop, continuous circulation with 15-minute count intervals and total count durations of 1.25 to 3 hours. Headspace radon activities measured with the RAD7 were converted to water sample radon activities:

$$Rn = (Rn_{air}V_{air} + \alpha V)V^{-1} \quad (1)$$

where Rn = pore water or nearshore seawater sample radon activity (Bq L^{-1}), Rn_{air} = radon activity in the air loop (Bq L^{-1}), V_{air} = volume of the air loop (1.5 L + V_{air} of pore water sample bottle headspace), α = radon air-water partition coefficient, and V = volume of the pore water or nearshore seawater sample. The radon air-water partition coefficient was calculated following Weigel (1978):

$$\alpha = 0.105 + 0.405\, e^{-0.0502\,T} \quad (2)$$

where T = temperature of the pore water sample. A temperature of 21.5°C was used in all radon calculations, which was the equilibrium temperature determined for a pore water sample incubated in the laboratory for 5 days.

Equilibrium pore water radon activity sample collection and analysis

Equilibrium radon activity samples (Rn_{eq}) were collected at multiple locations along the shore-normal transects at two study sites, East Campus and Manzanita. Approximately 50 mL of sand was collected from the top of the water table and mixed in an approximate 1:4 to 1:5 volume ratio with unfiltered nearshore seawater in radon bottles. The sand-seawater mixture was initially purged for 20 minutes with ambient laboratory air to remove initial radon and incubated in the laboratory for two weeks (16.6 ± 3.3 days) to allow ingrowth of radon, at which point they were analyzed using a closed-loop, continuous circulation on the RAD7 as described above. Equilibrium radon activity was calculated as:

$$Rn_{eq} = \varphi\,(1 - \theta)\left(\frac{Rn_{air}V_{air} + Rn_{pw}V_{pw}}{M_{sand}\,\theta^{-1}}\right) \quad (3)$$

where Rn_{eq} = equilibrium radon activity (Bq L^{-1}), M_{sand} = mass of sand (g), φ = sand density (g L^{-1}), and θ = porosity (dimensionless).

Radon residence time calculations

Nearshore seawater is deficient in radon relative to pore water (Table 1). Once this seawater infiltrates into beach sands, becoming pore water, it begins to accumulate radon from the decay of ^{226}Ra, and will do so until the rate of radon production is equal to radon decay, yielding the equilibrium radon activity (Rn_{eq}). Pore water residence times can therefore be calculated using the disequilibrium between the pore water sample radon activity

(Rn_{pw}) and mean equilibrium radon activity ($\overline{Rn}_{eq}$) (Bertin and Bourg, 1994; Colbert et al., 2008):

$$\tau = -\frac{1}{\lambda}\ln\left(1 - \frac{Rn_{pw}}{\overline{Rn}_{eq}}\right) \quad (4)$$

where τ = pore water sample residence time (days), λ = radon decay constant (0.18 days), Rn_{pw} = pore water sample radon activity (Bq L^{-1}), and $\overline{Rn}_{eq}$ = mean equilibrium radon activity (Bq L^{-1}). Nearshore seawater radon activities (Rn_{sw}) were subtracted from pore water radon sample activities, yielding pore water radon activities corrected for the initial seawater activity and nearshore seawater residence times of 0 days.

Residence time distribution (RTD) modeling

A two-parameter gamma distribution was used to model the probability density distribution of pore water sample residence times:

$$h(\tau) = \frac{\tau^{\alpha-1}}{\beta^{\alpha}\Gamma(\alpha)}\mathrm{e}^{-\tau/\beta} \quad (5)$$

where h = probability density of residence times (0 – 1), τ = residence time of pore water sample, α = shape parameter, $\beta = \tau_{mean}/\alpha$ (τ_{mean} = mean residence time), and $\Gamma(\alpha)$ = gamma function (a normalization constant making the area under the distribution equal to 1). A Kolmogorov-Smirnov test was used to assess the goodness of fit of the two-parameter gamma distribution to the pore water RTD.

Salinity sample collection and analysis

Specific electrical conductance values were measured using a YSI 3100 conductivity instrument (Yellow Springs) and were converted to salinity using a simplified general equation for salinity (Schemel, 2001) originally described by Lewis (1980).

Results and Discussion

The mixing of fresh groundwater into saline pore water can potentially alter residence time determinations, due to the radon in fresh groundwater. Using our measured pore water radon activities and an assumed fresh groundwater radon activity of 23.2 Bq L^{-1}, which is the mean groundwater radon activity for the Santa Barbara, California region (City of Santa Barbara Public Works), we calculated the radon activity due solely to beach sand production for pore water samples that had seawater percentages < 100% by using a two end-member mixing model based on salinity measurements, which assumes that pore water is a two-component mixture of recirculating seawater and fresh groundwater:

$$Rn_s = [Rn_{s+gw}(100) - Rn_{gw}P_{gw}]P_{sw}^{-1} \quad (6)$$

where Rn_s = pore water sample radon activity due to radon production in beach sands, Rn_{s+gw} = pore water sample radon activity resulting from both beach sand and fresh groundwater aquifer production, Rn_{gw} = mean radon activity in fresh groundwater (23.2 Bq L^{-1}), and P_{sw} = percentage of seawater in pore water sample. We used these fresh groundwater-corrected pore water radon activities to derive residence times using Eq. (4). We note that this method yields maximum differences between residences times calculated with and without a fresh groundwater component, as radon in fresh groundwater is essentially unsupported once entering the beach pore water and constitutes a progressively smaller proportion of the radon activity in pore water as it decays through time. Fifteen of the 53 pore water samples from

the radon dataset had a seawater percentage < 100%. Removal of the radon activity of the fresh groundwater for these samples showed that the mean difference between residence times calculated with and without the fresh groundwater radon activity was 2.8 ± 4.3 days, with a median difference of 1.2 days.

Dissolved inorganic nitrogen (DIN) temporal evolution in pore water

We used modeled DOC:TDN ratios from the radon dataset (Fig. 1a) and the negative exponential relationship between DIN and DOC:TDN (Fig. 1b) for the entire dataset to calculate DIN concentrations over the range of observed residence times in beach pore water (Fig. 2a). Further, we used two combinations of the equilibrium DOC:TDN ratio (1.4 in Fig. 1a) from the radon dataset, and DIN y-intercept (642 μM in Fig. 1b) from the overall dataset, to capture the range in observed DIN concentrations. To model the highest (lowest) DIN concentrations, we used the lower 95% CI (upper 95% CI) estimate of the equilibrium DOC:TDN ratio of 0.7 (2.1), and upper 95% CI (lower 95% CI) estimate of the DIN y-intercept of 767 μM (518 μM). These modeled DIN temporal evolution (i.e., DIN-te) curves are shown as "DIN-te (high)" ("DIN-te (low)") curves in Fig. 2a. The DIN-te curves showed that the pore water DIN concentration was initially ~ 10 μM in infiltrating seawater (i.e., mean of seawater DIN concentrations), and rapidly increased between ~ 1 to 3 days, attaining asymptotically maximum DIN concentrations ranging from a low of 62 μM (i.e., DIN-te (low)) to a high of 373 μM (DIN-te (high) around residence times of ~ 6 to 8 days, remaining more or less constant thereafter (Fig. 2a).

The decline in the pore water DOC:TDN ratio from 10.9 in infiltrating seawater to approach a low DOC:TDN of 1.4 at longer residence times (Fig. 1a) was in large part caused

by the rapid increase in the DIN concentration as primarily ammonium (Figs. 2a and 3b). This DIN increase likely resulted from the relative absence of labile DOC from photoautotrophic activity (Biddanda and Benner, 1997; Biersmith and Benner, 1998; Hama and Yanagi, 2001) and thus an increasing reliance of microbial metabolism on DON compounds such as amino acids, which are hydrolyzed from proteins via microbial extracellular enzymes (Pantoja et al., 1997; Vetter et al., 1998) and deaminated to produce ammonium. The photosynthetic activity of photoautotrophs in seawater can provide DOC substrates, such as dissolved carbohydrates (DCHO), which are highly labile and therefore rapidly consumed to fuel microbial metabolism (Amon et al., 2001; Arnosti et al., 1994). The absence of a renewed source of these DCHO compounds, such as would be the case in the dark pore water environment, would shift the reliance of the microbial community to other compounds that were present in higher abundance, such as more nitrogen-rich DOM compounds from algal detritus and microbial biomass (Burdige and Zheng, 1998; Burney, 1986; Canuel and Martens, 1993). The mean POC:PON ratio of 7.6 ± 1.8 was similar throughout all pore water samplings (Fig. 4), indicating that the main source of POM to pore water was algal- and microbially-derived and fairly constant throughout the year (Rusch and Huettel, 2000; Santos et al., 2009; Seidel et al., 2014). In contrast, the DOC:DON ratios were more variable (10.9 ± 15.3) (Fig. 4), and became lower as the pore water DON concentration increased with residence time (Figs. 3c and 4), illustrating the shift to more nitrogen-rich DOM compounds with increasing residence time (Seidel et al. 2014; Schmidt et al. 2011). In addition, dehydration (i.e., condensation) reactions, which cause aromatization of microbial degradation products and fulvic and humic substance formation (Nissenbaum and Kaplan, 1972; Schmidt et al., 2011), and bonding of ammonium with reactive functional

groups of DOM (McKee and Hatcher, 2010), can decrease the lability of pore water DOM. These processes may explain why DIN concentrations asymptote around residence times of 6 to 8 days (Fig. 2a) despite high pore water DOC concentrations (Fig. 3a), as microbial activity becomes substrate-limited by the decrease in labile DOM, either through exhaustive consumption or production of less labile forms through the above mechanisms.

Volume-weighted mean (VWM) dissolved inorganic nitrogen (DIN) concentrations

Although the pore water volume in the beach is unknown, the proportion of the pore water volume with residence time equal to or less than a given residence time τ can be described by the cumulative RTD (Bolin and Rodhe, 1973):

$$v(\tau) = V \int_0^\tau P(\tau)\, d\tau \quad (7)$$

where τ = pore water residence time (days), v = volume of pore water with residence time $\leq \tau$, V = total volume of pore water within a defined beach domain, and P = pore water residence time cumulative probability density function. The derivate of the pore water residence time cumulative probability density function P is the pore water probability density function p, which defines the probability density at any residence time τ. Therefore, if V is normalized to 1 (V/V), then the proportional pore water volume equal to τ within the defined beach domain is given by the residence time probability density at τ, and the pore water VWM DIN concentration can be calculated as:

$$VWM\ DIN = \int_0^n p(\tau)\, DIN(\tau)\, d\tau \quad (8)$$

where *VWM DIN* = pore water volume-weighted mean DIN concentration (μM), p = pore water residence time probability density at τ, and *DIN* = pore water DIN concentration at τ.

A Kolmogorov-Smirnov test showed that the two-parameter gamma distribution was a good fit to the pore water RTD ($D = 0.18$; $p = 0.51$). We used the shape parameter α (3.6) from the modeled RTD for the overall radon dataset ($n = 53$) to model two additional RTDs using the shortest and longest mean residence times observed for pore water sampling events ($\beta = \tau_{mean}/\alpha$), thereby representing the observed range in pore water RTDs (Table 1; Fig. 2b). We used these three probability density distributions of pore water residence times (Fig. 2b), in combination with the DIN-te modeled curves (Fig. 2a), to calculate pore water volume weighted-mean DIN concentrations (VWM DIN) (Table 2) according to Eq. (8). VWM DIN concentrations account for both residence time and DIN concentration variability in beach pore water since they are the integrated product of the RTDs and DIN-te curves.

The RTD is not the same as the transit time distribution (TTD), which describes the time elapsed from the initial infiltration of a volume of pore water into beach sands to its ultimate exfiltration to the coastal ocean, versus the residence time which describes the time elapsed from the initial infiltration of a volume of pore water into beach sands to the location of its extraction. Therefore the TTD provides the most accurate estimate of the VWM DIN concentration of pore water discharge. However, the similar mean residence times for the fore and back beach, 5.4 and 5.7 days, respectively, and similar shape of the residence time distributions (i.e., gamma; $D_{front} = 0.10$, $p = 0.88$, $n = 34$ and $D_{back} = 0.18$, $p = 0.50$, $n = 19$) (Figs. 5b and 5c) indicated that the overall RTD was a close approximation to the TTD (Fig. 5a). If this were not the case, we would expect to observe a significant shift toward shorter residence times in the fore beach RTD, as the fore beach is both the hydrologic source and sink region where seawater infiltrates and exfiltrates our marine-dominated study beaches (i.e., mean pore water sample seawater composition was 93%, and ranged from a minimum

of 85% to a maximum of 100%; Table 3). Such a shift to lower residence times in the fore beach would also cause a larger difference in mean residence times and distributional shape between the fore and back beach RTDs, which we did not observe (Figs. 5b and 5c).

Tides exert a dominant control on pore water circulation in all coastal regions with SGD, regardless of the proportion of recirculating seawater versus fresh groundwater (Li et al., 1999; Li et al., 2009; Robinson et al., 2007; Swarzenski et al., 2007; Taniguchi, 2002). This tidal effect is evident in our study as a positive correlation between pore water mean residence time and tidal amplitude ($r^2 = 0.75$; $F_{1,4} = 11.8$; $p < 0.05$; Fig. 7). The tidal amplitude was measured as the height difference between the higher high and lower low tide for the days on which pore water sampling was conducted. These variations in tidal amplitude result in a VWM DIN concentration (for a given DIN-te curve) for the RTD modeled using the longest mean residence time that is 1.5 times (50%) larger than that modeled using the shortest mean RTD (Table 2; Fig. 2b). Our VWM DIN concentrations presume no variation in the magnitude of pore water discharge, but higher tidal amplitudes are associated with higher pore water discharge (Li et al., 1999; Li et al., 2009; Taniguchi, 2002), so the increase in DIN flux would be even greater than the 50% elevation that we observed here. In addition, variation in POM and DOM source loading over shorter timescales on the order of pore water flushing (15.5 days, or ~ 2 weeks) can induce further VWM DIN concentration variability, making our observed 50% elevation in VWM DIN concentration the most conservative estimate. Macroalgal deposition onto Santa Barbara beaches, composed predominantly of *Macrocystis pyrifera* (giant kelp), is hypothesized to be a major source of DIN in beach pore water (Dugan et al. 2011; Barreiro et al. 2013), perhaps explaining the large range in asymptotic modeled DIN concentrations (i.e., from 62 μM to

373 μM) observed in pore water at later residence times (Fig. 2a). Thus, if a giant kelp deposition event were to occur during a spring tidal phase, DIN produced from the decomposition of this material could enrich beach pore water to a maximum concentration of 373 μM, thereby resulting in a VWM DIN concentration of 279 μM (i.e., DIN-te high, long mean RTD scenario; Table 2). This DIN could then be flushed from beach pore water via the concurrent removal of giant kelp by advection offshore and rapid decomposition over the following ~ 2 weeks as the tidal phase transitioned from spring to neap. In the absence of the source of DIN enrichment, the beach pore water asymptotic DIN concentration would then decrease to 62 μM, which would result in a VWM DIN concentration of 31 μM (i.e., DIN-te low, short mean RTD scenario; Table 2). Therefore the spring-neap tidal transition, in combination with varying POM and DOM source loading, would produce a situation where the VWM DIN was 9 times (800%) greater during the 'spring tide, giant kelp' loading phase (279 μM) than the following 'neap tide, absence of giant kelp' loading phase (31 μM) (Table 2).

We observed a 1.5-fold difference in the VWM DIN concentration due to variable RTDs for a given DIN-te curve, but for a given RTD, there is a 6.1-fold difference in the VWM DIN concentration between the DIN-te high and DIN-te low curves, which can increase to a 9-fold difference when considering a concurrent RTD and DIN-te shift (Table 2). However, the smaller difference in VWM DIN concentrations over the range of RTDs is belied by the fact that SGD is positively correlated with tidal amplitudes (Li et al., 1999; Li et al., 2009; Taniguchi, 2002), thus increasing the variability in DIN fluxes over spring-neap tidal phases and elevating the DIN flux difference beyond 50%. This tidal influence on DIN flux differences would be greater for coastal regions that experience larger tidal amplitude

swings, resulting in larger shifts in RTDs over the spring-neap tidal phase. Therefore, in coastal regions that experience microtidal regimes (i.e., lowest tidal amplitudes), biogeochemical variability is likely the primary factor governing VWM DIN concentrations in recirculating seawater (saline pore water), as the pore water RTD is relatively invariant. However, inland hydraulic gradient changes in coastal aquifers could alter saline pore water circulation (Robinson et al., 2007), in turn inducing higher RTD temporal variability, although primarily as a fresh groundwater rather than tidal influence.

Our study demonstrates that variability in pore water RTDs and DIN vs. residence time relationships (DIN-te curves) can interactively influence the pore water VWM DIN concentration, and that the resultant differences in VWM DIN concentrations can range from 1.5- to 9-fold, equivalent to 50% to 800% increases, respectively, from the minimum to maximum VWM DIN concentrations over the range in RTDs and DIN-te curves (Table 2). This suggests that using a single end-member DIN concentration to calculate SGD DIN flux over periods longer than the timescale of pore water residences times and flushing can result in large errors by failing to account for interactive pore water hydrologic and biogeochemical dynamics. Since SGD contains a high volumetric proportion of recirculating seawater (ranging from 50% to > 99%) in coastal regions both with and without significant fresh groundwater contributions (Li et al., 1999; Martin et al., 2007; Robinson et al., 2007; Urish and McKenna, 2004), accounting for temporal variability in RTD and DIN concentrations is necessary to obtain accurate estimates of DIN delivery to coastal oceans. Perhaps more importantly though, using radon as a residence time tracer may reveal the temporal biogeochemical dynamics of other compounds to provide a better understanding of the dual

role of beach pore water environments in mitigating land-derived pollutants and maintaining coastal marine biogeochemical cycles.

Tables and Figures

Table 1. Nearshore seawater radon activity, mean pore water radon activity (± 1σ), mean equilibrium radon activity, and mean residence time for Manzanita and East Campus study beaches.

Site	Sample date	n	Seawater ^{222}Rn (Bq L^{-1})	Pore water ^{222}Rn (Bq L^{-1})	Equilibrium ^{222}Rn (Bq L^{-1})	τ_{mean} (days)
Manzanita	12 Jul 2012	6	0.03	3.4 ± 1.0	6.9 ± 2.7	4.0 ± 1.8
	30 Aug 2012	6	0.15	4.1 ± 1.7	6.9 ± 2.7	6.8 ± 4.9
	27 Mar 2013	10	0.08	3.4 ± 1.1	5.5 ± 0.8	5.5 ± 2.9
	26 Jun 2013	13	0.07	3.6 ± 1.2	5.3 ± 0.9	5.9 ± 3.2
East Campus	17 Jul 2012	7	0.32	3.5 ± 1.2	4.7 ± 1.3	5.0 ± 2.8
	29 Aug 2012	11	0.07	3.0 ± 0.8	4.7 ± 1.3	5.4 ± 2.3

Table 2. Volume-weighted mean (VWM) dissolved inorganic nitrogen (DIN) concentrations (μM) for combinations of three DIN-te curves (Fig. 2a) and three pore water residence time distributions (RTDs) (Fig. 2b).

	DIN-te low	DIN-te mid	DIN-te high
Mean τ short (4.0 days)	31	78	189
Mean τ (5.5 days)	43	107	258
Mean τ long (6.8 days)	46	116	279

Table 3. Mean (1σ) values of pore water salinity, seawater percentage, dissolved inorganic nitrogen (DIN: ammonium and nitrate), total dissolved nitrogen (TDN), dissolved organic nitrogen and carbon (DON and DOC), and particulate organic carbon and nitrogen (POC and PON) for all study beaches.

Site	Sample date	n	Salinity	Seawater %[a]	Ammonium (µM)	Nitrate (µM)	Total dissolved nitrogen (µM)	Dissolved organic nitrogen (µM)	Dissolved organic carbon (µM)	Particulate organic carbon (µM)	Particulate organic nitrogen (µM)
East Campus	17 Jul 2012	8	32.9 (1.9)	100 (5)	158.8 (233.8)	2.0 (0.2)	266.2 (387.1)	94.9 (148.1)	276.2 (153.8)	382.4 (180.3)	57.3 (20.1)
	29 Aug 2012	11	32.8 (1.4)	100 (4)	137.3 (92.1)	5.7 (5.5)	199.1 (170.8)	57.8 (74.1)	239.3 (211.3)	330.5 (118.6)	41.5 (14.9)
	31 Jan 2013	13	30.6 (1.9)	94 (5)	185.1 (248.9)	10.3 (34.0)	259.1 (264.6)	62.5 (31.1)	435.4 (220.6)	310.4 (319.2)	34.5 (31.9)
	28 Feb 2013	5	30.6 (1.8)	94 (5)	192.6 (115.0)	23.5 (31.5)	249.4 (131.2)	47.2 (28.2)	386.9 (122.0)	314.1 (221.3)	41.5 (22.2)
	21 Apr 2013	3	30.8 (2.0)	95 (6)	145.8 (106.9)	1.3 (1.0)	184.0 (136.9)	62.0 (18.7)	349.6 (204.1)	158.9 (36.8)	21.6 (7.9)
Manzanita	12 Jul 2012	6	32.9 (1.1)	99 (3)	39.9 (52.5)	146.9 (222.0)	209.8 (190.2)	20.7 (15.0)	213.9 (111.0)	257.2 (105.8)	38.3 (24.5)
	30 Aug 2012	6	32.0 (3.1)	97 (8)	31.4 (31.8)	149.8 (303.6)	154.5 (215.3)	8.1 (4.2)	235.4 (210.5)	164.2 (66.2)	21.6 (7.1)
	27 Mar 2013	10	33.3 (0.7)	100 (2)	154.3 (104.9)	0.3 (0.2)	213.9 (126.7)	55.0 (29.6)	314.0 (177.8)	241.3 (123.4)	31.5 (15.1)
	26 Jun 2013	13	33.6 (2.1)	100 (6)	180.0 (156.2)	1.4 (1.8)	274.6 (178.0)	87.6 (84.7)	338.6 (250.0)	NS	NS
Isla Vista	02 Feb 2013	14	31.6 (1.5)	97 (4)	159.2 (207.5)	1.6 (3.1)	199.0 (250.9)	43.9 (46.0)	180.6 (134.7)	192.7 (158.2)	23.1 (16.2)
	02 Mar 2013	13	31.5 (1.1)	97 (3)	100.1 (191.3)	1.3 (2.9)	139.6 (225.5)	36.3 (46.4)	153.7 (102.6)	231.8 (131.8)	35.3 (16.8)
	23 Apr 2013	10	28.0 (4.3)	86 (12)	35.3 (33.2)	106.5 (184.8)	167.4 (174.2)	24.8 (24.0)	261.3 (303.3)	164.5 (53.7)	25.1 (10.6)
Gaviota	01 Feb 2013	15	30.8 (6.2)	94 (18)	8.1 (8.4)	28.0 (56.4)	39.6 (38.5)	10.8 (3.5)	141.9 (185.9)	184.2 (49.0)	27.8 (7.8)
	01 Mar 2013	12	31.7 (2.9)	98 (8)	14.8 (19.1)	27.3 (64.9)	57.4 (83.2)	15.0 (22.0)	113.5 (75.7)	138.3 (46.8)	23.9 (8.6)
	17 Apr 2013	12	27.4 (10.2)	85 (29)	11.1 (9.6)	16.3 (33.9)	41.2 (36.1)	14.6 (6.0)	161.2 (149.1)	122.8 (22.8)	16.4 (3.9)

[a] Seawater % was calculated as $P_{sw} = [S_{sample} - S_{gw}(1 - P_{sw})]S_{sw}^{-1} \times 100$, where P_{sw} = seawater percentage, S_{sample} = measured sample salinity, S_{gw} = fresh groundwater salinity (assumed to be 0), and S_{sw} = measured seawater salinity

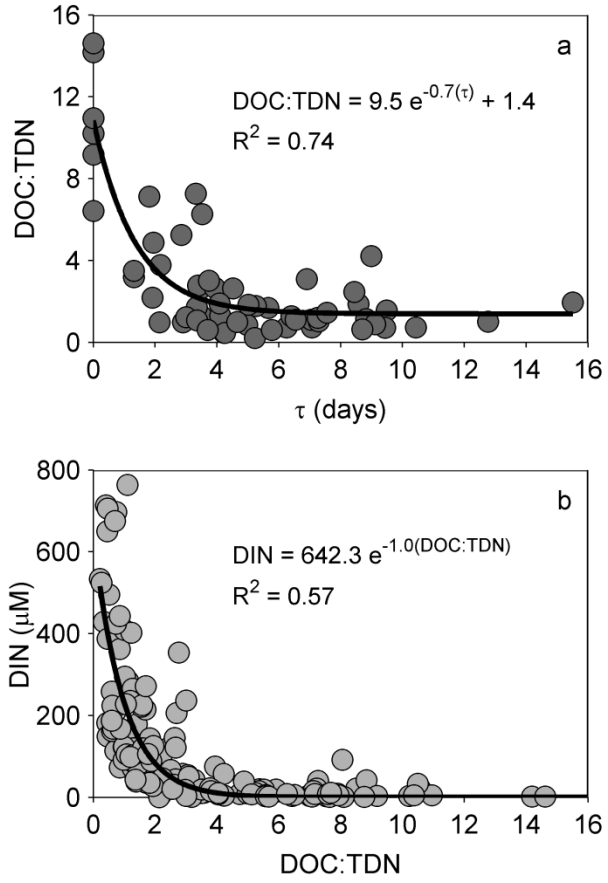

Fig. 1. (a) Negative exponential relationship between pore water dissolved organic carbon (DOC) to total dissolved nitrogen (TDN) ratio and residence time (n = 59). (b) Negative exponential relationship between pore water dissolved inorganic nitrogen (DIN) concentration and DOC:TDN ratio (n = 166).

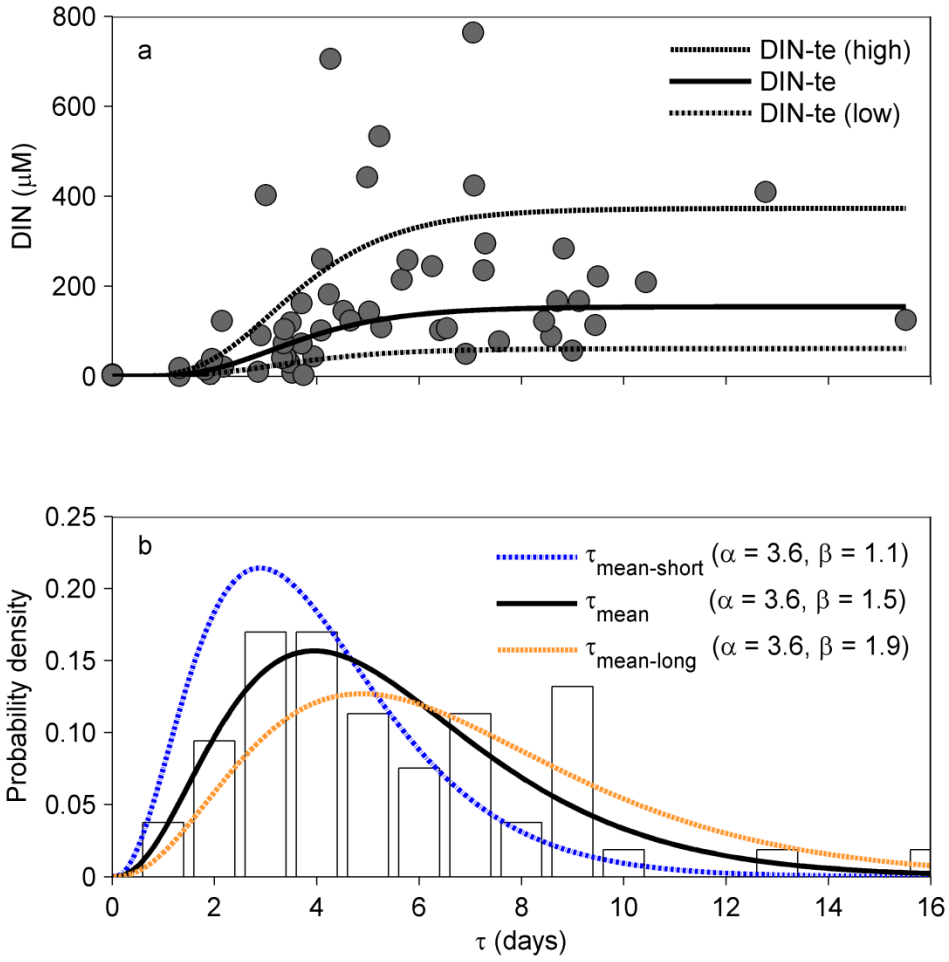

Fig. 2. (a) Modeled pore water residence time probability density distributions (gamma) for three observed mean pore water residence times; short (4.0 days), overall mean (5.5 days), and long (6.8 days). Empirical pore water residence time distribution for entire radon dataset (i.e., overall mean) shown as histogram (bars). (b) Seawater and pore water dissolved inorganic nitrogen (DIN) concentration vs. residence time. The three modeled DIN-te (i.e., DIN temporal evolution) curves were calculated using the modeled DOC:TDN ratio vs. residence time (Fig. 1a) and DIN vs. DOC:TDN relationships (Fig. 1b).

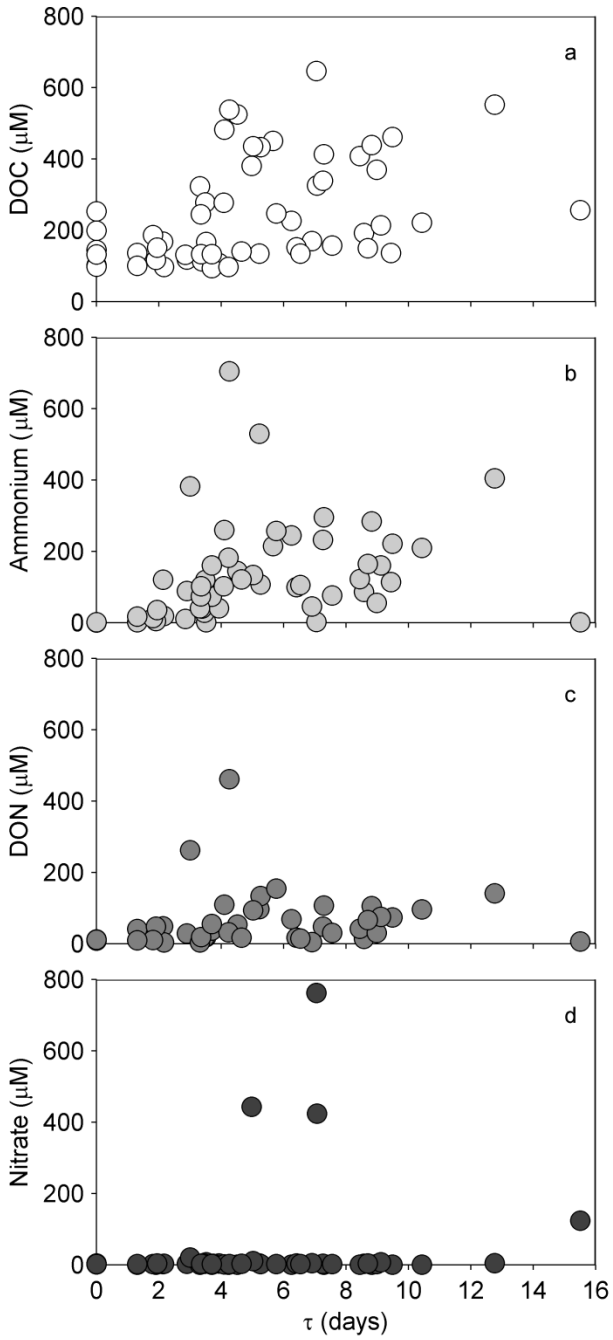

Fig. 3. Residence time relationships for nearshore seawater and pore water analytes (n = 60) (a) dissolved organic carbon (DOC), (b) ammonium, (c) dissolved organic nitrogen (DON), and (d) nitrate.

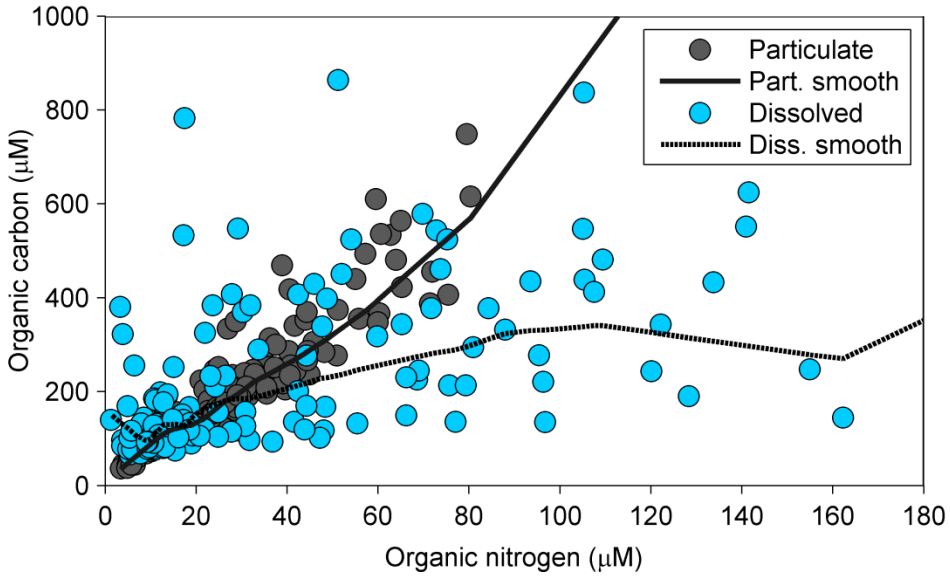

Fig. 4. Organic carbon vs. organic nitrogen scatterplot for particulate and dissolved fractions. Robust locally-weighted scatterplot smooths (Cleveland, 1981) shown for particulate and dissolved fractions with smoothing parameter (f) of 0.35. Five outlier points are not shown for visual presentation purposes: (DOC, DON) points of (1091, 41), (1057, 348), (819, 262), and (538, 461); (POC, PON) point of (1336, 137).

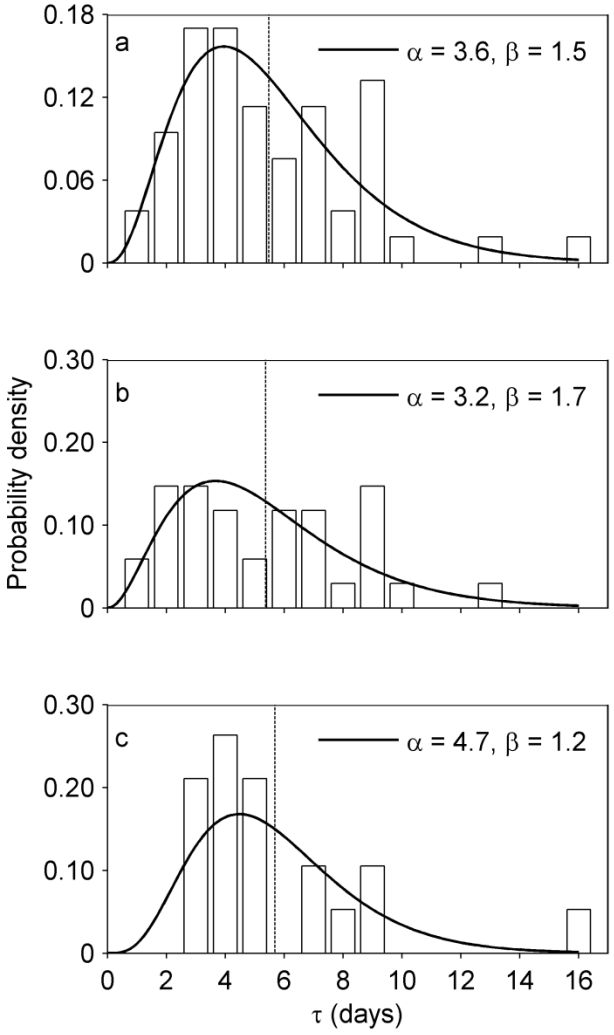

Fig. 5. Pore water residence time probability density distributions for (a) entire radon dataset, (b) fore beach (normalized shore-perpendicular distances > 0.5), and (c) back beach (normalized shore-perpendicular distances < 0.5) regions with fitted gamma distributions. Mean pore water residence times shown as vertical dashed lines.

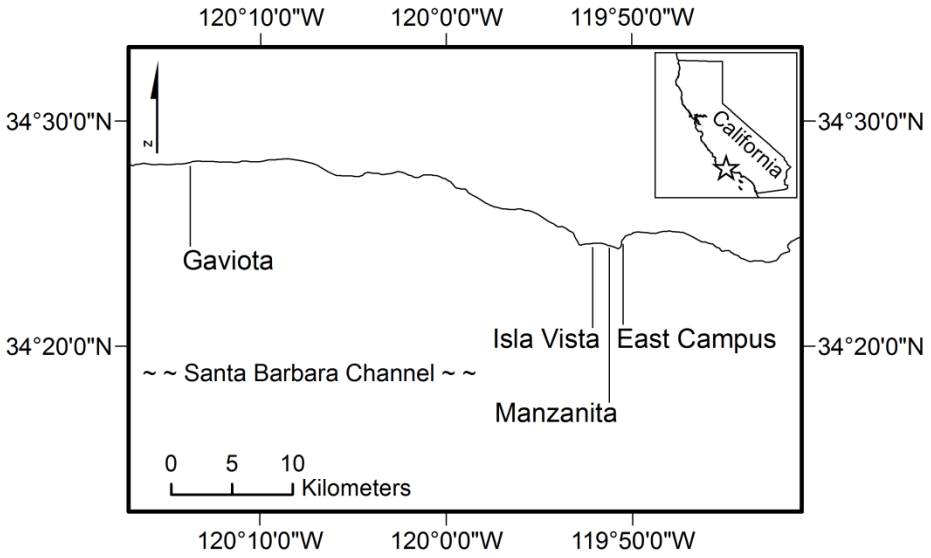

Fig. 6. Study beach locations along the Santa Barbara, California coastline.

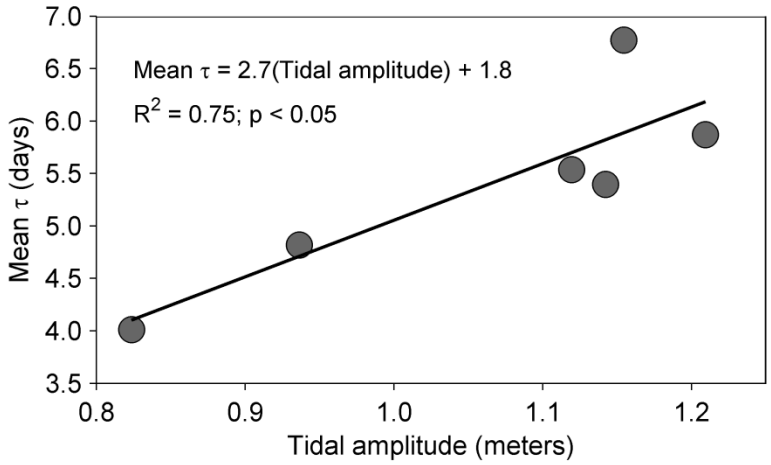

Fig. 7. Mean pore water residence time (τ) vs. tidal amplitude relationship with fitted linear equation (n = 53). Tidal amplitude was calculated as the difference between the higher high and lower low tidal elevations (semi-diurnal tide) for the day on which individual pore water sampling events occurred.

Chapter 4. Influence of seawater and pore water dissolved organic matter composition on bacterioplankton dissolved inorganic nitrogen uptake

Introduction

Marine interstitial environments, such as intertidal and subtidal sediments, play key roles in the carbon and nitrogen cycles of shallow coastal ocean regions (Boudreau et al., 2001). Seawater circulation through porous sandy sediments, a dominant sedimentary type in high-energy shallow waters, is driven by waves, tides, and bottom currents (Precht and Huettel, 2003; Rusch and Huettel, 2000). Particulate organic matter (POM) from the open water column is introduced with this seawater, and undergoes rapid conversion to dissolved organic matter (DOM), carbon dioxide (CO_2), and dissolved inorganic nitrogen (DIN, initially in the form of ammonium) via sedimentary heterotrophic microbial activity (Billerbeck et al., 2006; de Beer et al., 2005). Interstitial environments therefore act as biocatalytic filters that convert POM to DOM and dissolved inorganic nitrogen (DIN). This DIN can be taken up by primary producers and heterotrophic bacterioplankton communities in overlying and adjacent seawater, thereby forming a recycling loop between open water and interstitial environments.

Interstitial environments have significantly higher DIN and dissolved organic nitrogen (DON) concentrations than open water marine environments (Burdige and Zheng, 1998), in large part due to the dominance of heterotrophic microbial activity (Lomstein et al., 2009). Heterotrophic microbial biomass is nitrogen-rich (i.e., low biomass C:N ratios) due to high cellular protein content (Fukuda et al., 1998). The turnover of this biomass, caused by viral lysis, grazing, and enzymatic hydrolysis of dead biomass, results in higher

concentrations of DON in pore water relative to seawater (Epstein, 1997; Meyer-Reil, 1987; Wilhelm and Suttle, 1999). Further, the relative absence of an autotrophic influence in dark interstitial settings, in the form of provision of dissolved organic carbon (DOC) compounds such as dissolved carbohydrates (DCHO), likely contributes to high DIN concentrations due to carbon-limitation of microbial biomass and therefore greater reliance on DON compounds (Burdige and Martens, 1988). DON compounds such as amino acids are deaminated to form ammonium, which accumulates in pore water, thereby elevating the pore water DIN concentration and making interstitial environments a source of DIN to primary producers and bacterioplankton.

The amount of pore water DIN that is taken up by bacterioplankton is highly dependent on the lability, and hence composition, of DOM sources that enable bacterioplankton growth and metabolism (Kirchman et al., 1990; Wheeler and Kirchman, 1986). In addition to the often large difference in DIN and DON concentration between seawater and pore water, DOM composition often differs between seawater and pore water as well, which can alter the lability of DOM compounds to bacterioplankton, and therefore magnitude of bacterioplankton DIN uptake. Fluorescence spectroscopy has been used to examine differences in the composition of DOM through the identification of important chemical compound classes in marine environments, such as humic substances (HS) and amino acids (e.g., tyrosine and tryptophan), which fluoresce when exposed to ultraviolet (UV) and visible light (Coble et al., 1990; Stedmon and Markager, 2005).

The respiratory quotient (RQ), which is the ratio of the production of CO_2 to the consumption of dissolved oxygen (O_2), is a complementary measure to fluorescence spectroscopy that can indicate the broad compound classes of DOM that are respired by

bacterioplankton communities (Berggren et al., 2011). RQs less than 1 can indicate metabolism of O-poor DOM, such as amino acids and lipids, whereas RQs greater than 1 can indicate metabolism of O-rich substrates such as carbohydrates (Dilly, 2001). In addition, assumed RQs, in the range of 0.7 to 1.2, are routinely used as conversion factors to derive CO_2 production estimates from O_2 consumption data in studies of microbial respiration in marine environments (Berggren et al., 2011). However, RQs can be temporally variable, reflecting changes in available DOM sources and consequently the apportionment of the carbon (C) and oxygen (O) contained within the DOM toward respiratory (i.e., ATP-generating) and biosynthetic (i.e., biomass and enzyme formation) pathways (Dilly, 2001). Bacterioplankton are the primary mineralizers of DOM in marine environments, therefore making accurate assessments of CO_2 production derived from O_2 consumption (i.e. RQs) important in accurately describing dissolved organic and inorganic carbon dynamics in marine systems.

In this study, I assessed how DOM composition and temporal alterations in DOM composition in seawater and pore water influence DIN uptake, using a combination of excitation emission matrix (EEM) fluorescence spectroscopy, respiratory quotient determinations, and DIN (i.e., ammonium and nitrate) concentration analysis in a 7-day time-series dark incubation. I hypothesized that the mixing of seawater and pore water would provide labile DOC sources from water column primary production (i.e., DCHO) that would allow higher DIN uptake than that observed for seawater or pore water alone (i.e., 100% seawater or 100% pore water).

Methods

Seawater and pore water collection

Seawater and pore water samples were collected in beaches along the Santa Barbara, California coastline over two sampling periods (May 2014 and June/July 2014). Twenty liters of seawater were collected at ~ 0.5 m depth in the surf zone by submerging a carboy underwater and filling to capacity. For pore water collection, a stainless-steel, hollow point piezometer tipped with a 2 cm slotted screen was hand-driven into the sand approximately 0.3 m into the seepage face of the beach. Tygon tubing was attached to the top of the piezometer and connected to a peristaltic pump (GeoTech, Inc.). Sixteen liters of pore water was pumped at a rate of ~ 0.5 L min^{-1} into a 20 L carboy. Both the seawater and pore water carboys (20 L each) were immediately returned to the laboratory and placed in a 14°C cold room with caps loosely screwed on to allow gas exchange. The average coastal sea surface temperature in Santa Barbara is 14°C (NOAA).

Seawater and pore water incubation preparation and sampling

Collected seawater and pore water were allowed to sit in the 14°C cold room for a period of ~ 24 hours. After this period, seawater and pore water were gravity-filtered through 142 mm 0.2 µm pore size nitrocellulose filters with a 1.2 µm nitrocellulose pre-filter (Millipore) and apportioned into 5 L multi-layer gas sampling bags (Restek) fitted with 3/16" polypropylene inlet valves, hereafter referred to as treatment bags. Seawater and pore water carboys were continuously stirred using magnetic stir bars and stir plates for the duration of the filtering and establishment of the treatment bags. Three different volumetric combinations of filtered seawater and pore water were established with two treatment bags per combination—4 L seawater/0 L pore water (SW treatment), 2 L seawater/2 L pore water

(SW/PW treatment), and 0 L seawater/4 L pore water (PW treatment). After the volumes of seawater and pore water were distributed into their respective bags (total of 6 treatment bags, 2 bags per volume combination), 1 L of inoculum was gravity-fed into each treatment bag in sequence through a 47 mm 2.7 μm pore size glass-fiber filter. All volumes were determined gravimetrically using a mean measured seawater density of 1.01 g mL^{-1}. Treatment bags were each placed on an oscillating shaker for 10-15 minutes to allow water to mix and homogenize. Treatment bags remained in a 14°C cold room and were subsequently gravity-sampled daily for a range of analytes (see below) for the duration of a 10-day (May) and 7-day (June/July) incubation period. The duration of each incubation was determined by the period over which CO_2 production and O_2 consumption was linear. On each day of sampling, treatment bags were placed on an oscillating shaker for 5-10 minutes prior to sample collection to mix and homogenize treatment water inside the bag before sample collection.

Dissolved carbon and nitrogen sample collection and analysis

Dissolved organic carbon (DOC) and total dissolved nitrogen (TDN) water samples were gravity-filtered with 0.7 μm GFF filters and collected in duplicate in 40 mL Qorpak Kaptclean vials. Ammonium (NH_4^+) and nitrate ($NO_2^- + NO_3^-$) samples were gravity-filtered with 0.7 μm GFF filters and collected in duplicate in 14 mL polycarbonate tubes. Both DOC and TDN and ammonium and nitrate samples were frozen after collection.

DOC and TDN were measured by high temperature combustion (HTC) using a Shimadzu (Shimadzu) TOC-V_{CSH} system coupled with a Shimadzu Total N analyzer (Letscher et al., 2013). The N oxidation product nitric oxide (NO) was quantified by reaction

with ozone and detection of the resulting chemiluminescence. The precision for DOC and TDN was ± 1 to 2 µmol L^{-1}. Ammonium and nitrate concentrations were determined on a Lachat Flow Injection Autoanalyzer (Hach Company). Ammonium was measured by adding base to the sample stream, which converted NH_4^+ to NH_3. Nitrate was measured using the Griess-Ilosvay reaction after cadmium reduction. The detection limit for both ammonium and nitrate was 0.5 µmol L^{-1}, precision was ± 0.4 µmol L^{-1} for ammonium and ± 0.1 µmol L^{-1} for nitrate, and accuracy was ± 6% for both ammonium and nitrate. Dissolved organic nitrogen (DON) was calculated as the difference between TDN and the sum of ammonium and nitrate.

pCO_2, pH, dissolved O_2, and temperature sample collection and analysis

Dissolved O_2 samples were gravity-collected unfiltered in 125 mL rectangular polycarbonate bottles and measured using a YSI ProODO (YSI Inc.,Yellow Springs, OH) optical dissolved oxygen unit. Immediately after collection the optical probe was inserted into the mouth of the 125 mL bottle and excess sample water was displaced, ensuring the probe remained fully submersed. Sample temperature was allowed to equilibrate for 10 minutes, whereupon dissolved O_2 (in both concentration and % saturation units), barometric pressure, and temperature (T) measurements were recorded. Dissolved O_2 concentrations were corrected for specific conductance and temperature following Benson and Krause (1984). Accuracy of dissolved O_2 measurements per manufacturer specification was ± 3 µM.

Forty mL of sample water for CO_2 samples were gravity-collected unfiltered in a 140 mL polycarbonate syringe and subsequently shaken and equilibrated with 100 mL of ambient air for 1 minute. Background air CO_2 (ppmv) was recorded before injecting the sample

headspace into an EGM-4 infra-red gas analyzer (PP Systems). The sample CO_2 measurement was allowed to stabilize for ~ 10 – 20 seconds before recording. Water CO_2 concentration (μM) was calculated using the CO_2 solubility coefficient at the measured water temperature and seawater density (Weiss, 1974) with correction for background air CO_2.

pH samples were collected in 50 mL Falcon tubes, and measured within 1 to 2 hours of sampling on an Oakton Ion 510 series pH meter using a temperature compensation probe. A 3-point calibration was performed using pH buffer solutions of 4.0, 7.0, and 10.0. Accuracy per manufacturer specifications was ± 0.01 pH.

Respiratory quotients (RQs)

The respiratory quotient (RQ), which is the ratio of CO_2 production to O_2 consumption, was calculated for each treatment bag using the ratio of the linear regression slopes for CO_2 and O_2 measurements (m_{CO2} and m_{O2}) for the 7-day incubation ($RQ = m_{CO2}/m_{O2}$) (Berggren et al., 2011). Nitrification can potentially bias O_2 consumption estimates since O_2 is a required substrate for the oxidation of ammonium and nitrite (Dilly, 2003); two moles of O_2 are consumed per 1 mole of nitrate produced in a complete nitrification reaction (Ebeling et al., 2006). I used the mean nitrate concentrations observed on day 7 for each treatment to calculate a mean nitrate production rate over the 7-day incubation. Although nitrate formation did not begin until around days 4 to 5, the 7-day average rate is calculated over the same interval as the CO_2 production and O_2 consumption estimates, and therefore can be subtracted from the O_2 consumption rate to yield O_2 consumption due solely to DOM oxidation (i.e. not resulting from consumption by nitrification).

Fluorescent dissolved organic matter (FDOM) sample collection and analysis

Fluorescent dissolved organic matter (FDOM) samples were collected and analyzed for the June/July incubation only. Samples were gravity-filtered with 0.7 μm GFF filters and collected in 14 mL Falcon tubes, and were then analyzed on a Varian Cary Eclipse fluorimeter using a 10 mm quartz cuvette (Helma Analytics). Samples were scanned over excitation wavelengths of 240 to 450 nm and emission wavelengths of 300 to 600 nm, with a band pass of 10 nm for excitation and 2 nm for emission scans. Two Nanopure water blanks were run for discrete sample sets, with their fluorescence intensities subtracted from sample fluorescence intensities. All samples were Raman-calibrated using the Raman fluorescence peak between the 370 and 428 nm emission wavelengths for an excitation wavelength of 350 nm. First and second order Rayleigh scatter peaks were removed from all excitation-emission matrices (EEMs) Blank subtraction and Raman-calibration yielded fluorescence intensity values in Raman Units (RU). Excitation-emission matrices (EEMs) were constructed from FDOM data measured for each treatment bag during each sampling day (n = 42 for 7-day incubation period) using the fluorescence intensities (RU) measured over the range in excitation (240 to 450 nm) and emission (300 to 600 nm) wavelengths.

Results

Ammonium was the dominant form of dissolved inorganic nitrogen in the SW/PW and PW treatments, but was undetectable for the duration of the incubation in the SW treatment (Table 1). On day 1 of the incubation ammonium concentration was initially 41.3 ± 0.6 μM (mean ± 1 standard deviation) and 42.0 ± 0.1 μM in the two PW treatment bags,

and 21.4 ± 0.4 µM and 21.1 ± 0.1 µM in the two SW/PW treatment bags. Ammonium showed apparent slight to no decrease by the end of the incubation in the PW treatment bags, dropping to only 39.7 ± 0.1 µM and 41.9 ± 0.2 µM on day 7 (Figure 1). In the SW/PW treatment bags, ammonium showed larger decreases than the PW treatment bags, with ammonium concentration decreasing to 14.9 ± 0.1 µM and 14.6 ± 0.1 µM on day 7 (Figure 1). Nitrate was initially undetectable in all treatment bags, but increased to 0.9 ± 0.5 µM in one of the SW treatment bags (the other remained undetectable), 2.0 ± 1.3 µM and 1.9 ± 0.9 µM in the SW/PW treatment bags, and 1.3 ± 1.1 µM and 1.3 ± 1.0 µM in the PW treatment bags.

For the May incubation, carbon dioxide (CO_2) production was highest for the PW treatment at 1.8 and 2.8 µM CO_2 d^{-1} and lowest for the SW/PW treatment at 1.1 and 1.2 µM CO_2 d^{-1} (Table 1). Dissolved oxygen (O_2) consumption was highest for the PW treatment at 2.5 and 4.5 µM CO_2 d^{-1} and lowest for the SW/PW treatment at 1.2 and 1.5 µM CO_2 d^{-1} (Table 1). For the June/July incubation, CO_2 production was highest for the SW/PW treatment at 4.2 and 5.6 µM CO_2 d^{-1} and lowest for the SW treatment at 0.6 µM CO_2 d^{-1} and negative in the second SW treatment bag (indicating consumption of CO_2) (Figure 2; Table 1). Dissolved oxygen consumption was highest for the SW/PW treatment at 8.8 and 9.9 µM O_2 d^{-1} and lowest for the SW treatment at 4.0 and 4.8 µM O_2 d^{-1} (Figure 2; Table 1). The pH values for the SW, SW/PW, and PW treatments bags for the May incubation were 7.74 ± 0.02 and 7.79 ± 0.03, 7.72 ± 0.02 and 7.73 ± 0.02, and 7.58 ± 0.03 and 7.62 ± 0.03, respectively, and for the June/July incubation were 8.12 ± 0.01 and 8.15 ± 0.02, 7.85 ± 0.03 and 7.83 ± 0.04, and 7.55 ± 0.02 and 7.55 ± 0.02, respectively (Table 1). Variability in pH

was due to uniform pH declines in all treatments. Water temperatures in all treatments for the May incubation were 15.0 ± 0.1°C and for the June/July incubation were 14.8 ± 0.2°C.

Respiratory quotients (RQs) ranged from 0.46 to 1.03 in the May incubation for all treatments, and from 0.30 to 0.59 in the June/July incubation for SW/PW and PW treatments (Table 1). Due to the low CO_2 production rate for one of the SW treatment bags, and negative production (i.e., consumption) of CO_2 for the other SW treatment bag in the June/July incubation, RQs for the SW treatment were 0.16 and -0.06 even after correcting for O_2 consumption due to nitrification (Table 1). Nitrification-corrected RQs for the SW/PW and PW treatments, ranging from 0.31 to 0.63, were similar to the uncorrected RQs and indicated minor influence of nitrification on RQs in these two treatments.

Three excitation-emission regions of maximal FDOM fluorescence were identified, corresponding to UV and visible humic-like regions at excitation/emission wavelengths of 250/427 nm and 335/426 nm, respectively, and one protein-like peak at 240/313 nm (Figure 3). All three treatments showed similar increases in protein-like peak fluorescence over the 7-day period (Figure 4). PW FDOM fluorescence was initially highest at 0.02 and 0.03 RU, with SW lowest at 0.01 to 0.02 RU. The SW/PW and SW FDOM fluorescence showed a linear increase between days 2 and 5, whereas PW FDOM showed a maximal increase between days 2 and 3 and appeared to asymptote around 0.06 RU. The SW/PW and SW FDOM showed a decrease from days 5 to 6, and then the highest rates of fluorescence increase from day 6 to 7. By day 7, the SW/PW FDOM had attained the highest fluorescence (0.09 and 0.13 RU), SW was second highest at 0.07 and 0.08 RU, and PW was lowest at 0.06 and 0.07 RU (Figure 4). In addition, the emission wavelength of peak fluorescence for the protein-like peak exhibited a red-shift (i.e., increase in wavelength) for PW FDOM relative to

SW FDOM, with the SW/PW FDOM samples appearing to be intermediate between the two wavelengths

UV and visible humic-like fluorescence (excitation/emission wavelengths of 250/427 and 335/426) showed a similar pattern in all three treatments, with PW consistently highest, SW/PW intermediate, and SW lowest in fluorescence intensity (Figures 5 and 6). Initial fluorescence intensities for PW, SW/PW, and SW FDOM were ~ 0.22, 0.14, and 0.06 RU, respectively, for the UV humic-like peak, and ~ 0.11, 0.06, and 0.01 RU for the visible humic-like peak, respectively. There was a sharp increase in the fluorescence intensity of all treatments between days 2 and 3 (Figures 5 and 6). Thereafter fluorescence intensities for both visible and UV humic-like regions remained elevated and more or less constant. However, the visible humic-like mean fluorescence intensities for the SW/PW treatment (average of both treatment bags per day) and the UV humic-like mean fluorescence intensities for the PW treatment showed significant declines from day 3 to 7, at -0.003 RU d^{-1} (95% confidence interval (CI) = -0.005, -0.001) and -0.010 RU d^{-1} (95% CI = -0.017, -0.003), respectively (Figures 5 and 6).

Discussion

The very low and negative RQs observed for the SW treatment bags over the course of the 7-day June/July incubation were perplexing, as I was able to detect small but significant increases in CO_2 production for the May SW treatment (1.4 and 1.6 µM d^{-1}), and I detected higher O_2 consumption rates in the June/July SW incubation (4.2 and 5.0 µM d^{-1}) than in the May incubation (2.4 and 3.6 µM d^{-1}), indicating active DOM oxidation by the bacterioplankton community. The low RQs in the June/July incubation are likely explained

by $CaCO_3$ (calcite) formation, as pH was very high (8.13 and 8.17) for the SW treatment bags at the beginning of the June/July incubation (Berggren et al., 2011; Hammes and Verstraete, 2002). In contrast, pH values were lower (7.75 and 7.76) for the SW treatment bags in the May incubation. High pH and alkalinity, as seen in the June/July SW incubation, can convert much of the respired CO_2 to $CaCO_3$ (Hammes and Verstraete, 2002). Regardless of this CO_2 loss, the SW treatment bags had the lowest RQs in the May incubation, and likely also the lowest for the June/July incubation since the pattern in the magnitude of RQs was identical (i.e., SW/PW RQ > PW RQ > SW RQ).

A strong negative relationship has been observed between RQ and net autotrophy in an analysis of freshwater lake ecosystems (Berggren et al., 2011). I saw a similar pattern in our coastal marine ecosystem, as pore water is a heterotrophic-dominated system relative to the seawater. In seawater, active phytoplankton communities can contribute a higher abundance of relatively O-poor cellular substrates that bacterioplankton respire (Hedges et al., 2002). Although phytoplankton exude O-rich substrates, such as carbohydrates, that can periodically elevate the O:C ratio of DOM (Larsson and Hagström, 1979), the RQs for the SW treatment bags indicate that these exudates were either not abundant in the water column at the time of sampling, or were not used at the same rate as O-poor cellular substrates.

Overall, the RQs for all treatments for both May and June/July incubations ranged from a low of 0.31 to a high of 1.03, indicating bacterioplankton oxidation of reduced, relatively O-poor DOM compounds (e.g., lipids, proteins) relative to RQs observed in other marine studies (Oviatt et al., 1986). The RQs from the SW treatment bags for the May incubation, 0.46 and 0.58, are 17% to 62% lower than the RQs (0.7 to 1.2) that are typically assumed for open water bacterioplankton respiration (Berggren et al., 2011; Oviatt et al.,

1986), and all but three of the measured RQs fell below 0.7 (Table 1). The SW/PW and PW treatments both had higher RQs than the SW treatment, indicating bacterioplankton oxidation of relatively O-rich DOM, although this SW/PW and PW DOM would still be considered O-poor compared to environments with more abundant carbohydrate sources that elevate the RQ to 1 or higher (Oviatt et al., 1986). Marine humic substances (HS) can have relatively high O content, ~ 30 – 50% (ash-free dry mass), due to the presence of carboxyl and carbonyl functional groups (Rashid and King, 1971). HS comprise a large fraction of DOM and are often considered refractory due their complex structure and high aromaticity (McKnight et al., 2001), although some studies have shown that this is not necessarily the case, and some HS may be biologically labile (Miller and Moran, 1997; Nieto-Cid et al., 2006). Important precursor molecules in the formation of marine HS are carbohydrates and amino acids derived from phytoplankton cells. These compounds are progressively degraded by microbial activity, allowing for abiotic condensation reactions that can form HS and contribute O-containing functional groups to HS chemical structures (Obernosterer and Herndl, 2000; Tranvik, 1993). Carbohydrates and amino acids are often found in higher concentration in marine pore water compared to seawater environments, and their active degradation can result in higher concentrations of HS in pore water relative to seawater (Henrichs, 1992). I observed a pattern of overall higher peak fluorescence intensities in pore water relative to seawater for both humic-like peaks (UV and visible; Figures 5 and 6), indicating that pore water likely had a higher concentration of HS than seawater.

Both the FDOM and RQ data indicate that relatively O-rich HS may have contributed to bacterioplankton respiration in the 7-day June/July incubation. Theoretical RQs for the oxidation of a model terrestrial HS compound ($C_{308}H_{328}O_{90}N_5$) range from 0.29 to 0.91

(Dilly, 2001), and the RQ values for PW treatment bags fall within this range (0.42 and 0.63 for the June/July incubation). Further, there was a significant decline in peak fluorescence intensities in the UV humic-like peak for PW from days 3 to 7 (Figures 5 and 6). This decline was not observed in the SW treatment, which showed essentially no change in fluorescence over that time period (i.e., increase of 0.001 RU) (Figure 5). For the visible humic-like peak, there was a significant decline in peak fluorescence intensity in the SW/PW treatment and no change in the SW treatment from days 3 to 7 (i.e., decrease of 0.001 RU) (Figure 6). The FDOM compounds that contribute to the visible humic-like fluorescence peak are considered more labile than those contributing to UV humic-like fluorescence (Stubbins et al., 2014).

The declines in both UV and visible peak fluorescence indicate a loss of HS that can only be due to bacterioplankton oxidation, as treatments were incubated in the dark and therefore not subject to potential photochemical oxidation. In natural marine settings, photochemical degradation is one of the main causes of HS oxidation, although bacterioplankton oxidation is also important. The latter is particularly enhanced by photochemical oxidation that produces smaller molecular weight HS that are more easily metabolized by the bacterioplankton community (Amador et al., 1989; Miller and Moran, 1997). Photochemical oxidation can explain the lower initial fluorescence in SW on day 1 of the incubation, and perhaps the absence of decreases in peak UV and visible humic-like fluorescence that is seen in the SW/PW and PW treatments over the 7-day incubation (Figures 5 and 6). Photochemical oxidation in seawater produces CO_2 and CO from HS, decreasing O:C ratios of the residual HS. The low RQs in the SW treatment bags could in part be a product of bacterioplankton oxidation of photochemically-altered HS with low O:C

ratios, although at lower rates than the SW/PW and PW treatment bags as indicated by the lower O_2 consumption rate in the SW treatment bags (Table 1). Therefore the 7-day incubation may have been too short to detect a decrease in SW UV and visible humic-like fluorescence. Longer time-series incubations could identify whether there is indeed a decrease in humic-like fluorescence for SW.

The dramatic increase in both UV- and visible-like fluorescence intensities from day 2 to 3 in all treatments (Figures 5 and 6) indicated rapid production of HS, which is commonly observed in other studies of HS production due to bacterioplankton degradation (Lønborg et al., 2009; Nieto-Cid et al., 2006; Yamashita and Tanoue, 2003). Further, this increase coincided with an increase in protein-like fluorescence (excitation/emission wavelengths of 240/313), which is also consistent with rapid mineralization of DOM, producing DON substrates (e.g., amino acids). The degradation products of these substrates are important precursors to the formation of HS (Nissenbaum and Kaplan, 1972). The rate of increase in protein-like fluorescence between days 2 and 3 was highest for the PW treatment, but thereafter PW increases appeared to be overall lower than both the SW/PW and SW treatments (Figure 4), likely due to the onset of bacterioplankton carbon-limitation. This onset is apparent in the ammonium concentration data of both PW treatment bags, as ammonium decreased for the first 3 days of the incubation, but then increased on day 4, and remained at or slightly lower than ammonium concentrations on day 1 (Figure 1). The increase on day 4 was likely the result of amino acid respiration under limiting supply of C-rich substrate. Carbon-limitation can also explain the decrease in UV- and visible-like fluorescence between days 3 to 7. During this period bacterioplankton were likely non-discriminatively metabolizing any carbon sources available, including HS, which are

typically less labile than other DOM forms. This pattern is also observed in the SW/PW treatment bags up until days 5 through 7. At this time, ammonium in the SW/PW incubations linearly declined to reach a concentration that was ~ 6 – 7 µM lower on day 7 than that of day 1, compared to ammonium concentrations on day 7 in the PW treatment bags, which were 0.6 µM higher and 2.3 µM lower than day 1 (Figure 1). The PW treatment bags therefore showed ammonium changes by day 7 that were 6% lower and 2% higher than initial ammonium concentrations on day 1, whereas the SW/PW treatments bags showed ammonium changes that were 29% and 32% lower by day 7 relative to day 1 (Figure 1). This pattern, as well as higher CO_2 consumption rates in the SW/PW treatment (Table 1), indicated that the lability of seawater DOM and/or HS produced under SW/PW mixing is likely greater than that of pore water DOM, which allowed higher % usage of DIN (ammonium) from pore water.

In summary, I have shown that RQs ranged from 0.31 to 1.02 (Table 1) over the 7-day incubation period, indicating oxidation of reduced compounds such as proteins, lipids, and possibly humic substances (HS). Plots of peak fluorescence intensity showed rapid increases in both UV and visible humic-like fluorescence in all treatments between days 2 and 3, followed by significant decreases in UV humic-like fluorescence for PW and visible humic-like fluorescence for SW/PW for day 3 through 7 (Figures 5 and 6). No change in the SW treatment was seen for either types of humic-like fluorescence between days 3 and 7 (Figures 5 and 6). The significant decline for the SW/PW treatment visible humic-like fluorescence, not seen in the SW or PW treatments, may indicate different pathways of HS formation and chemical structures of HS produced under seawater and pore water mixing. Combining the plot of peak protein-like fluorescence with the ammonium concentration

time-series indicated that the decrease in UV humic-like fluorescence seen in the PW treatment was likely the result of C-limitation inducing oxidation of less labile compounds such as HS, as ammonium concentration declined from day 1 through 3 but peaked on day 4 and remained elevated for the remainder of the incubation (Figure 1). This coincided with protein-like fluorescence intensities for the PW treatment that remained fairly constant from day 3 through 7, indicating greater reliance on oxidation of DON compounds such as amino acids than the SW/PW treatment, which showed an overall greater increase in protein-like fluorescence (Figure 4) and greater decrease in ammonium concentration (Figure 1). Mixing of seawater and pore water (SW/PW treatment) lead to ammonium concentration declines between 29% and 32%, whereas pore water alone (PW treatment) only showed a decline of 6% and increase of 2% over the course of the incubation (Figure 1). This illustrates the important coupling between interstitial and seawater environments in shallow coastal marine areas, where seawater and pore water mixing can enhance bacterioplankton uptake of the DIN produced within sediments. This enhanced DIN uptake may be the product of more labile seawater DOM and/or the formation of more labile DOM (e.g., HS) under seawater and pore water mixing.

Tables and Figures

Table 1. Mean ammonium and nitrate concentrations (± 1 SD), mean pH, CO_2 production rates, O_2 production rates, and respiratory quotients (RQs) for May and June/July dark incubations

			Ammonium (µM)	Nitrate (µM)	pH	m CO2 (µM d^{-1})	m O2 (µM d^{-1})	Respiratory quotient (RQ)
May	SW	1	-	-	7.74 ± 0.02	1.6	3.6	0.46
		2	-	-	7.79 ± 0.03	1.4	2.4	0.58
	SW/PW	1	-	-	7.72 ± 0.02	1.1	1.5	0.78
		2	-	-	7.73 ± 0.02	1.2	1.2	1.03
	PW	1	-	-	7.58 ± 0.03	2.8	4.5	0.63
		2	-	-	7.62 ± 0.03	1.8	2.5	0.72
June/July	SW	1	0.5	0.7 ± 0.5	8.12 ± 0.01	*0.6*	4.0	0.16
		2	0.5	0.5	8.15 ± 0.02	*-0.3*	4.8	-0.06
	SW/PW	1	17.9 ± 2.3	0.9 ± 0.8	7.85 ± 0.03	5.6	8.8	0.63
		2	18.0 ± 2.0	0.9 ± 0.7	7.83 ± 0.04	4.2	9.9	0.42
	PW	1	39.9 ± 1.9	0.8 ± 0.5	7.55 ± 0.02	3.5	7.9	0.44
		2	40.7 ± 2.3	0.7 ± 0.4	7.55 ± 0.02	*2.2*	7.1	0.31

Italics = not significant at 95% confidence level

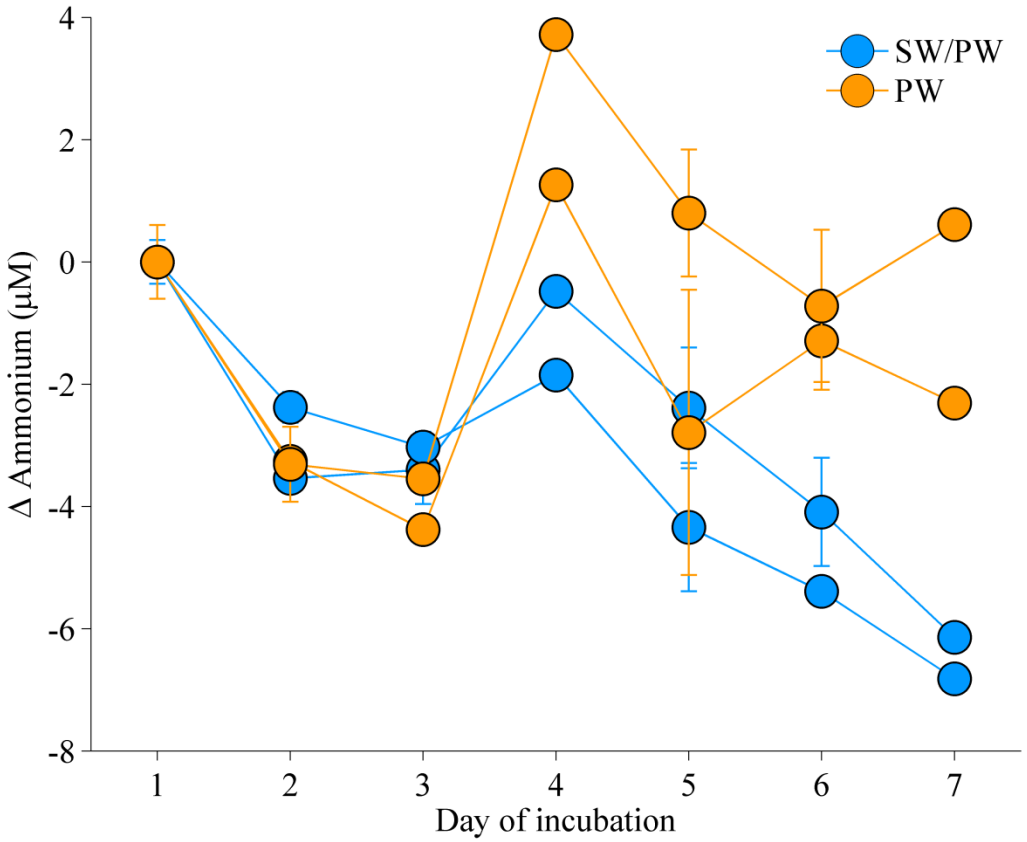

Figure 1. Time series of ammonium concentration changes for the June/July incubation. Values are normalized by subtraction of ammonium concentrations observed on day 1 of the incubation for each treatment bag.

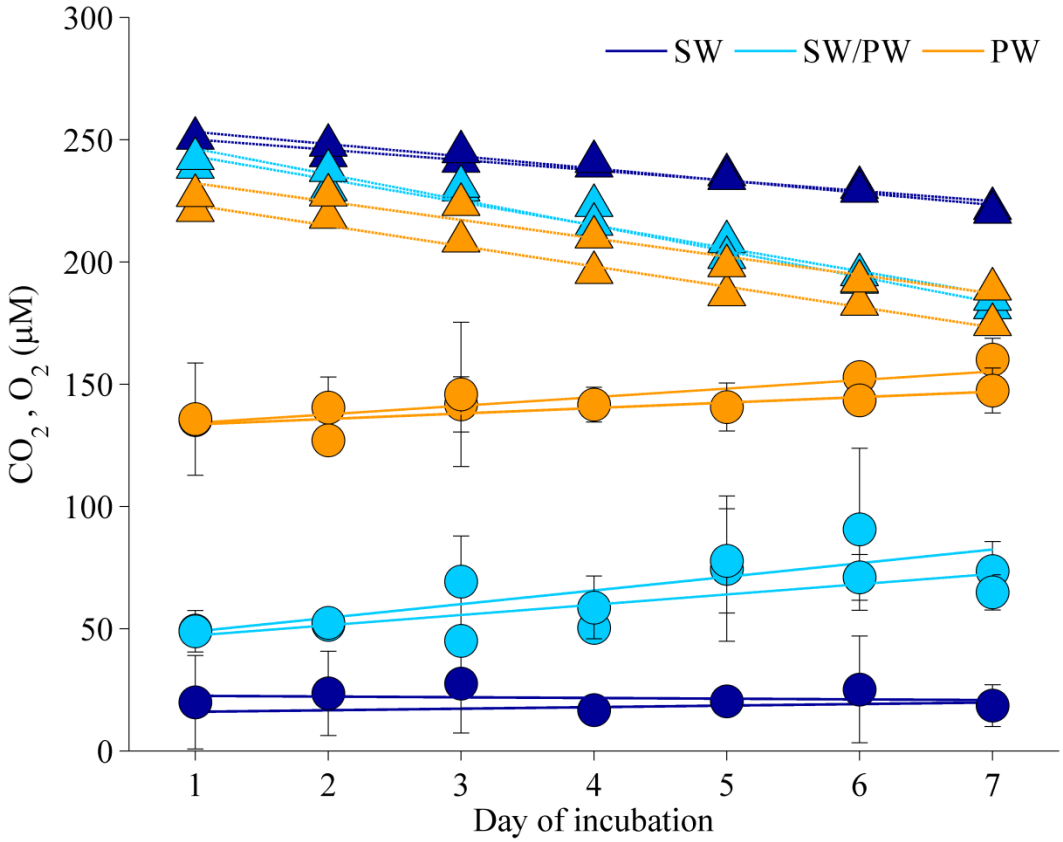

Figure 2. Time series of CO_2 (circles) and O_2 (triangles) concentrations for all treatments in the June/July incubation with linear fits. Error bars denote ± 1 standard deviation.

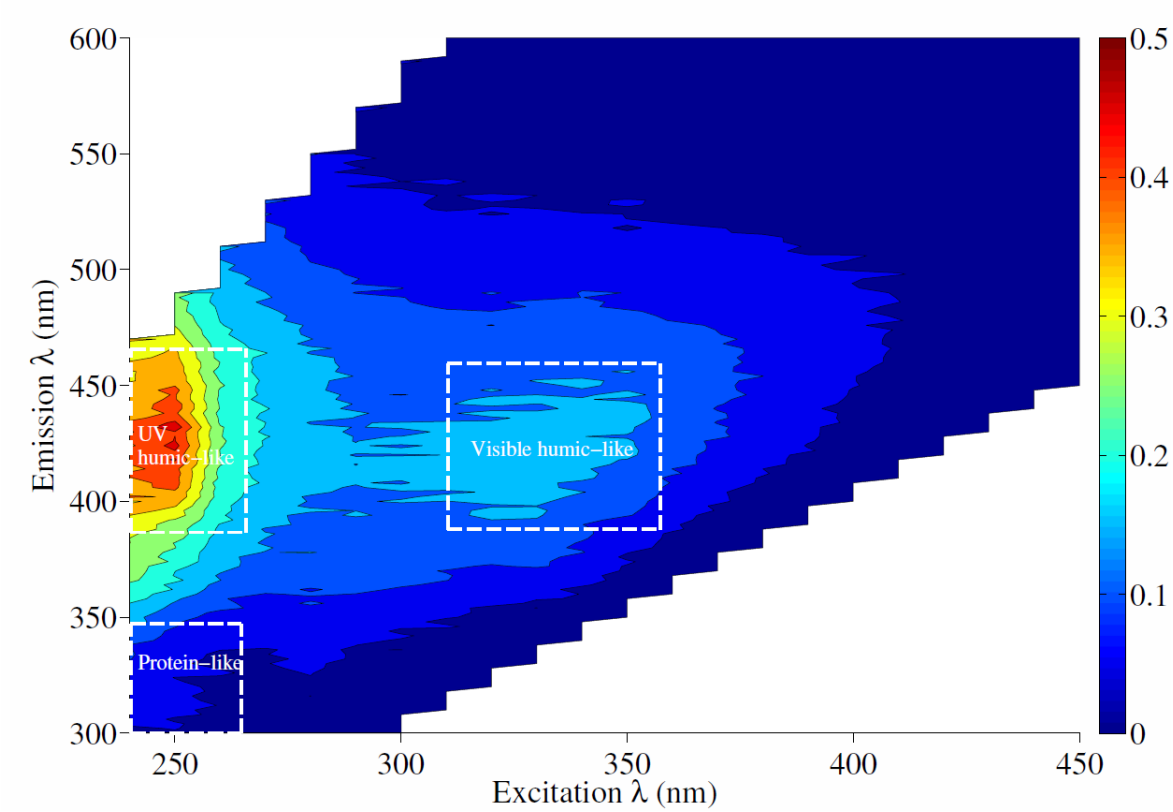

Figure 3. Example of excitation-emission matrix (EEM) showing three identified peak fluorescence regions: UV humic-like, visible humic-like, and protein-like. The z-axis is in Raman Units (RU).

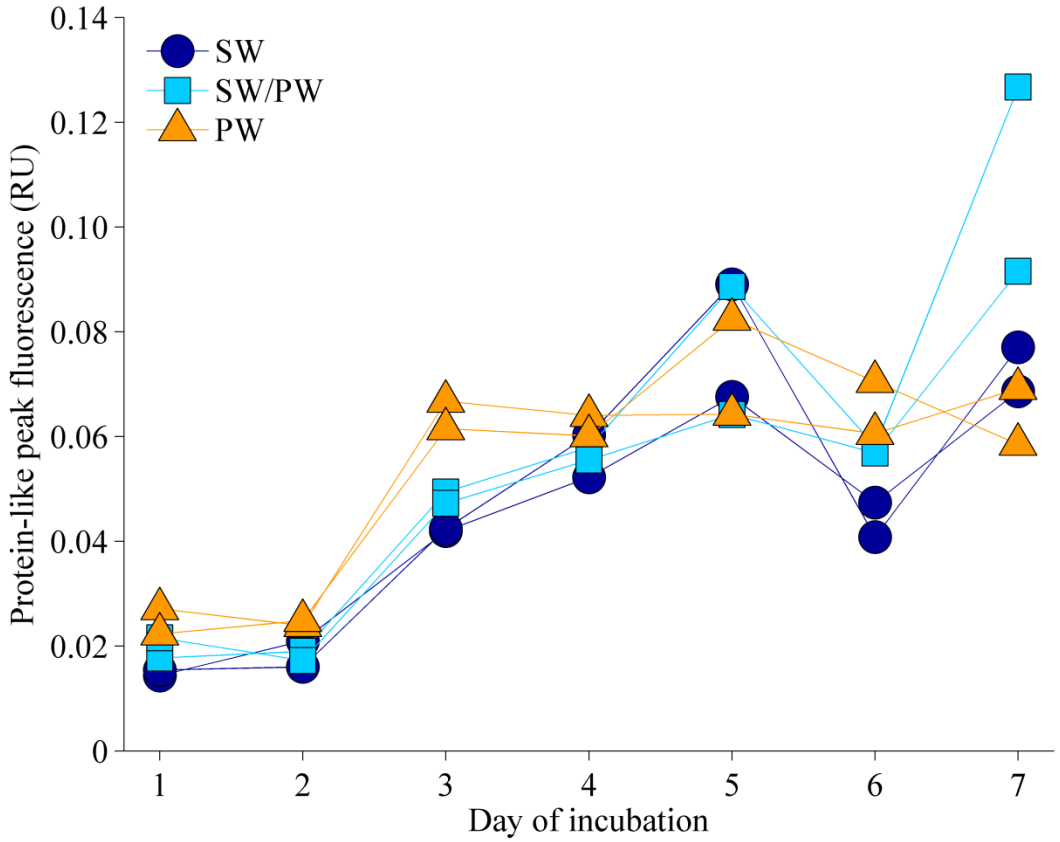

Figure 4. Time series of protein-like peak fluorescence intensities for three treatments in the June/July incubation.

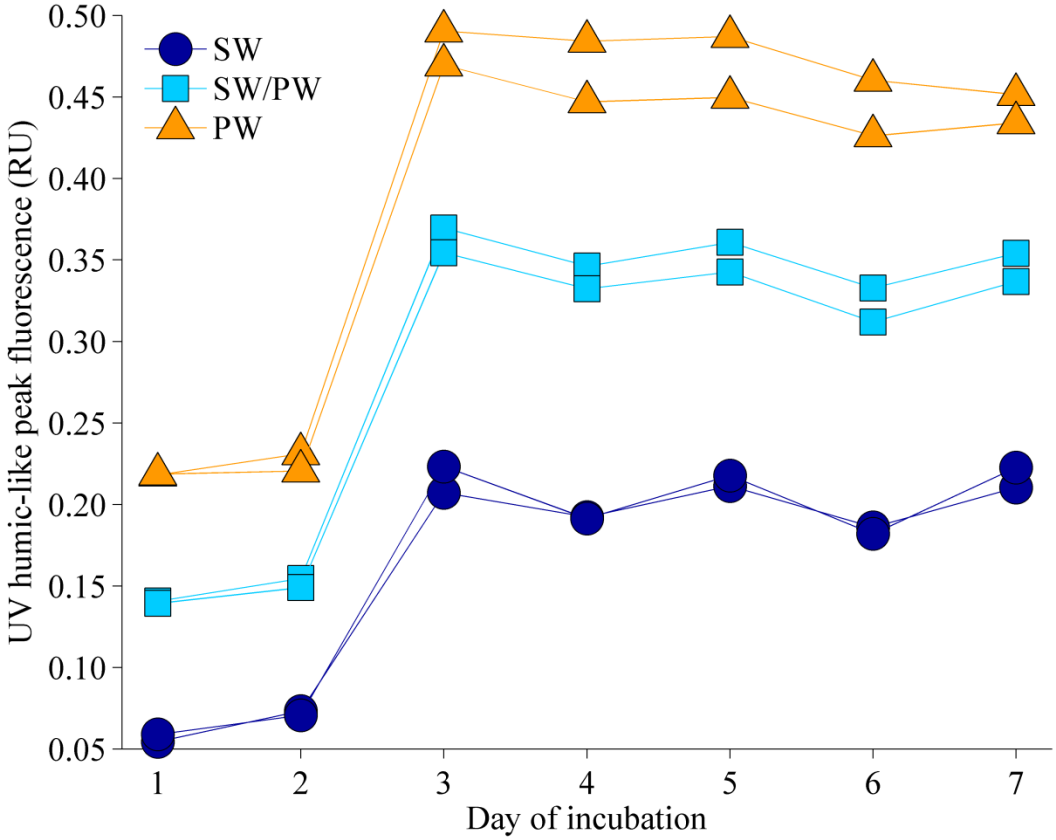

Figure 5. Time series of UV humic-like peak fluorescence intensities for three treatments in the June/July incubation.

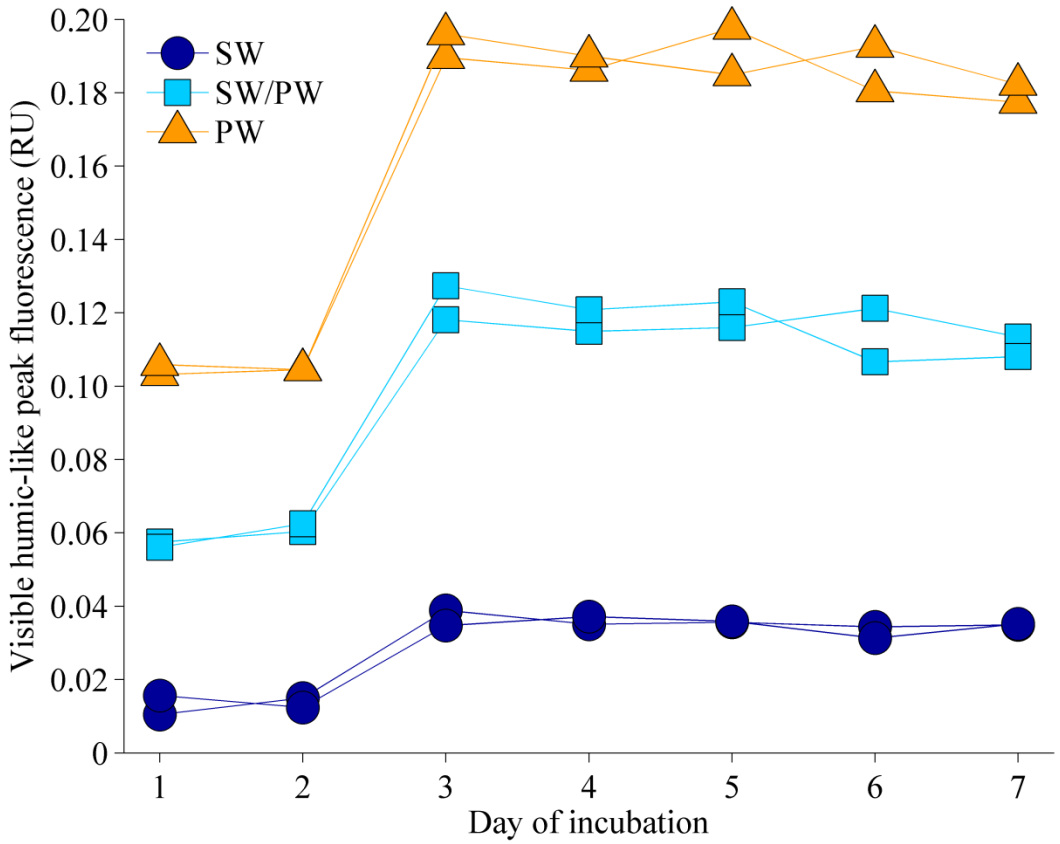

Figure 6. Time series of visible humic-like peak fluorescence intensities for three treatments in the June/July incubation.

References

Alexander, R.B., Boyer, E.W., Smith, R.A., Schwarz, G.E. and Moore, R.B., 2007. The role of headwater streams in downstream water quality. Journal of the American Water Resources Association, 43(1): 41-59.

Almasri, M.N. and Kaluarachchi, J.J., 2004. Assessment and management of long-term nitrate pollution of ground water in agriculture-dominated watersheds. Journal of Hydrology, 295(1-4): 225-245.

Amador, J.A., Alexander, M. and Zika, R.G., 1989. Sequential photochemical and microbial degradation of organic molecules bound to humic acid. Applied and Environmental Microbiology, 55(11): 2843-2849.

Amon, R.M., Fitznar, H.-P. and Benner, R., 2001. Linkages among the bioreactivity, chemical composition, and diagenetic state of marine dissolved organic matter. Limnology and Oceanography, 46(2): 287-297.

Anderson, D.M., Glibert, P.M. and Burkholder, J.M., 2002. Harmful algal blooms and eutrophication: nutrient sources, composition, and consequences. Estuaries, 25(4): 704-726.

Arnosti, C., Repeta, D. and Blough, N., 1994. Rapid bacterial degradation of polysaccharides in anoxic marine systems. Geochimica et Cosmochimica Acta, 58(12): 2639-2652.

Avila, A., Pinol, J., Roda , F. and Neal, C., 1992. Storm solute behaviour in a montane Mediterranean forested catchment. Journal of Hydrology, 140(1-4): 143-161.

Barco, J., Hogue, T.S., Curto, V. and Rademacher, L., 2008. Linking hydrology and stream geochemistry in urban fringe watersheds. Journal of Hydrology, 360(1-4): 31-47.

Barreiro, F., Gómez, M., López, J., Lastra, M. and De la Huz, R., 2013. Coupling between macroalgal inputs and nutrients outcrop in exposed sandy beaches. Hydrobiologia, 700(1): 73-84.

Basu, N.B. et al., 2010. Nutrient loads exported from managed catchments reveal emergent biogeochemical stationarity. Geophysical Research Letters, 37(23): L23404.

Beighley, R.E., Dunne, T. and Melack, J.M., 2008. Impacts of climate variability and land use alterations on frequency distributions of terrestrial runoff loading to coastal waters in Southern California. Journal of the American Water Resources Association, 44(1): 62-74.

Beighley, R.E., Melack, J.M. and Dunne, T., 2003. Impacts of California's climatic regimes and coastal land use change on streamflow characteristics. Journal of the American Water Resources Association, 39(6): 1419-1433.

Belnap, J., Welter, J.R., Grimm, N.B., Barger, N. and Ludwig, J.A., 2005. Linkages between microbial and hydrologic processes in arid and semiarid watersheds. Ecology, 86(2): 298-307.

Benson, B. and Krause, D., Jr., 1984. The concentration and isotopic fractionation of oxygen dissolved in fresh and seawater in equilibrium with the atmosphere. Limnology and Oceanography, 29(3): 620-632.

Berggren, M., Lapierre, J.-F. and del Giorgio, P.A., 2011. Magnitude and regulation of bacterioplankton respiratory quotient across freshwater environmental gradients. The ISME Journal, 6(5): 984-993.

Bernal, S., Butturini, A., Riera, J., Vazquez, E. and Sabater, F., 2004. Calibration of the INCA model in a Mediterranean forested catchment: the effect of hydrological inter-

annual variability in an intermittent stream. Hydrology and Earth System Sciences, 8(4): 729-741.
Bernal, S., Butturini, A. and Sabater, F., 2005. Seasonal variations of dissolved nitrogen and DOC:DON ratios in an intermittent Mediterranean stream. Biogeochemistry, 75(2): 351-372.
Bernot, M.J. and Dodds, W.K., 2005. Nitrogen retention, removal, and saturation in lotic ecosystems. Ecosystems, 8(4): 442-453.
Bertin, C. and Bourg, A.C., 1994. Radon-222 and chloride as natural tracers of the infiltration of river water into an alluvial aquifer in which there is significant river/groundwater mixing. Environmental Science & Technology, 28(5): 794-798.
Bethke, C.M. and Johnson, T.M., 2008. Groundwater age and groundwater age dating. Annual Review of Earth and Planetary Sciences, 36: 121-152.
Biddanda, B. and Benner, R., 1997. Carbon, nitrogen, and carbohydrate fluxes during the production of particulate and dissolved organic matter by marine phytoplankton. Limnology and Oceanography, 42(3): 506-518.
Biersmith, A. and Benner, R., 1998. Carbohydrates in phytoplankton and freshly produced dissolved organic matter. Marine Chemistry, 63(1–2): 131-144.
Billerbeck, M. et al., 2006. Surficial and deep pore water circulation governs spatial and temporal scales of nutrient recycling in intertidal sand flat sediment. Marine Ecology Progress Series, 326: 61-76.
Biron, P.M. et al., 1999. The effects of antecedent moisture conditions on the relationship of hydrology to hydrochemistry in a small forested watershed. Hydrological Processes, 13(11): 1541-1555.
Bolin, B. and Rodhe, H., 1973. A note on the concepts of age distribution and transit time in natural reservoirs. Tellus, 25(1): 58-62.
Boudreau, B.P. et al., 2001. Permeable marine sediments: overturning an old paradigm. Eos, Transactions American Geophysical Union, 82(11): 133-136.
Boyer, E.W. et al., 2006. Riverine nitrogen export from the continents to the coasts. Global Biogeochemical Cycles, 20(1): GB1S91.
Burdige, D.J. and Martens, C.S., 1988. Biogeochemical cycling in an organic-rich coastal marine basin: 10. The role of amino acids in sedimentary carbon and nitrogen cycling. Geochimica et Cosmochimica Acta, 52(6): 1571-1584.
Burdige, D.J. and Zheng, S., 1998. The biogeochemical cycling of dissolved organic nitrogen in estuarine sediments. Limnology and Oceanography, 43(8): 1796-1813.
Burnett, W.C., Bokuniewicz, H., Huettel, M., Moore, W.S. and Taniguchi, M., 2003. Groundwater and pore water inputs to the coastal zone. Biogeochemistry, 66(1-2): 3-33.
Burney, C.M., 1986. Bacterial utilization of total in situ dissolved carbohydrate in offshore waters. Limnology and Oceanography, 31(2): 427-431.
Burns, D.A. et al., 2001. Quantifying contributions to storm runoff through end-member mixing analysis and hydrologic measurements at the Panola Mountain Research Watershed (Georgia, USA). Hydrological Processes, 15(10): 1903-1924.
Buttle, J.M., 1994. Isotope hydrograph separations and rapid delivery of pre-event water from drainage basins. Progress in Physical Geography, 18(1): 16-41.
Butturini, A. and Sabater, F., 2002. Nitrogen concentrations in a small Mediterranean stream: 1. Nitrate 2. Ammonium. Hydrology and Earth System Sciences, 6(3): 539-550.

Canuel, E.A. and Martens, C.S., 1993. Seasonal variations in the sources and alteration of organic matter associated with recently-deposited sediments. Organic Geochemistry, 20(5): 563-577.
Caraco, N.F. and Cole, J.J., 1999. Human impact on nitrate export: an analysis using major world rivers. Ambio, 28(2): 167-170.
Carpenter, S.R. et al., 1998. Nonpoint pollution of surface waters with phosphorus and nitrogen. Ecological Applications, 8(3): 559-568.
Chamran, F., Gessler, P.E. and Chadwick, O.A., 2002. Spatially explicit treatment of soil-water dynamics along a semi-arid catena. Soil Science Society of America Journal, 66(5): 1571-1583.
Christophersen, N., Neal, C., Hooper, R.P., Vogt, R.D. and Andersen, S., 1990. Modeling streamwater chemistry as a mixture of soilwater end-members: a step towards second-generation acidification models. Journal of Hydrology, 116(1-4): 307-320.
Cleveland, W., 1979. Robust locally weighted regression and smoothing scatterplots. Journal of the American Statistical Association, 74(368): 829-836.
Cleveland, W.S., 1981. LOWESS: A program for smoothing scatterplots by robust locally weighted regression. The American Statistician: 54-54.
Cleveland, W.S. and Devlin, S.J., 1988. Locally weighted regression: an approach to regression analysis by local fitting. Journal of the American Statistical Association, 83: 596-610.
Cloern, J.E., 2001. Our evolving conceptual model of the coastal eutrophication problem. Marine Ecology Progress Series, 210(2001): 223-253.
Coble, P.G., Green, S.A., Blough, N.V. and Gagosian, R.B., 1990. Characterization of dissolved organic matter in the Black Sea by fluorescence spectroscopy. Nature(348): 432-435.
Colbert, S.L., Berelson, W.M. and Hammond, D.E., 2008. Radon-222 budget in Catalina Harbor, California: 2. Flow dynamics and residence time in a tidal beach. Limnology and Oceanography, 53(2): 659-665.
de Beer, D. et al., 2005. Transport and mineralization rates in north sea sandy intertidal sediments, Sylt-Rømø Basin, Wadden Sea. Limnology and Oceanography, 50(1): 113-127.
DeFries, R. and Eshleman, K.N., 2004. Land-use change and hydrologic processes: a major focus for the future. Hydrological Processes, 18(11): 2183-2186.
Dennis, R.H. and Hirsch, R.M., 1993. Statistical methods in water resources. Elsevier, Amsterdam, Netherlands.
Di, H.J. and Cameron, K.C., 2002. Nitrate leaching in temperate agroecosystems: sources, factors and mitigating strategies. Nutrient Cycling in Agroecosystems, 64(3): 237-256.
Diaz, R.J. and Rosenberg, R., 2008. Spreading Dead Zones and Consequences for Marine Ecosystems. Science, 321(5891): 926-929.
Dillon, P.J. and Molot, L.A., 1990. The role of ammonium and nitrate retention in the acidification of lakes and forested catchments. Biogeochemistry, 11(1): 23-43.
Dilly, O., 2001. Microbial respiratory quotient during basal metabolism and after glucose amendment in soils and litter. Soil Biology and Biochemistry, 33(1): 117-127.
Dilly, O., 2003. Regulation of the respiratory quotient of soil microbiota by availability of nutrients. FEMS Microbiology Ecology, 43(3): 375-381.

Driscoll, C.T. et al., 2003. Nitrogen pollution in the northeastern United States: sources, effects, and management options. BioScience, 53(4): 357-374.
Dugan, J.E., Hubbard, D.M., Page, H.M. and Schimel, J.P., 2011. Marine macrophyte wrack inputs and dissolved nutrients in beach sands. Estuaries and Coasts, 34(4): 839-850.
Ebeling, J.M., Timmons, M.B. and Bisogni, J., 2006. Engineering analysis of the stoichiometry of photoautotrophic, autotrophic, and heterotrophic removal of ammonia–nitrogen in aquaculture systems. Aquaculture, 257(1): 346-358.
Epstein, S.S., 1997. Microbial food webs in marine sediments. I. Trophic interactions and grazing rates in two tidal flat communities. Microbial Ecology, 34(3): 188-198.
Fierer, N. and Schimel, J.P., 2002. Effects of drying-rewetting frequency on soil carbon and nitrogen transformations. Soil Biology and Biochemistry, 34(6): 777-787.
Freeman, M.C., Pringle, C.M. and Jackson, C.R., 2007. Hydrologic connectivity and the contribution of stream headwaters to ecological integrity at regional scales. JAWRA Journal of the American Water Resources Association, 43(1): 5-14.
Fukuda, R., Ogawa, H., Nagata, T. and Koike, I., 1998. Direct determination of carbon and nitrogen contents of natural bacterial assemblages in marine environments. Applied and Environmental Microbiology, 64(9): 3352-3358.
Galloway, J.N. et al., 2003. The nitrogen cascade. BioScience, 53(4): 341-356.
Galloway, J.N. et al., 2004. Nitrogen Cycles: Past, Present, and Future. Biogeochemistry, 70(2): 153-226.
Godsey, S.E., Kirchner, J.W. and Clow, D.W., 2009. Concentration–discharge relationships reflect chemostatic characteristics of US catchments. Hydrological Processes, 23(13): 1844-1864.
Hama, T. and Yanagi, K., 2001. Production and neutral aldose composition of dissolved carbohydrates excreted by natural marine phytoplankton populations. Limnology and Oceanography, 46(8): 1945-1955.
Hammes, F. and Verstraete, W., 2002. Key roles of pH and calcium metabolism in microbial carbonate precipitation. Reviews in Environmental Science and Biotechnology, 1(1): 3-7.
Hantszche, N.N. et al., 2003. Septic System Sanitary Survey for Santa Barbara County, California. Questa Engineering Corporation, Point Richmond, California.
Hedges, J.I. et al., 2002. The biochemical and elemental compositions of marine plankton: A NMR perspective. Marine Chemistry, 78(1): 47-63.
Henrichs, S.M., 1992. Early diagenesis of organic matter in marine sediments: progress and perplexity. Marine Chemistry, 39(1): 119-149.
Hill, A.R. and Warwick, J., 1987. Ammonium transformations in springwater within the riparian zone of a small woodland stream. Canadian Journal of Fisheries and Aquatic Sciences, 44(11): 1948-1956.
Hoehn, E. and Von Gunten, H., 1989. Radon in groundwater: A tool to assess infiltration from surface waters to aquifers. Water Resources Research, 25(8): 1795-1803.
Hooper, R.P., Christophersen, N. and Peters, N.E., 1990. Modeling streamwater chemistry as a mixture of soilwater end-members: an application to the Panola Mountain catchment, Georgia, U.S.A. Journal of Hydrology, 116(1-4): 321-343.
Howarth, R.W., 1988. Nutrient limitation of net primary production in marine ecosystems. Annual Review of Ecology and Systematics: 89-110.

Howarth, R.W. and Marino, R., 2006. Nitrogen as the limiting nutrient for eutrophication in coastal marine ecosystems: evolving views over three decades. Limnology and Oceanography, 51(1): 364-376.
Jaworski, N.A., Howarth, R.W. and Hetling, L.J., 1997. Atmospheric deposition of nitrogen oxides onto the landscape contributes to coastal eutrophication in the northeast United States. Environmental Science & Technology, 31(7): 1995-2004.
Johnson, N.M., Likens, G.E., Bormann, F.H., Fisher, D.W. and Pierce, R.S., 1969. A working model for the variation in stream water chemistry at the Hubbard Brook Experimental Forest, New Hampshire. Water Resources Research, 5(6): 1353-1363.
Jordan, T.E., Correll, D.L. and Weller, D.E., 1997. Relating nutrient discharges from watersheds to land use and streamflow variability. Water Resources Research, 33(11): 2579-2590.
Kemp, M.J. and Dodds, W., 2002. Comparisons of nitrification and denitrification in prairie and agriculturally influenced streams. Ecological Applications, 12(4): 998-1009.
Kim, G. and Hwang, D.-W., 2002. Tidal pumping of groundwater into the coastal ocean revealed from submarine 222Rn and CH4 monitoring. Geophysical Research Letters, 29(14): 23-1-23-4.
Kim, T.-H., Waska, H., Kwon, E., Suryaputra, I. and Kim, G., 2012. Production, degradation, and flux of dissolved organic matter in the subterranean estuary of a large tidal flat. Marine Chemistry, 142-144: 1-10.
Kirchman, D.L., Keil, R.G. and Wheeler, P.A., 1990. Carbon limitation of ammonium uptake by heterotrophic bacteria in the subarctic Pacific. Limnology and Oceanography, 35(6): 1258-1266.
Kirchner, J.W., 2003. A double paradox in catchment hydrology and geochemistry. Hydrological Processes, 17(4): 871-874.
Kummerow, J., Alexander, J.V., Neel, J.W. and Fishbeck, K., 1978. Symbiotic nitrogen fixation in Ceanothus roots. American Journal of Botany, 65(1): 63-69.
Larsson, U. and Hagström, A., 1979. Phytoplankton exudate release as an energy source for the growth of pelagic bacteria. Marine Biology, 52(3): 199-206.
Latron, J., Llorens, P. and Gallart, F., 2009. The hydrology of Mediterranean mountain areas. Geography Compass, 3(6): 2045-2064.
Laudon, H. and Slaymaker, O., 1997. Hydrograph separation using stable isotopes, silica and electrical conductivity: an alpine example. Journal of Hydrology, 201(1-4): 82-101.
Lerner, D.N., 1986. Leaking pipes recharge ground water. Ground Water, 24(5): 654-662.
Letscher, R.T., Hansell, D.A., Carlson, C.A., Lumpkin, R. and Knapp, A.N., 2013. Dissolved organic nitrogen in the global surface ocean: distribution and fate. Global Biogeochemical Cycles, 27(1): 141-153.
Lewis, E., 1980. The practical salinity scale 1978 and its antecedents. IEEE Journal of Oceanic Engineering, 5(1): 3-8.
Li, L., Barry, D.A., Stagnitti, F. and Parlange, J.Y., 1999. Submarine groundwater discharge and associated chemical input to a coastal sea. Water Resources Research, 35(11): 3253-3259.
Li, X., Hu, B.X., Burnett, W.C., Santos, I.R. and Chanton, J.P., 2009. Submarine ground water discharge driven by tidal pumping in a heterogeneous aquifer. Ground Water, 47(4): 558-568.

Lischeid, G., 2008. Combining hydrometric and hydrochemical data sets for investigating runoff generation processes: tautologies, inconsistencies and possible explanations. Geography Compass, 2(1): 255-280.
Lomstein, B.A., Niggemann, J., Jorgensen, B.B. and Langerhuus, A.T., 2009. Accumulation of prokaryotic remains during organic matter diagenesis in surface sediments off Peru. Limnology and Oceanography, 54(4): 1139.
Lønborg, C., Álvarez-Salgado, X.A., Davidson, K. and Miller, A.E., 2009. Production of bioavailable and refractory dissolved organic matter by coastal heterotrophic microbial populations. Estuarine, Coastal and Shelf Science, 82(4): 682-688.
Martin, J.B., Cable, J.E., Smith, C., Roy, M. and Cherrier, J., 2007. Magnitudes of submarine groundwater discharge from marine and terrestrial sources: Indian River Lagoon, Florida. Water Resources Research, 43(5).
Matsubayashi, U., Velasquez, G.T. and Takagi, F., 1993. Hydrograph separation and flow analysis by specific electrical conductance of water. Journal of Hydrology, 152(1-4): 179-199.
McDonnell, J.J., Stewart, M.K. and Owens, I.F., 1991. Effect of catchment-scale subsurface mixing on stream isotopic response. Water Resources Research, 27(12): 3065-3073.
McKee, G.A. and Hatcher, P.G., 2010. Alkyl amides in two organic-rich anoxic sediments: A possible new abiotic route for N sequestration. Geochimica et Cosmochimica Acta, 74(22): 6436-6450.
McKnight, D.M. et al., 2001. Spectrofluorometric characterization of dissolved organic matter for indication of precursor organic material and aromaticity. Limnology and Oceanography, 46(1): 38-48.
Meixner, T. and Fenn, M., 2004. Biogeochemical budgets in a Mediterranean catchment with high rates of atmospheric N deposition – importance of scale and temporal asynchrony. Biogeochemistry, 70(3): 331-356.
Meyer-Reil, L.A., 1987. Seasonal and spatial distribution of extracellular enzymatic activities and microbial incorporation of dissolved organic substrates in marine sediments. Applied and Environmental Microbiology, 53(8): 1748-1755.
Miller, A.E., Schimel, J.P., Meixner, T., Sickman, J.O. and Melack, J.M., 2005. Episodic rewetting enhances carbon and nitrogen release from chaparral soils. Soil Biology and Biochemistry, 37(12): 2195-2204.
Miller, W.L. and Moran, M.A., 1997. Interaction of photochemical and microbial processes in the degradation of refractory dissolved organic matter from a coastal marine environment. Limnology and Oceanography, 42(6): 1317-1324.
Mitsch, W.J. et al., 2001. Reducing nitrogen loading to the Gulf of Mexico from the Mississippi River Basin: strategies to counter a persistent ecological problem. BioScience, 51(5): 373-388.
Mulholland, P.J. et al., 2008. Stream denitrification across biomes and its response to anthropogenic nitrate loading. Nature, 452(7184): 202-205.
Nieto-Cid, M., Álvarez-Salgado, X.A. and Pérez, F.F., 2006. Microbial and photochemical reactivity of fluorescent dissolved organic matter in a coastal upwelling system. Limnology and Oceanography, 51(3): 1391-1400.
Nissenbaum, A. and Kaplan, I., 1972. Chemical and isotopic evidence for the in situ origin of marine humic substances. Limnology and Oceanography, 17(4): 570-582.

Nolan, B.T., Ruddy, B.C., Hitt, K.J. and Helsel, D.R., 1997. Risk of nitrate in groundwaters of the United States: a national perspective. Environmental Science & Technology, 31(8): 2229-2236.

Obernosterer, I. and Herndl, G.J., 2000. Differences in the optical and biological reactivity of the humic and nonhumic dissolved organic carbon component in two contrasting coastal marine environments. Limnology and Oceanography, 45(5): 1120-1129.

Ostrom, N.E., Hedin, L.O., von Fischer, J.C. and Robertson, G.P., 2002. Nitrogen transformations and nitrate removal at the soil-stream interface: a stable isotope approach. Ecological Applications, 12(4): 1027-1043.

Oviatt, C.A., Rudnick, D.T., Keller, A.A., Sampou, P.A. and Almquist, G.T., 1986. A comparison of system (O 2 and CO 2) and C-14 measurements of metabolism in estuarine mesocosms. Marine Ecology Progress Series, 28: 57-67.

Pantoja, S., Lee, C. and Marecek, J.F., 1997. Hydrolysis of peptides in seawater and sediment. Marine Chemistry, 57(1): 25-40.

Patsch, K. and Griggs, G., 2008. A sand budget for the Santa Barbara Littoral Cell, California. Marine Geology, 252(1–2): 50-61.

Pellerin, B.A., Wollheim, W.M., Feng, X. and Vörösmarty, C.J., 2008. The application of electrical conductivity as a tracer for hydrograph separation in urban catchments. Hydrological Processes, 22(12): 1810-1818.

Peters, J.H. et al., 2005. Existing conditions study of the Arroyo Burro, Mission, Sycamore, and Laguna Creek watersheds, Questa Engineering Corporation, Santa Barbara, California.

Peterson, B.J. et al., 2001. Control of nitrogen export from watersheds by headwater streams. Science, 292(5514): 86-90.

Pilgrim, D.H., Huff, D.D. and Steele, T.D., 1979. Use of specific conductance and contact time relations for separating flow components in storm runoff. Water Resources Research, 15(2): 329-339.

Poor, C.J. and McDonnell, J.J., 2007. The effects of land use on stream nitrate dynamics. Journal of Hydrology, 332(1-2): 54-68.

Precht, E. and Huettel, M., 2003. Advective pore water exchange driven by surface gravity waves and its ecological implications. Limnology and Oceanography, 48(4): 1674-1684.

Rademacher, L., Clark, J. and Boles, J., 2003. Groundwater residence times and flow paths in fractured rock determined using environmental tracers in the Mission Tunnel; Santa Barbara County, California, USA. Environmental Geology, 43(5): 557-567.

Rashid, M. and King, L., 1971. Chemical characteristics of fractionated humic acids associated with marine sediments. Chemical Geology, 7(1): 37-43.

Roberts, D.A. et al., 1998. Mapping chaparral in the Santa Monica Mountains using multiple endmember spectral mixture models. Remote Sensing of Environment, 65(3): 267-279.

Robinson, C., Li, L. and Barry, D.A., 2007. Effect of tidal forcing on a subterranean estuary. Advances in Water Resources, 30(4): 851-865.

Robinson, T.H., Leydecker, A., Keller, A.A. and Melack, J.M., 2005. Steps towards modeling nutrient export in coastal Californian streams with a Mediterranean climate. Agricultural Water Management, 77(1-3): 144-158.

Rusch, A. and Huettel, M., 2000. Advective particle transport into permeable sediments-evidence from experiments in an intertidal sandflat. Limnology and Oceanography, 45(3): 525-533.
Ryther, J.H. and Dunstan, W.M., 1971. Nitrogen, phosphorus, and eutrophication in the coastal marine environment. Science, 171(3975): 1008-1013.
Salmon, C.D., Walter, M.T., Hedin, L.O. and Brown, M.G., 2001. Hydrological controls on chemical export from an undisturbed old-growth Chilean forest. Journal of Hydrology, 253(1-4): 69-80.
Santos, I.R. et al., 2008. Nutrient biogeochemistry in a Gulf of Mexico subterranean estuary and groundwater-derived fluxes to the coastal ocean. Limnology and Oceanography, 53(2): 705-718.
Santos, I.R., Burnett, W.C., Dittmar, T., Suryaputra, I.G.N.A. and Chanton, J., 2009. Tidal pumping drives nutrient and dissolved organic matter dynamics in a Gulf of Mexico subterranean estuary. Geochimica et Cosmochimica Acta, 73(5): 1325-1339.
Schemel, L., 2001. Simplified conversions between specific conductance and salinity units for use with data from monitoring stations. IEP Newsletter, 14(1): 17-18.
Schlesinger, W.H., Gray, J.T. and Gilliam, F.S., 1982. Atmospheric deposition processes and their importance as sources of nutrients in a chaparral ecosystem of southern California. Water Resources Research, 18(3): 623-629.
Schmidt, F. et al., 2011. Diagenetic transformation of dissolved organic nitrogen compounds under contrasting sedimentary redox conditions in the Black Sea. Environmental Science & Technology, 45(12): 5223-5229.
Seidel, M. et al., 2014. Biogeochemistry of dissolved organic matter in an anoxic intertidal creek bank. Geochimica et Cosmochimica Acta.
Seitzinger, S. et al., 2006. Denitrification across landscapes and waterscapes: a synthesis. Ecological Applications, 16(6): 2064-2090.
Sercu, B., Werfhorst, L.C.V.D., Murray, J. and Holden, P.A., 2008. Storm drains are sources of human fecal pollution during dry weather in three urban Southern California watersheds. Environmental Science & Technology, 43(2): 293-298.
Shields, C.A. et al., 2008. Streamflow distribution of non-point source nitrogen export from urban-rural catchments in the Chesapeake Bay watershed. Water Resources Research, 44(9): W09416.
Shuman, L.M., 2001. Phosphate and nitrate movement through simulated golf greens. Water, Air, & Soil Pollution, 129(1): 305-318.
Silva, S.R. et al., 2002. Forensic applications of nitrogen and oxygen isotopes in tracing nitrate sources in urban environments. Environmental Forensics, 3(2): 125-130.
Sobota, D., Harrison, J. and Dahlgren, R., 2009. Influences of climate, hydrology, and land use on input and export of nitrogen in California watersheds. Biogeochemistry, 94(1): 43-62.
Spalding, R.F. and Exner, M.E., 1993. Occurrence of Nitrate in Groundwater: A Review. Journal of Environmental Quality, 22(3): 392-402.
Stedmon, C.A. and Markager, S., 2005. Tracing the production and degradation of autochthonous fractions of dissolved organic matter by fluorescence analysis. Limnology and Oceanography, 50(5): 1415.
Stubbins, A. et al., 2014. What's in an EEM? Molecular signatures associated with dissolved organic fluorescence in boreal Canada. Environmental Science & Technology.

Swarzenski, P.W. and Izbicki, J.A., 2009. Coastal groundwater dynamics off Santa Barbara, California: combining geochemical tracers, electromagnetic seepmeters, and electrical resistivity. Estuarine, Coastal and Shelf Science, 83(1): 77-89.
Swarzenski, P.W., Porcelli, D., Andersson, P.S. and Smoak, J.M., 2003. The behavior of U- and Th-series nuclides in the estuarine environment. Reviews in Mineralogy and Geochemistry, 52(1): 577-606.
Swarzenski, P.W., Simonds, F.W., Paulson, A.J., Kruse, S. and Reich, C., 2007. Geochemical and geophysical examination of submarine groundwater discharge and associated nutrient loading estimates into Lynch Cove, Hood Canal, WA. Environmental Science & Technology, 41(20): 7022-7029.
Taniguchi, M., 2002. Tidal effects on submarine groundwater discharge into the ocean. Geophysical Research Letters, 29(12): 2-1.
Tranvik, L.J., 1993. Microbial transformation of labile dissolved organic matter into humic-like matter in seawater. FEMS Microbiology Ecology, 12(3): 177-183.
Urish, D.W. and McKenna, T.E., 2004. Tidal effects on ground water discharge through a sandy marine beach. Ground Water, 42(7): 971-982.
USACE, 2005. HEC-RAS Hydraulic Reference Manual. Hydrologic Engineering Center, Davis, California.
Valiela, I. et al., 1990. Transport of groundwater-borne nutrients from watersheds and their effects on coastal waters. Biogeochemistry, 10(3): 177-197.
Vetter, Y.A., Deming, J.W., Jumars, P.A. and Krieger-Brockett, B.B., 1998. A predictive model of bacterial foraging by means of freely released extracellular enzymes. Microbial Ecology, 36(1): 75-92.
Vitousek, P.M. et al., 1997. Human alteration of the global nitrogen cycle: sources and consequences. Ecological Applications, 7(3): 737-750.
Vitousek, P.M., Gosz, J.R., Grier, C.C., Melillo, J.M. and Reiners, W.A., 1982. A comparative analysis of potential nitrification and nitrate mobility in forest ecosystems. Ecological Monographs, 52(2): 155-177.
Wakida, F.T. and Lerner, D.N., 2005. Non-agricultural sources of groundwater nitrate: a review and case study. Water Research, 39(1): 3-16.
Weigel, F., 1978. Radon. Chemiker-Zeitung, 102(9): 287-299.
Weiss, R.F., 1974. Carbon dioxide in water and seawater: the solubility of a non-ideal gas. Marine Chemistry, 2(3): 203-215.
Wheeler, P.A. and Kirchman, D.L., 1986. Utilization of inorganic and organic nitrogen by bacteria in marine systems. Limnology and Oceanography: 998-1009.
Wilhelm, S.W. and Suttle, C.A., 1999. Viruses and nutrient cycles in the sea. BioScience, 49(10): 781-788.
Woessner, W.W., 2007. Building a compact, low-cost, and portable peristaltic sampling pump. Ground Water, 45(6): 795-797.
Wong, J.W.C., Chan, C.W.Y. and Cheung, K.C., 1998. Nitrogen and phosphorus leaching from fertilizer applied on a golf course: lysimeter study. Water, Air, & Soil Pollution, 107(1): 335-345.
Yamashita, Y. and Tanoue, E., 2003. Chemical characterization of protein-like fluorophores in DOM in relation to aromatic amino acids. Marine Chemistry, 82(3): 255-271.
Yang, Y., Lerner, D.N., Barrett, M.H. and Tellam, J.H., 1999. Quantification of groundwater recharge in the city of Nottingham, UK. Environmental Geology, 38(3): 183-198.